https://ntrs.nasa.gov/search.jsp?R=19700002800 2020-03-12T04:44:00+00:00Z

General Disclaimer

One or more of the Following Statements may affect this Document

- This document has been reproduced from the best copy furnished by the organizational source. It is being released in the interest of making available as much information as possible.

- This document may contain data, which exceeds the sheet parameters. It was furnished in this condition by the organizational source and is the best copy available.

- This document may contain tone-on-tone or color graphs, charts and/or pictures, which have been reproduced in black and white.

- This document is paginated as submitted by the original source.

- Portions of this document are not fully legible due to the historical nature of some of the material. However, it is the best reproduction available from the original submission.

Produced by the NASA Center for Aerospace Information (CASI)

NATIONAL AERONAUTICS AND SPACE ADMINISTRATION

Technical Memorandum 33-435

Proceedings of the Conference on Effects of Lithium Doping on Silicon Solar Cells

Held at the Jet Propulsion Laboratory Pasadena, California May 9, 1969

Edited by
Paul A. Berman

N70-12104 (ACCESSION NUMBER) N70-12111 (THRU)
70 (PAGES) 1 (CODE)
CR#106770 (NASA CR OR TMX OR AD NUMBER) 03 (CATEGORY)
FACILITY FORM 602

JET PROPULSION LABORATORY
CALIFORNIA INSTITUTE OF TECHNOLOGY
PASADENA, CALIFORNIA

August 15, 1969

NATIONAL AERONAUTICS AND SPACE ADMINISTRATION

Technical Memorandum 33-435

Proceedings of the Conference on Effects of Lithium Doping on Silicon Solar Cells

Held at the Jet Propulsion Laboratory
Pasadena, California
May 9, 1969

Edited by
Paul A. Berman

JET PROPULSION LABORATORY
CALIFORNIA INSTITUTE OF TECHNOLOGY
PASADENA, CALIFORNIA

August 15, 1969

Prepared Under Contract No. NAS 7-100
National Aeronautics and Space Administration

Preface

This conference was held at the Jet Propulsion Laboratory, Pasadena, California, on April 9, 1969. The purpose of the conference was to discuss in depth the work being done in the area of lithium-doped silicon solar cells. Six organizations presently under contract to the Jet Propulsion Laboratory were invited to present their final briefing, as contractually required, at this meeting in order to give others in this field an opportunity to listen and discuss the results. Other scientists in the field were also invited to make presentations concerning their investigations; two organizations, the Naval Research Laboratory and Gulf General Atomics, accepted. During the latter part of the afternoon, an open forum was held to present an opportunity for detailed discussion of pertinent points and for some general philosophizing. The meeting was attended by people having a wide variety of interests ranging from solid state and radiation physics to flight program administration and management, thus rendering the open forum extremely interesting and meaningful.

The conference and the publishing of the papers thereof was under the auspices of the Guidance and Control Division of the Jet Propulsion Laboratory.

I would like to thank all those who attended and participated in the meeting, and in particular Mr. Arvin Smith of NASA Headquarters for his support of the JPL Solar Cell Radiation Effects Program.

P. A. Berman
Conference Chairman

Foreword

Significant progress has been made over the past year in understanding many of the characteristics of lithium-doped solar cells and in fabricating uniform, reproducible lithium-doped solar cells. At the present time, however, there is no proven theoretical model that completely describes the effect of irradiation on the lithium-doped solar cell, and some of the cell fabrication processes could be significantly improved.

The presented material and subsequent discussions in this progress conference on lithium-doped solar cells has provoked the following subjective observations.

(1) Lithium-doped cell efficiences have increased, especially for cells fabricated from crucible-grown material, to the point where they can be as high as good state-of-the-art N/P cells (11–11.5% AM0, 28°C).

(2) An interesting hypothesis, stimulated by the foregoing observation, might be made:

(a) Nonlithium-doped P/N cell efficiency distributions are normally one efficiency percent lower than N/P cells.

(b) Lithium-doped P/N cells can be made with efficiencies equal to N/P cells.

(c) If manufacturing techniques for fabricating nonlithium-doped P/N cells are improved to the levels of N/P cells, so that nonlithium P/N and N/P cell efficiencies are equivalent, then lithium-doped P/N cells might be an efficiency percent higher than nonlithium-doped N/P cells.

(3) The diffusion of boron into N-type silicon by the BCl_3 process appears to cause significant embrittlement of the silicon, probably the result of strains introduced by this process. This would be expected to reduce the ultimate efficiency in the resultant cell, and appears to be an area where major improvements can be made, even for nonlithium-doped P/N cells.

(4) Crucible-grown cells, in general, have higher efficiency, due mainly to higher V_{oc}, than float-zone cells having similar lithium diffusion schedules.

(5) An optimized contact sintering schedule might increase the efficiency of lithium-doped cells.

(6) The recombination centers created by the introduction of lithium into silicon are no more effective that those introduced by more conventional dopants such as antimony or arsenic and, in fact, may be less effective.

(7) Changes in lithium diffusion schedule appear to affect primarily the long-wavelength cell response.

Foreword (contd)

(8) Lithium-doped cells fabricated from crucible-grown silicon stored at elevated temperatures (60–100°C) behave almost identically like lithium-doped cells fabricated from float-zone material stored at 28°C. Thus, fast recovery of crucible-grown lithium cells can be expected for cells operated at 1-AU conditions where the cells would attain a temperature of about 60°C.

(9) Different defect centers appear to be formed in lithium-doped crucible-grown and float-zone silicon. In crucible-grown silicon, the primary defect center is probably a lithium-oxygen-vacancy combination; while, in float-zone silicon, the defect is most likely a lithium-vacancy combination.

(10) It appears that both complexing and disassociation of the lithium-vacancy combination occurs in float-zone material at room temperature, while only complexing of the lithium-oxygen-vacancy combination occurs for crucible-grown silicon at room temperature.

(11) The lithium-oxygen-vacancy center is far more stable than the lithium-vacancy center.

(12) Despite the indications that different defect centers are formed in lithium-doped crucible-grown and float-zone silicon at temperatures of 28°C or above, the gross cell characteristics behave as though the main difference is a diffusion associated phenomenon [reference item (8) above].

(13) The term "redegradation" might be a misnomer since there are indications that the phenomenon is really a nonirradiation (or shelf-life) associated degradation. Perhaps the phenomenon would be more accurately termed "radiation independent degradation."

(14) Two types of "redegradation" have been observed:

(a) "Redegradation" of the cell short-circuit current. This is most apparent in highly lithium-doped (greater than 5×10^{15} Li/cm^3 near the P/N junction) cells fabricated from float-zone material.

(b) "Redegradation" of the cell curve-shape, especially open-circuit voltage with little or no change in the short-circuit current.

(15) After irradiation of lithium-doped silicon, two processes occur concurrently: a decrease in the concentration of free lithium and lithium oxygen pairs, and a decrease in the concentration of radiation-induced acceptor levels. It is postulated that two lithium ions are involved with the disappearance of each acceptor level.

Contents

Development of The Lithium-Diffused Solar Cell 1
E. L. Ralph and P. Payne

Development of Lithium-Diffused Solar Cells 9
D. Kendall

Lithium Cell Fabrication and Characteristics 11
P. A. Iles

The Effect of Lithium Doping on Silicon Solar Cells 23
R. G. Downing

Electrical Studies of Electron-Irradiated Lithium-Containing Silicon and Silicon-Solar Cells 31
G. J. Brucker

Annealing of Electron Damage in Lithium-Doped Silicon at 300°K 45
J. E. Stannard

Production and Annealing of Defects in Li-Diffused Silicon After 30-MeV Electron Irradiation at 300°K 51
J. A. Naber, H. Horiye, and R. A. Berger

Study of Dopants for Radiation-Resistant Silicon 57
O. L. Curtis, Jr. and R. F. Bass

PRECEDING PAGE BLANK NOT FILMED.

List of Attendees

ABBOTT, DOREECE D.
Boeing Company, Seattle, Wash.

ALBERT, DANIEL J.
System Science and Software,
La Jolla, Calif.

ANSPAUGH, BRUCE
Jet Propulsion Laboratory, Pasadena, Calif.

BASS, R. F.
Northrop Corporate Laboratories,
Hawthorne, Calif.

BEAUMONT, FRANK
Electro-Optical Systems, Inc.,
Pasadena, Calif.

BERMAN, PAUL
Jet Propulsion Laboratory, Pasadena, Calif.

BERRY, E. R.
Aerospace Corp., Los Angeles, Calif.

BRUCKER, GEORGE J.
Astro-Electronics Division,
Radio Corporation of America,
Highstown, N. J.

CARTER, J. R., JR.
TRW Systems, Redondo Beach, Calif.

CURTIS, ORLIE
Northrop Corporate Laboratories,
Hawthorne, Calif.

DAYTON, R. R.
Lockheed Nuclear Laboratory,
Dawsonville, Ga.

DOWNING, R. G.
TRW Systems, Redondo Beach, Calif.

ERTEL, ALFRED
Centralab Semiconductor Division,
El Monte, Calif.

FARADAY, BRUCE J.
Naval Research Laboratory,
Washington, D. C.

FLARITY, EARL
Jet Propulsion Laboratory, Pasadena, Calif.

FRIEDLANDER, S. A.
Electro-Optical Systems, Inc.,
Pasadena, Calif.

GOLDSMITH, JOHN
Jet Propulsion Laboratory, Pasadena, Calif.

GOLDSMITH, PAUL
Jet Propulsion Laboratory, Pasadena, Calif.

ILES, PETER A.
Centralab Semiconductor Division,
Globe-Union Inc., El Monte, Calif.

KENDALL, D.
Texas Instruments Inc., Dallas, Tex.

LOFERSKI, J. J.
Division of Engineering,
Brown University, Providence, R. I.

LOTT, D. R.
Lockheed Missiles and Space Company,
San Jose, Calif.

LUFT, W.
TRW Systems, Redondo Beach, Calif.

NABER, J. A.
Gulf General Atomic, San Diego, Calif.

PALMER, JAMES M.
Centralab Semiconductor Division,
Globe-Union Inc., El Monte, Calif.

PASSENHEIM, B. C.
Gulf General Atomic, San Diego, Calif.

PAYNE, PAT
Heliotek, Sylmar, Calif.

RAHILLY, PAT
AFAPL, Wright-Patterson Air Force Base,
Dayton, Ohio

RALPH, E. L.
Heliotek, Sylmar, Calif.

REYNARD, DUNCAN L.
SRS Division, Philco-Ford Corp.,
Palo Alto, Calif.

SARGENT, G. A.
Materials Science Dept.,
University of Kentucky, Lexington, Ky.

SMITH, ARVIN H.
NASA Headquarters, Washington, D. C.

STANNARD, JOHN
U. S. Naval Research Laboratory,
Washington, D. C.

STOFEL, ED
Aerospace Corp., Los Angeles, Calif.

WILLIAMS, RICHARD A.
SRS Division, Philco-Ford Corp.,
Palo Alto, Calif.

YASUI, ROBERT
Jet Propulsion Laboratory, Pasadena, Calif.

N70-12105

Development of the Lithium-Diffused Solar Cell

E. L. Ralph and P. Payne

Heliotek
A Division of Textron, Incorporated
Sylmar, California

I. Introduction

This paper summarizes the lithium-doped solar cell research and development program carried out over the past year under JPL Contract 952247. Details of the work discussed will be found in the contract final report. The work performed can be separated into two basic areas: (1) experimental work aimed at the improvement of cell efficiencies, and (2) the fabrication of a quantity of various lithium solar cell types that were characterized statistically.

The lithium cell fabrication procedure used was essentially the same as that reported in an earlier work.* The pertinent steps included a boron diffusion using a BCl_3 source, a lithium diffusion using an oil suspension paint on source, the redistribution of the lithium, the evaporation of the Ti-Ag contacts, and the evaporation of a SiO antireflection coating.

*Heliotek Final Report for Goddard Space Flight Center Contract NAS 5-10272, August 24, 1967.

II. Experimental Studies

The main experimental areas studied were lithium diffusion techniques, boron diffusion techniques, heat treatment effects, antireflection coatings, and storage stability studies.

An investigation was made to determine the effect of repeated lithium diffusions in the same diffusion tube. It was discovered that the initial lithium diffusions made in a clean tube produced cells with short-circuit currents that were 10% lower than normal. Two diffusions in the tube were required before good cell characteristics were obtained.

In another lithium diffusion study it was found that similar cell output performance was achieved regardless of whether the boron diffused layer was or was not removed from the back of the cell before lithium diffusion. The lithium diffused through the boron layer with no adverse effects, thus the masking and etching steps were eliminated from the procedure.

An investigation of the effect of cell position on the boat during boron diffusions showed that the cells first to be exposed to the BCl_3 gas as it traveled down the tube were etched more and had lower outputs than the "downstream" cells. For a group of cells that were boron diffused in the same tube at the same time, the average short-circuit current of cells at the front of the boat was found to be 56.7 mA in a tungsten light source as compared to an average of 61.1 mA for cells "downstream" on the boat. As a result of this experiment, the use of dummy silicon slices at the front of the boat was included in cell processing for all but the first lot of cells sent to JPL during this program.

Sintering or heating of the Ti-Ag contacts has not been utilized as a standard process for lithium solar cells, since the unheated contacts have good ohmic low series resistance and the heat treatments change the lithium concentration profile appreciably. Figure 1 shows the changes in a lithium cell I-V characteristic curve as measured in an AM0 simulator at 140 mW/cm^2 with the cell subjected to three successive 10-min sinterings at 600°C. Each successive heat treatment increased the short-circuit current, probably as a result of a gettering action along with a decrease in the lithium concentration. The first heating increased series resistance significantly, however, a good recovery was made with the second heating and the maximum power output increased to a value slightly higher than that used initially. The third heating again increased the series resistance and lowered the output.

Some heating experiments have shown much greater increases in short-circuit current, especially with very low I_{sc} cells. This effect was demonstrated by heating the two discrete groups of lithium cells shown in Fig. 2. These cells were measured in a tungsten light source. The higher output group had typical output curves. All cells were lithium diffused in the same run and processed together, but they came from two different boron diffusion runs. Consequently, the loss in output was believed to be associated with boron diffusion induced stresses or impurities. After heating to 600°C for 10 min, the characteristic curves shown in Fig. 3 were obtained. All cells showed a short-circuit current increase as expected, however, the average for the low group increased 22%, while that for the higher output group increased only 2%.

An antireflection coating experiment showed that a SiO antireflection coating evaporated on the face of an etched P/N cell was superior to the dark blue coating that naturally develops during the boron diffusion. The average short-circuit current of the SiO coated cells in a solar

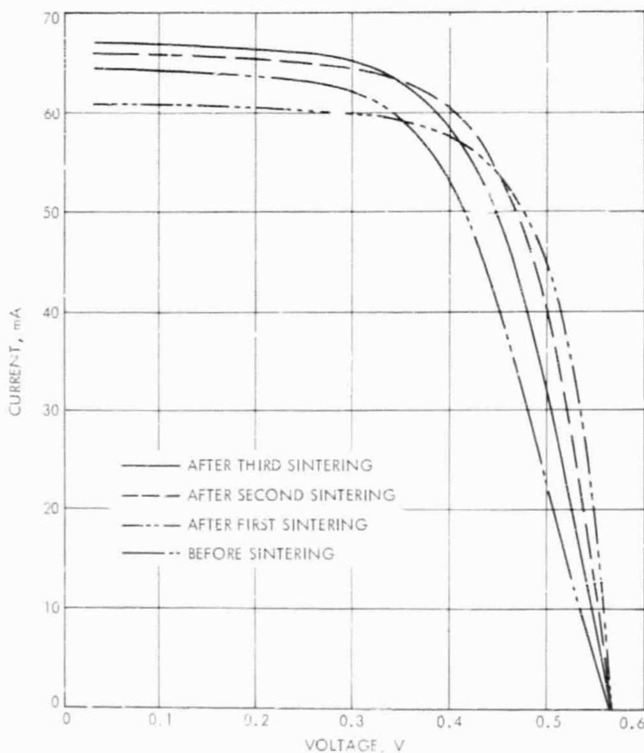

Fig. 1. I-V curves before and after sintering lithium-diffused P/N cells

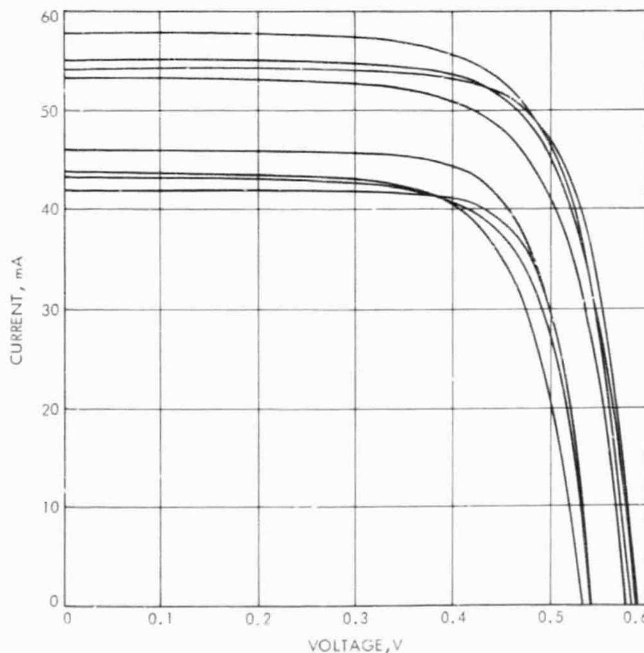

Fig. 2. I-V curves of an unsintered lot of lithium-diffused P/N cells

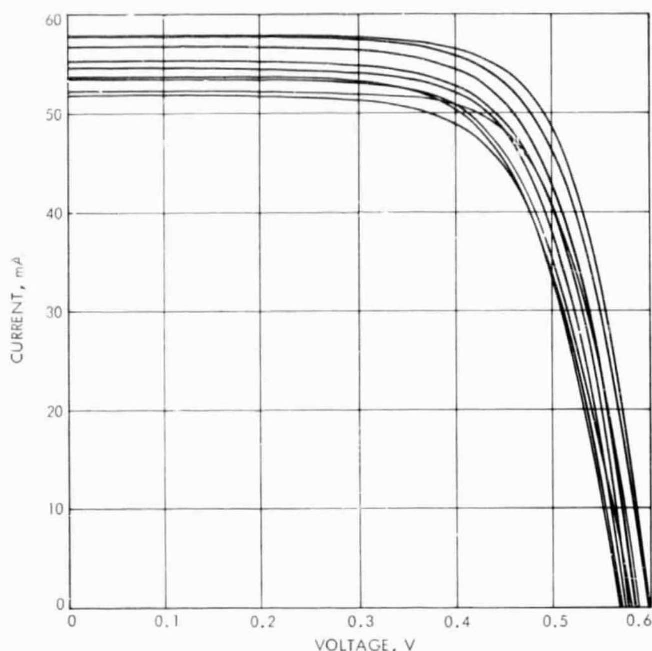

Fig. 3. I-V curves after sintering the lot of lithium-diffused P/N cells

simulator was 71.8 mA while the natural dark blue cells had an average I_{sc} of 66.0 mA, representing an 8.0% loss. Even evaporating SiO on top of the dark blue surface only brought the I_{sc} value up to 67.3 mA, indicating that the SiO coating on the etched surface was an optically superior antireflection layer.

Because lithium has the ability to move in the silicon lattice at room temperature, there has been concern that the cells may not be stable after long-term storage. Therefore, lithium cells were stored and periodically measured. One group of cells being monitored were fabricated, and initial measurements were made on these cells between September and November 1966. At that time, many different materials and diffusion variables were being investigated, thus a good selection of cells with different designs could be included in the storage life experiment. Table 1 shows the data initially obtained about October 1966, those obtained 14 months later in January 1968, and those obtained in March 1969 after about 2½ yr storage at room ambient temperature. The following significant observations have been made based upon the storage experiment data:

Table 1. Lithium cell characteristics after storage

Cell No.	Material		Conditions		Short-circuit current I_{sc}, mA			Open-circuit voltage V_{oc}, V			Maximum power P_{max}, mW		
	Resistivity, Ω-cm	Type[a]	Diffusion/redistribution, min	Temperature, °C	1[b]	2[c]	3[d]	1	2	3	1	2	3
48	1	CG	90/60	425	61.5	61.9	63.1	600	600	605	28.6	28.5	29.0
66	1	CG	90/60	425	62.0	62.5	64.0	594	600	600	27.1	27.6	28.1
71	1	CG	100/60	425	63.8	63.3	64.8	603	605	608	29.4	29.2	30.0
82	>100	CG	90/60	425	54.6	54.9	57.0	556	550	550	21.5	21.4	22.0
83	>100	CG	90/60	425	53.2	53.8	55.9	541	540	540	19.6	19.7	20.4
93	>100	CG	90/60	425	57.4	57.8	59.0	576	578	580	22.3	22.3	23.0
101	20	FZ	90/60	425	55.4	51.0	52.6	559	532	523	23.4	20.3	20.7
155	20	FZ	90/60	425	58.0	58.0	59.8	555	550	554	23.2	23.2	23.9
156	20	FZ	90/60	425	56.5	56.9	58.8	547	542	549	22.7	22.8	24.0
85	100	FZ	90/60	425	57.5	53.0	55.0	562	543	538	24.1	21.6	22.0
86	100	FZ	90/60	425	55.2	51.0	53.4	553	530	525	22.9	20.4	21.0
158	100	FZ	90/60	425	59.0	57.9	59.3	563	556	560	24.0	21.2	24.0
121	20	FZ	90/60	350	68.8	67.5	68.3	560	549	552	28.0	27.3	27.7
136	20	FZ	90/60	350	64.5	65.0	66.7	582	573	572	27.9	27.9	28.6
130	100	FZ	90/60	350	65.2	63.5	64.0	581	568	569	27.1	26.2	27.0
131	100	FZ	90/60	350	64.3	63.0	64.0	572	560	560	26.9	26.0	26.5
139	100	FZ	90/60	350	65.4	64.4	65.5	585	573	575	28.0	26.2	27.7

[a]CG = crucibe-grown silicon; FZ = float-zone cells.
[b]Initial measurements made ≈ October 1966.
[c]Measurements made January 1968.
[d]Measurements made March 1969.

(1) There were no cells with gross losses.

(2) There were three float-zone cells that had about 10% loss in P_{max}.

(3) These three float-zone cells had unusually large V_{oc} decreases.

(4) Not all cells in these float-zone groups above had a loss in power.

(5) All the Czochralski-grown cells had an increase in P_{max}.

(6) The Czochralski-grown cell increase was due to I_{sc} increases.

(7) The cells that were diffused at 350°C decreased and then recovered.

A similar storage-life test has been started on cells made during the past year. Results obtained from the cells stored about 7 mo show that Monex and float-zone cells from lots 3 and 4 have had significant short-circuit current losses of 2.5 to 4.0 mA, while the crucible-grown cells have not had any losses.

III. Fabrication and Characteristics of Delivered Cells

Ten lots of sixty lithium-doped cells each were shipped to JPL during the past year for radiation tests in other laboratories. Usually more than the required sixty were processed and tested so that a good selection was provided. In the statistical analyses of the characteristics, all cells were included to avoid any bias in the distributions.

Table 2 summarizes the cell design and output characteristics for all ten lots. The AM0 maximum power output distribution curves for all ten lots measured in the solar simulator at 140 mW/cm² are shown in Fig. 4.

Lot 1 (Fig. 4a) was the only one that did not use the dummy slices during the boron diffusion (discussed earlier). Lot 2 has two distribution curves as shown in Fig. 4b. The lower curve includes all cells (113 cells) made, while the upper curve (81 cells) has five consecutive diffusion runs eliminated, because all five runs were conspicuously lower than the cells from runs before and after.

Lot 6 had a distribution that was not normal, since it is the sum of two distinct distributions. The first 80 cells made, represented by the lower distribution curve (see Fig. 4e), were from one silicon ingot, while the upper curve was for cells made from a second ingot. Of interest, boron diffusions for a few cells from each ingot were done on the same day but not on the same run, and this large differential still existed with these cells; thus, these results would strongly indicate material variations.

The lot 8 cells were made to a special design that was not typical for standard lithium cells. There was a phosphorous region diffused into the silicon slice prior to the standard boron diffusion. This group of cells had a high percentage of shunting and a relatively low output. This

Table 2. Summary of delivered lithium cells lots

Shipment Lot	Material		Conditions		Maximum power, mW			Short-circuit current, mA		
	Resistivity, Ω-cm	Type[a]	Diffusion/ redistribution, min	Temperature, °C	5% of Cells ≥	50% of Cells ≥	95% of Cells ≥	5% of Cells ≥	50% of Cells ≥	95% of Cells ≥
1	>100	CG	90/60	425	29.8	26.0	21.0	68.2	62.0	54.2
2	20	CG	90/60	425	30.6	28.5	26.0	69.5	66.3	60.3
3	20	Monex	90/60	425	26.6	23.5	21.1	63.1	57.2	53.6
4	100	FZ	90/60	425	26.0	23.3	21.6	63.1	58.0	54.7
5	20	FZ	90/60	350	31.3	28.8	26.4	76.4	71.9	64.2
6	20	CG	90/60	450	31.7	24.4	22.3	68.6	58.5	54.0
7	20	Lopex	90/60	425	31.5	28.4	24.7	72.6	66.7	62.9
8	100	FZ[b]	90/60	425	27.8	23.7	21.0	66.9	60.3	53.6
9	20	FZ	90/60	425	29.0	27.1	25.2	67.1	62.9	59.8
10	20	CG	90/60	425	32.0	29.0	26.0	70.5	65.0	59.6

[a]CG = crucible-grown silicon; FZ = float-zone cells.

[b]Special cell with phosphorus region at the junction.

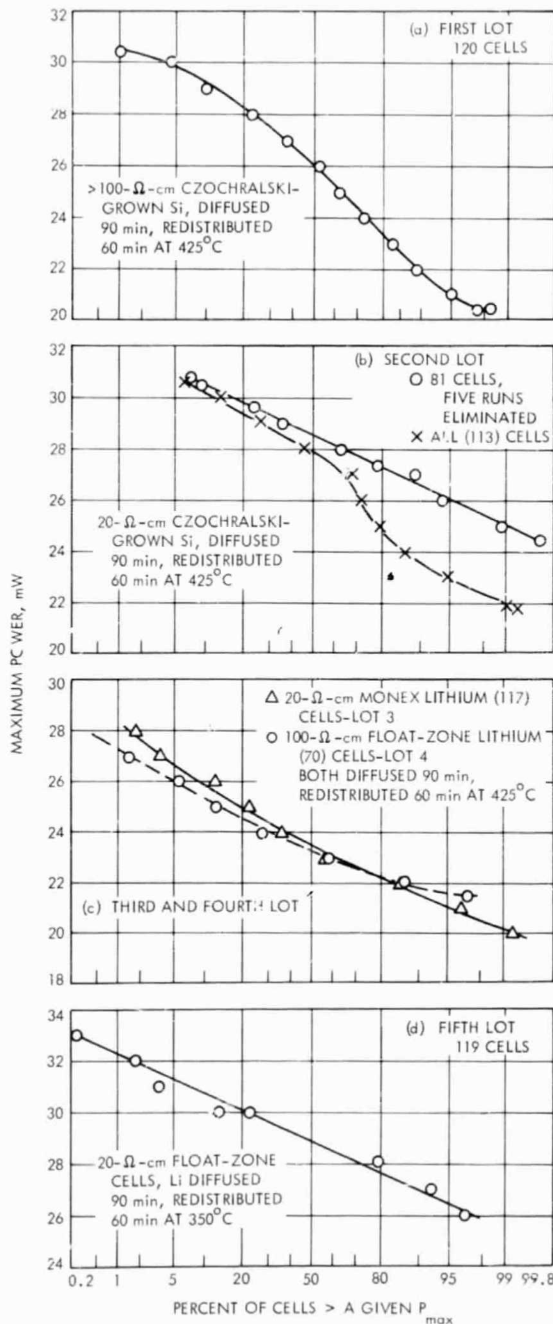

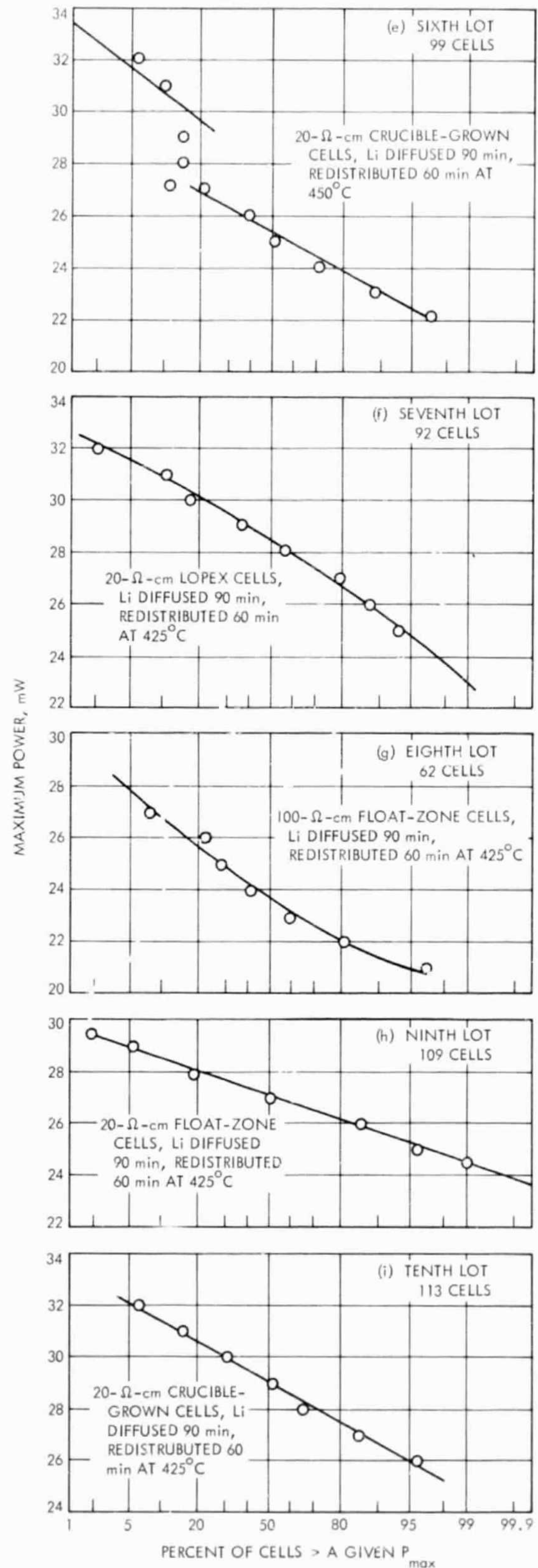

Fig. 4. Maximum power distribution of lithium cells fabricated for the ten shipment lots

experimental cell design is expected to provide unique radiation recovery characteristics; however, it should not be considered a state-of-the-art cell as is the case for the other nine lots.

Lots 2 and 10 were made with the same crucible-grown cell design. Consequently they provide an opportunity to compare two large groups of cells made at widely different time periods. Figure 5 shows that the maximum power distributions are very similar, indicating an ability to reproducibly fabricate this type of cell.

A comparison of float-zone (lot 9) and crucible-grown (lot 10) cells made from 20 Ω-cm silicon is shown in Fig. 6. The distribution of the float-zone cells was narrower; however, the outputs of the Czochralski-grown

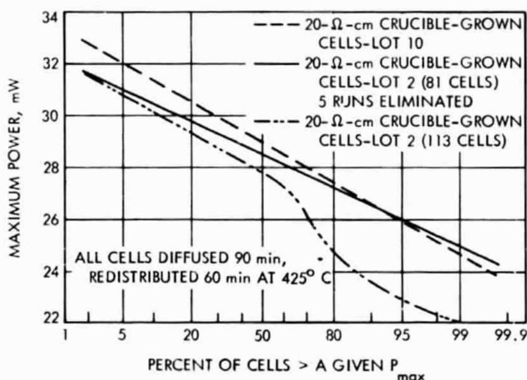

Fig. 5. Comparison of maximum power distributions of lots 2 and 10

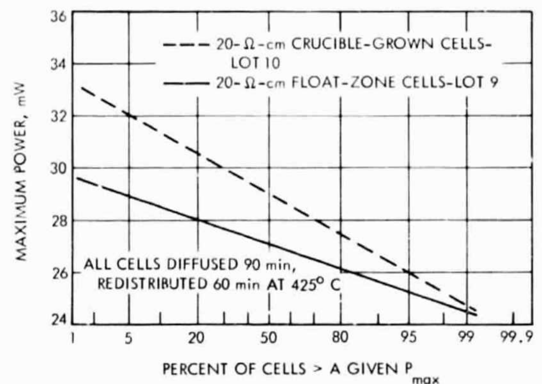

Fig. 6. Comparison of maximum power distributions of lots 9 and 10

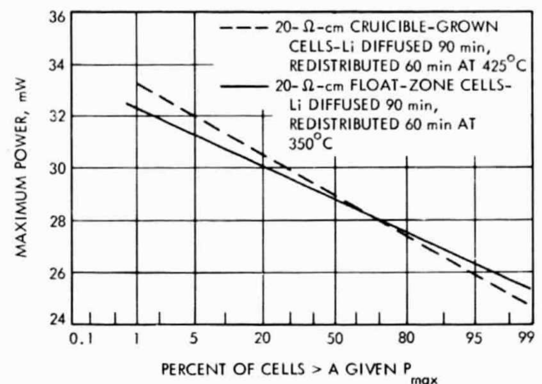

Fig. 7. Comparison of maximum power distributions of lots 9 and 10 at diffusion temperatures of 350 and 450°C

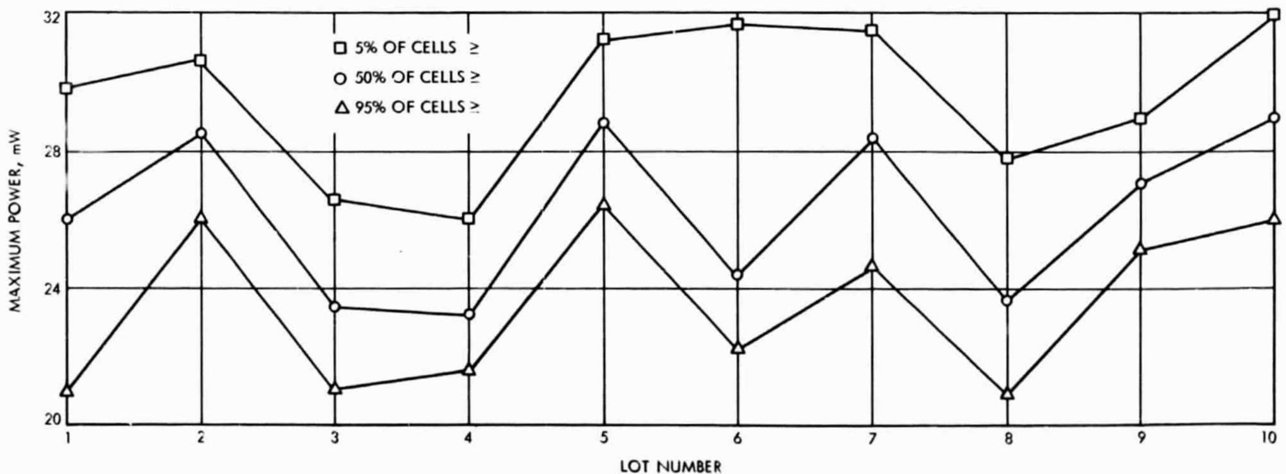

Fig. 8. Summary of maximum power distributions of all ten lots

cells were higher. A closer match in output was obtained, as shown in Fig. 7, when the diffusion temperature for the float-zone cells was reduced from 425 to 350°C.

Figure 8 summarizes the maximum power (5, 50, and 95%) distribution points obtained on all ten lots. The widest distributions were obtained for lots 1 and 6. Lot 1 did not use dummy cells in the boron diffusion and lot 6 had two distributions that correlated to two ingots. Lots 2 through 5 had very good narrow distributions. Lots 7 and 8 were not quite as good, with lot 7 being Lopex material and lot 8 being the special phosphorous-diffused cells. Lot 9 had the narrowest distribution of all lots. Lot 10, although the same design as lot 2, had a slightly wider distribution, but also slightly better output. In general, the lithium cells fabricated from crucible-grown silicon had the highest outputs.

In summary, the outputs for all cell designs show good improvements in efficiency over those obtained a year ago. If the radiation studies on these cells show the same recovery characteristics as the previous studies have shown, then the improved efficiencies will result in more power after radiation exposure than previously available with solar cells.

Acknowledgment

The authors wish to thank Mr. Paul Berman of JPL for his technical coordination, and JPL for the support of the program.

Development of Lithium-Diffused Silicon Solar Cells

D. Kendall

Texas Instruments Incorporated
Dallas, Texas

(Paper not available at time of publication.)

PRECEDING PAGE BLANK NOT FILMED.

N70-12106

Lithium Cell Fabrication and Characteristics

P. A. Iles

Centralab Semiconductor Division
Globe-Union, Incorporated
El Monte, California

I. Introduction

The objective of this work under JPL Contract 952250 is to develop high-efficiency solar cells, using lithium doping to improve cell stability in the charged particle environment in space. The method for this development is to improve the fabrication processes for lithium solar cells, to test their potential for use as power sources, and to provide well-controlled groups of cells with deliberately introduced variations for evaluation by various irradiation groups. A first requirement is to understand the pre-irradiation properties and then to relate these properties with the post-irradiation behavior.

This paper will survey the basic cell fabrication steps, the introduction and distribution of lithium in the cells, and the effect of the lithium and the silicon properties on cell performance. Also described will be some associated tests, the groups of cells shipped during the year, and trials of some different cell structures.

II. Basic Cell Fabrication Steps

A. Surface Finish

Tests have continued throughout the contract to improve the fabrication steps. Most cells have been made with a lightly etched, lapped finish slice, but good cells were also made from slices with a high optical finish.

B. Boron Diffusion

The P+ layer is produced by boron diffusion, and mostly boron trichloride gas has been used as the source. This method is convenient and has produced high-quality cells. However, there are several consequences of this gaseous process, which restrict work in some of the areas described later. These consequences are the removal of ½ to 1 mil of silicon by boron trichloride etching, stresses introduced into the silicon by the boron layer, and the need for a hybrid antireflective coating because the boron skin left on the silicon has different optical properties

PRECEDING PAGE BLANK NOT FILMED

from ordinary highly doped P− silicon. In practice, the coating procedure can be adjusted to allow collected currents under AM0 illumination as high as those measured in the best quality N/P cells. The gas etching complicates work where the P+/N cell must contain a thin layer to improve radiation properties. The stresses drastically increase the dislocation density of the silicon and prevent full evaluation of low dislocation density silicon. These stresses may also affect the behavior of lithium diffused into the silicon.

Because of these disadvantages of the BCl_3 process, alternative boron diffusion methods were found to produce good quality cells without the above disadvantages. More work is needed to build these methods into possible production processes.

C. Other Processes

In most cases, the P/N junction produced for lithium cells is of good quality. The titanium-silver contacts have generally been adequate for use in the present program. Tests have been made on other contact metals, and of these, aluminum has provided good cells. As expected, there were no difficulties in making lithium cells that were all or partly solder coated, or of larger size.

III. Introduction of Lithium into the Silicon

Several methods have been studied; a few have shown promise in some aspects, but more work is needed to find the best overall method. The methods tried are as follows:

(1) Paint-on using suspensions of lithium metal or compounds.

(2) Thermal evaporation of lithium metal, either in high vacuum or at relatively high inert gas pressures.

(3) Lithium vapor transport.

A. Suspensions

Oil suspensions were used most. They are convenient and gave consistent cells, but they have several disadvantages.

These disadvantages include a tendency for clusters of lithium metal to form deep pits by localized alloying, with great chance of breakage, and difficulty in covering the whole back surface of the slice. Full coverage could be obtained by depositing on a slice larger than the final cell and later shaping, but this procedure is not as convenient as correctly shaping the starting slice.

A solution of lithium aluminum hydride in ether was obtained from TRW Systems and tested. This solution gave reduced surface damage, maintaining the surface finish as it was before lithium diffusion. Better coverage near the edges was obtained but was still not complete. The lithium concentration at the surface and in the cell was slightly lower than that obtained from the oil suspensions, but compensating changes in diffusion schedule can remedy this condition.

B. Evaporation

Vacuum evaporation has several theoretical advantages including a clean source, clean deposition conditions, control of the slice temperature during deposition, full coverage on the exposed surfaces, and the possibility of shadow masking.

However, practical difficulties were found in this method. Sample heating during evaporation caused loss of lithium from the silicon, and this loss in turn led to a wide spread in the electrical characteristics of the cells, even if the diffusion was performed outside the vacuum system in an inert atmosphere. Cover layers evaporated over the lithium did not reduce the loss of lithium. Lately, improved evaporation boat design and procedures have given more consistent cells. The main remaining defect is that lithium vapor leaks to the front surface of the cell, either degrading the antireflective coating or, in extreme cases, degrading the P+ layer or contacts.

A variant of evaporation used relatively high vapor pressure (50 μm Hg) of argon between the lithium source and the samples. The main defect was uneven lithium distribution from gas flow patterns, and no advantage was found in this method.

For all these deposition methods, the carrier gas used during diffusion affected cell properties. Although more inert gases did not give greater surface concentration of lithium, they allowed more interaction between the lithium and the silicon, often increasing the cell breakage.

C. Lithium Vapor Transport

In this method, lithium metal was heated to above 700°C, and an argon stream carried the vapor down a furnace tube over silicon slices held at the diffusion temperature. Several practical difficulties were encountered as a result of this process. Lithium vapor was very reactive, necessitating great care in the choice and coverage of the furnace lining, and the gas flow patterns gave

uneven lithium coverage. The lithium vapor reacted with all surfaces of the silicon, and this reaction was a disadvantage if the attack degraded the front surface components of the cell.

However, it was also possible with this method to introduce lithium into the cell through the front surface P+ layer. The vapor method in principle could provide controllable (and lower) surface concentrations.

D. Summary

Paint-on methods have consistently produced closely controlled cell characteristics for all the ingots used. The lithium aluminum hydride suspension avoids several of the faults of the oil suspensions and is undergoing a more thorough evaluation.

Vacuum evaporation still shows promise for large scale usage.

IV. Distribution of Lithium in Cells

The amount and concentration gradient of lithium in the cells can affect cell properties before and after irradiation. Before irradiation, more lithium near the P/N junction reduced short-circuit current and the series resistance. More lithium near the back surface increased open-circuit voltage up to about 600 mV.

After irradiation, the amount of lithium affected the speed of recovery and the ability to recover after more severe fluences. The gradient of lithium near the P/N junction controls cell stability.

It is convenient to divide the various combinations of diffusion temperature and time into three classes:

(1) Tack-on cycle.

(2) Drive-in cycle.

(3) Redistribution.

A. Tack-on Cycle

The diffusion cycle is not severe, and a thin layer of lithium (several mils deep) is formed.

B. Drive-in Cycle

The diffusion cycle is more severe, and the lithium source is maintained in contact with the silicon. A deep layer, heavy with lithium, forms through most of the slice.

C. Redistribution

After either of the above cycles, the slices are cooled, the excess lithium is removed from the back surface, and the slice receives another diffusion cycle.

If redistribution at 450°C follows a tack-on cycle at 450°C for 5 min, the profile changes as shown in Fig. 1. If redistribution follows a drive-in cycle at 425°C for 90 min, the profile changes are as shown in Fig. 2.

Some redistribution cycles produced fairly uniform concentrations. However, there was generally a loss of lithium near each surface of the slice. The measured concentration gradient near the back surface appeared to be the result of out-diffusion. The loss near the P/N junction may have been dissolution of lithium in the diffused boron layer.

When a summation of the measurable donors was made after various redistribution cycles (by integrating under a linear plot of concentration versus distance), serious overall losses in lithium were found. Typically, for 30-min redistribution at 450°C, the amount of lithium fell by 70% for crucible-grown silicon, and by 40% for float-zone

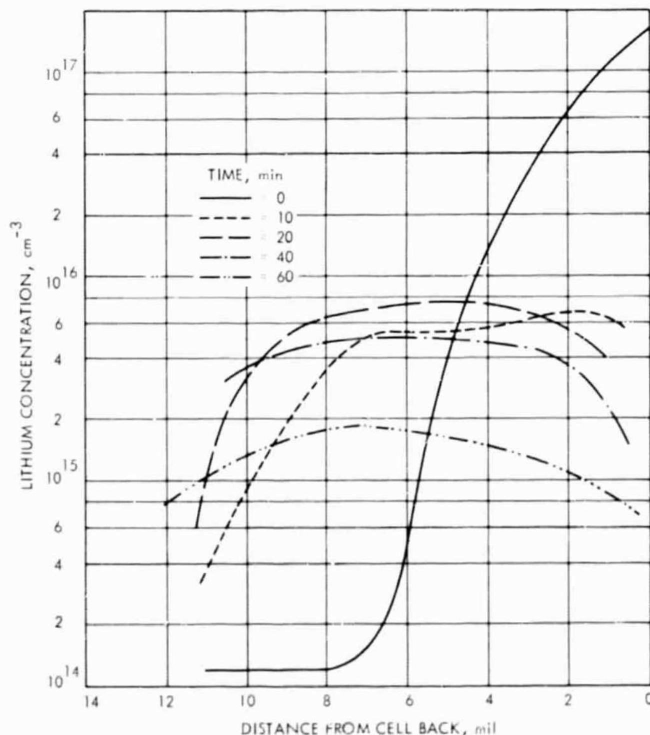

Fig. 1. Lithium concentration profiles following redistribution of a tack-on diffusion

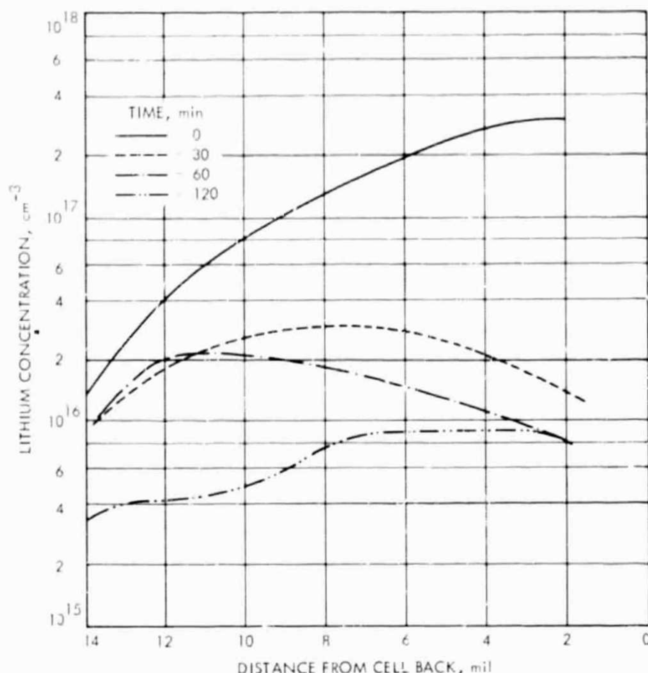

Fig. 2. Lithium concentration profiles following redistribution of a drive-in diffusion

silicon. Examination of the profiles in Figs. 1 and 2 showed that most cycles gave lithium concentrations above 10^{16} cm^{-3}, thus converting most of the bulk N-type silicon to low resistivity (< 1 Ω-cm) silicon.

It has been found that greater amounts of lithium near the P/N junction reduce I_{sc} (Fig. 3). Figure 4 shows that the I_{sc} changes after various redistribution cycles could be explained by the changes in lithium concentration shown in Figs. 1 and 2. The V_{oc} values are much less sensitive to these cycles.

D. Other Distributions

Diffusion at 600 C for 5 or 20 min gave low I_{sc}. Redistribution cycles increased I_{sc}, but it was still low.

Two groups of N-type silicon were given a tack-on and a drive-in lithium diffusion, respectively. They were then taken through the standard BCl_3 diffusion, corresponding to a very severe redistribution cycle. Measurements showed only the starting background level of donors, but the cells made from these two groups showed that the bulk perfection of the silicon had not been degraded by the introduction and loss of lithium. Cells with above 31-mW output were obtained.

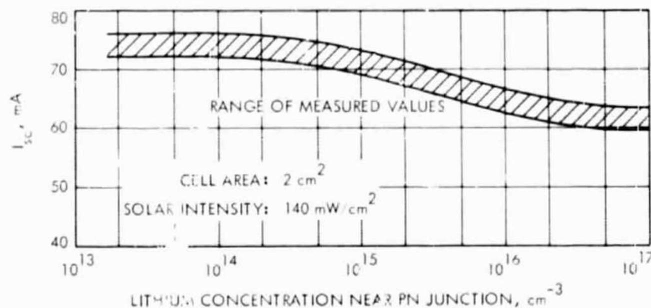

Fig. 3. I_{sc} versus lithium concentration near P/N junction

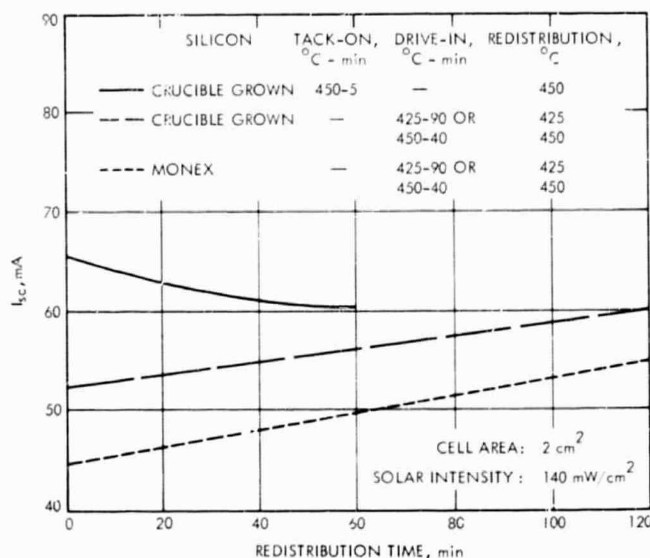

Fig. 4. I_{sc} as a function of redistribution time following either tack-on or drive-in lithium diffusion

V. Influence of Silicon Crystal Growth Method

Three major methods of growing silicon crystals have produced the silicon properties shown in Table 1.

Several separate tests have shown that if slices of the three growth variants were given identical BCl_3 diffusion,

Table 1. Properties of silicon grown by different methods

Method	Maximum resistivity, Ω-cm	Dislocation density, cm^{-2}	Oxygen content, cm^{-3}
Crucible grown	100	Low-medium (10^4)	High (~ 10^{18})
Float zone	1000	High (> 4 × 10^4)	Low (< 10^{16})
Lopex, Monex	1000	Very low (< 10^2)	Low (< 10^{16})

antireflective coatings, and lithium diffusion, there was a consistent difference in the I-V properties of the cells. Generally, the oxygen-lean silicon cells were similar, but all differed from the oxygen-rich crucible grown silicon. Table 2 summarizes the differences of the cells.

For the two forms of silicon, Fig. 5 compares the whole I-V curves, Fig. 6 the dark forward diode characteristics, and Fig. 7 the ln I_{sc}-V_{oc} plots for various light levels. The V_{oc} did not vary much with the diffusion cycle within

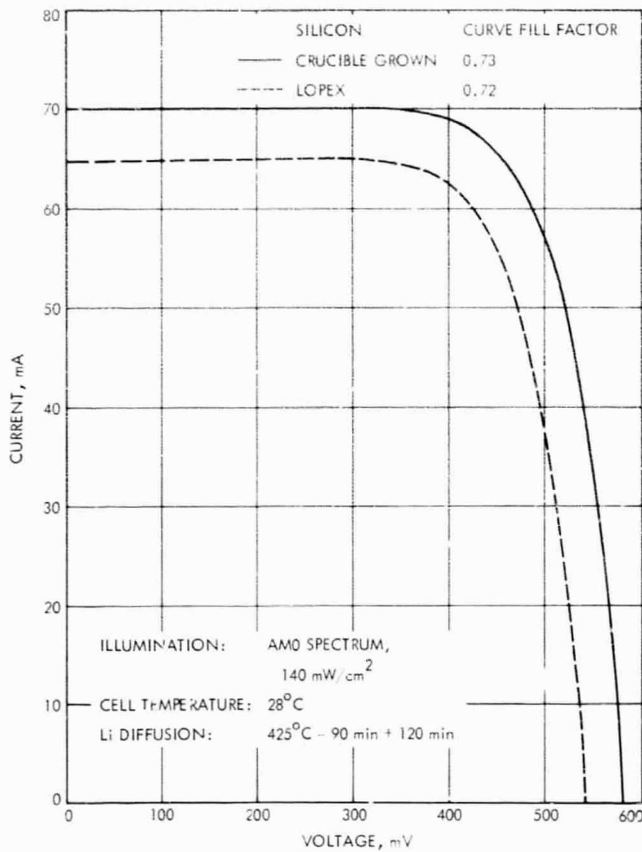

Fig. 5. I-V curves for two forms of silicon with same lithium diffusion schedule

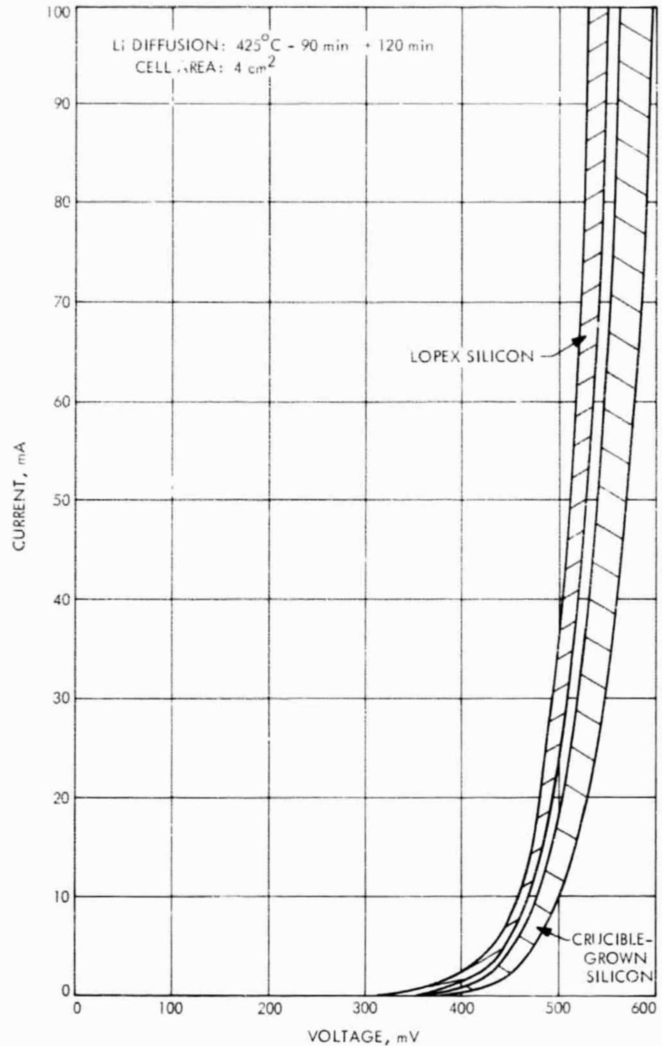

Fig. 6. Envelopes of dark forward I-V characteristics for two forms of silicon with same diffusion schedule

Table 2. Comparison of I-V characteristics for various kinds of silicon[a]

Lithium diffusion schedule, °C-min	Monex, Lopex, or float-zone silicon					Crucible-grown silicon				
	I_{sc}, mA	Tungsten only, mA	Xenon only, mA	I_{450}, mA	V_{oc}, mV	I_{sc}, mA	Tungsten only, mA	Xenon only, mA	I_{450}, mA	V_{oc}, mV
425-90	54.5	30	25	51	560	63.0	38.0	25.0	57.5	590
425-90 (+ 60)	59.5	34	28	55	555	65.0	40.0	25.0	60.0	590
425-90 (+ 120)	65.0	37	28	53	550	68.5	43.0	27.0	65.0	585
450-40	55.0	28	28	50	560	63.0	37.0	26.0	59.0	600
450-40 (+ 80)	63.5	36	29	57	550	69.0	42.5	26.5	65.0	580

[a]Test parameters: cells of 2 cm² and AM0 at 140 mW/cm².

each material type, and the difference between types was consistent. The I_{sc} depended more on the diffusion cycle, the differences becoming less pronounced for longer redistribution times. Measurement of the lithium concentration in the two groups of materials did not explain the differences. Generally, crucible-grown silicon had more lithium through the cell for an equivalent cycle, and this should have decreased I_{sc}. These material comparisons are being repeated using different boron diffusion methods to ensure that the dislocation density of the cells is close to that in the starting silicon.

At present, none of the obvious material differences provide a clear explanation of the observed differences in the cells.

VI. Associated Tests

A. Etch Pits

After etching to develop etch pits, the surface to which the lithium was applied had a "lumpy" appearance possibly caused by localized alloying. Often the etch pit density was lower in the area where the lithium was located, but it was possible that this effect was caused by a reduced preferential etch rate rather than by interaction of lithium and the dislocations.

B. Breaking Tests

Slices approximately 14-mil thick were center loaded until they broke. Although the breaking weights showed spread, possibly because of variable surface effects, three conclusions were possible:

(1) Lithium diffusion alone did not markedly decrease the strength, although it increased the spread.

(2) BCl_3 decreased the breaking weight.

(3) Lithium added to BCl_3 diffused slices did not alter the values obtained in conclusion (2).

C. Oxygen Concentration

Infrared absorption at 9 μm was used to compare the oxygen content of various crucible-grown ingots, and also to search for a diffused oxygen layer.

D. Test for Shelf Drift

Over a 3-mo period, tests on unirradiated cells showed that crucible-grown cells remained stable and a few Lopex cells were also steady, but cells made from float-zone silicon degraded.

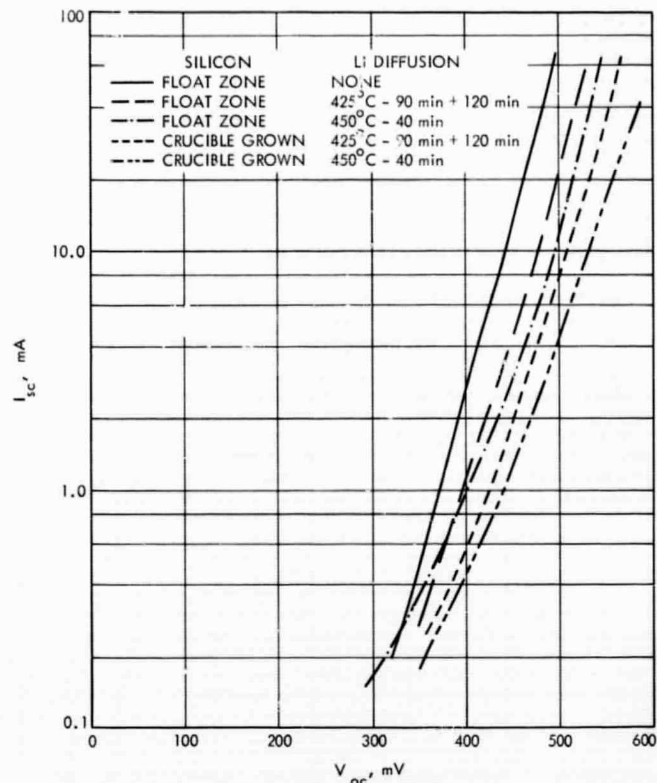

Fig. 7. Log-linear I_{sc}-V_{oc} plots for two forms of silicon with similar lithium diffusion schedules

Float-zone cells that had a drive-in diffusion showed decreases of 6.5mA at I_{sc}, 25mV at V_{oc}, and 6.5mA at I_{450}. For float-zone cells with a moderate redistribution cycle, I_{sc} remained stable, V_{oc} fell by 15mV, and I_{450} decreased 10.5mA. This latter degradation may have been caused by changes in contact resistance.

VII. Centralab Cell Shipments

To date, seven shipments have been made and the eighth is in preparation. Over 1200 slices were processed to form these shipments, and each group was analyzed to show the cumulative yield obtained. The cell shipment details are given in Table 3, and the yields are shown in Figs. 8, 9, and 10.

The group C-1 cells were lightly doped with lithium and did not show good recovery. The group C-2 cells had moderate lithium doping but showed no recovery at room temperature. To test whether the use of antimony as the starting dopant was the reason for this lack of recovery, group C-6 was fabricated. If antimony does not prove to be the reason, other possibilities such as a higher oxygen content in the ingot used for C-2 cells will be explored.

Table 3. Details of cell shipments

Shipment	Number of cells	Si	Resistivity, Ω-cm	Dopant	Li Diffusion, °C-min	Average AM0 I-V values			
						I_{sc}, mA	I_{450}, mA	P_{450}, mW	V_{oc}, mV
C1	60	CG[a]	30	As	450-5 (+40)	70.5	67.5	30.5	600
C2	60	CG	10	Sb	425-90 (+120)	69.5	67.5	30.5	590
C3	30	FZ[a]	65	P	350-30	70.0	57.5	27.0	550
	30	FZ	65	P	425-5	71.0	54.5	24.5	550
C4	12	Monex	100	P	425-90	54.0	50.0	22.5	560
	12	Monex	100	P	425-90 (+60)	59.5	54.0	24.5	555
	12	Monex	100	P	425-90 (+120)	65.0	53.0	24.0	555
	12	Monex	100	P	450-40	55.0	50.0	22.5	555
	12	Monex	100	P	450-40 (+80)	63.5	56.5	25.5	550
C5	30	CG	30	As	450-40	62.0	59.0	26.5	605
	30	CG	30	As	425-90 (+120)	69.0	64.5	29.0	585
	30	FZ	90	P	450-40	54.0	49.0	22.0	570
	30	FZ	90	P	425-90 (+120)	62.0	49.0	22.0	540
C6	40	CG	3–16	Sb	425-90 (+120)	68.0	63.0	28.5	585
	40	CG	17–85	Sb	425-90 (+120)	68.5	63.0	28.5	585
	40	CG	16–57	P	425-90 (+120)	69.0	63.0	28.5	585
C7	30	FZ	90	P	450-10	62.0	55.5	25.0	550
						Remarks			
C8	10	FZ	100	P	400-120	+ O_2-skin			
	10	Lopex	90	P	400-120				
	5	FZ	100	P	400-120	—			
	5	Lopex	90	P	400-120				
	10	FZ	100	P	400-10	Front and back surface			
	10	CG	30	As	400-10				
	5	FZ	100	P	400-120	Back surface only			
	5	CG	30	As	400-120				

[a]CG = crucible grown; FZ = float zone

Groups C-3 and C-7 used short tack-on cycles to leave the active region of the cell without lithium. These cells were then subjected to a sequence of irradiation dosages and redistribution cycles at 250°C, with monitoring of the cell performance. This procedure enabled the degradation and recovery processes to be followed as lithium was progressively moved into the active region.

Group C-4 used Monex silicon and a progressive sequence of lithium distributions. Their behavior under irradiation by 0.7 MeV electrons is shown in Fig. 11, and can be summarized as follows:

(1) For all lithium doping levels, the degradation under fluences of 10^{14}, 5×10^{14}, or 3×10^{15} e/cm^2 was more severe for cells with lower lithium concentration near the P/N junction. This difference in degradation may result from different annealing rates before the post-irradiation measurements.

(2) The degree of recovery of maximum power was most complete as follows:

Fluence	*Cell doping*
Low	Light lithium
Medium	Medium lithium
High	Heavy lithium

VIII. Different Cell Structures

Some structures differing from the conventional lithium cell are worth consideration, either to improve cell performance or to help understand the controlling processes.

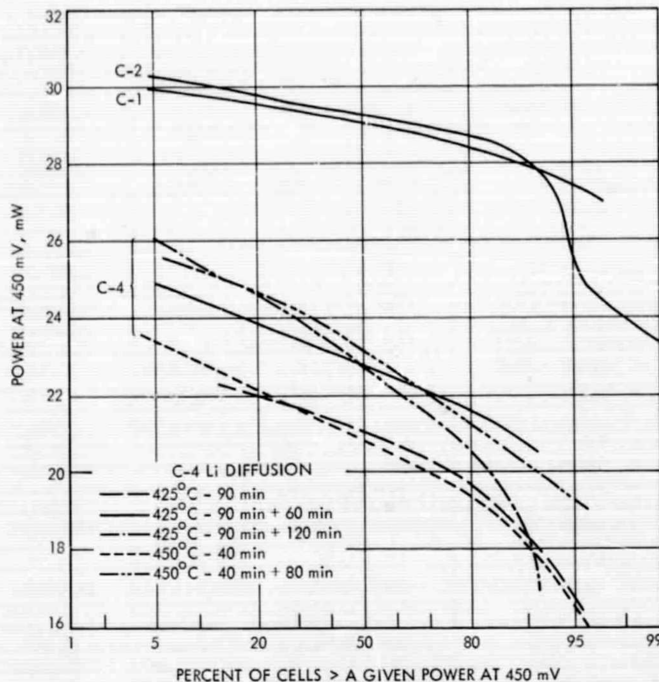

Fig. 8. Cumulative yields for cell shipment groups C-1, C-2, and C-4

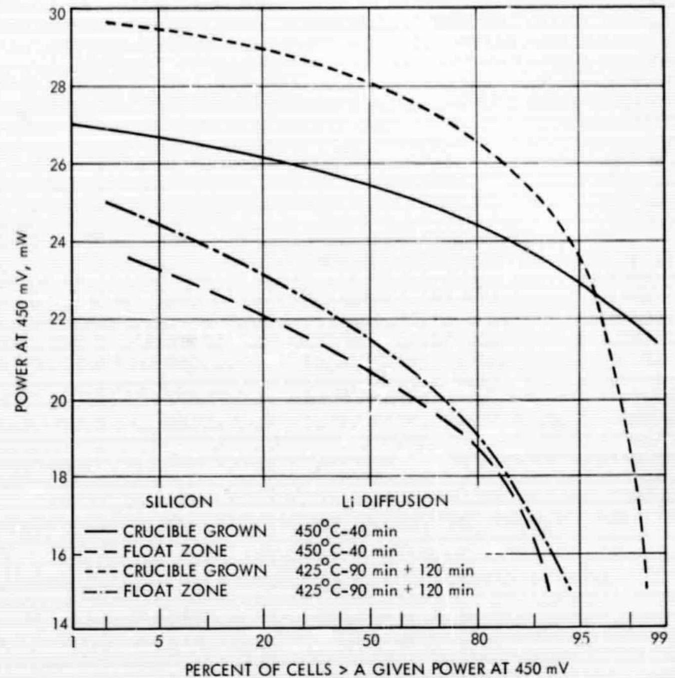

Fig. 9. Cumulative yields for cell shipment group C-5

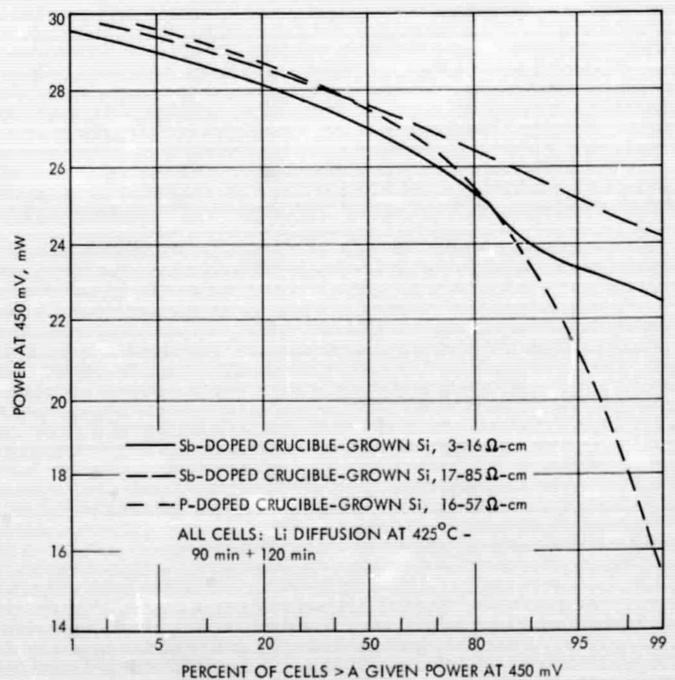

Fig. 10. Cumulative yields for cell shipment group C-6

A. P+/N+/N Configuration

This structure has already provided lithium cells with greater stability after heavy fluences. The P/N junction is formed at the N+ layer after boron diffusion, and this junction remains stable despite large decreases in lithium concentration near the junction. Work continues to improve the starting performance of cells made with this structure.

B. Oxygen Layer Structure

Oxygen-lean silicon generally gives lithium cells with the fastest recovery after irradiation; however, the same silicon can allow most instability after recovery. Oxygen-rich silicon gives the opposite behavior, namely slower recovery with good stability. Because the recovery processes depend on the silicon properties in the bulk of the cell, whereas instability depends more on the properties close to the P/N junction, a structure with a thin oxygen-rich layer at the front surface of a cell formed from oxygen-lean silicon seems worthy of study.

The fabrication sequence is shown in Fig. 12. An oxygen-rich layer approximately 1-mil thick is formed by diffusion in an oxidizing atmosphere. Then a P+ layer is formed, preferably without removal of any of the oxygen layer. Contacts and coating are applied to this P+ layer, and then lithium is diffused in from the back surface. Finally the back contact is applied.

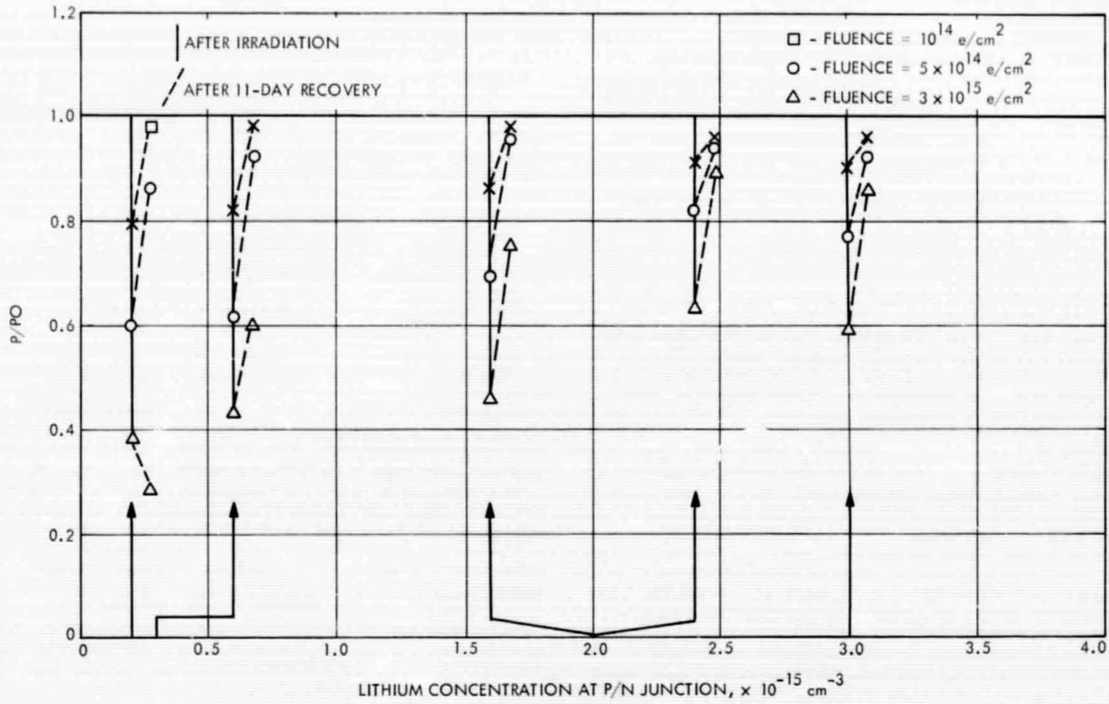

Fig. 11. P/PO ratio for five groups of C-4 cells

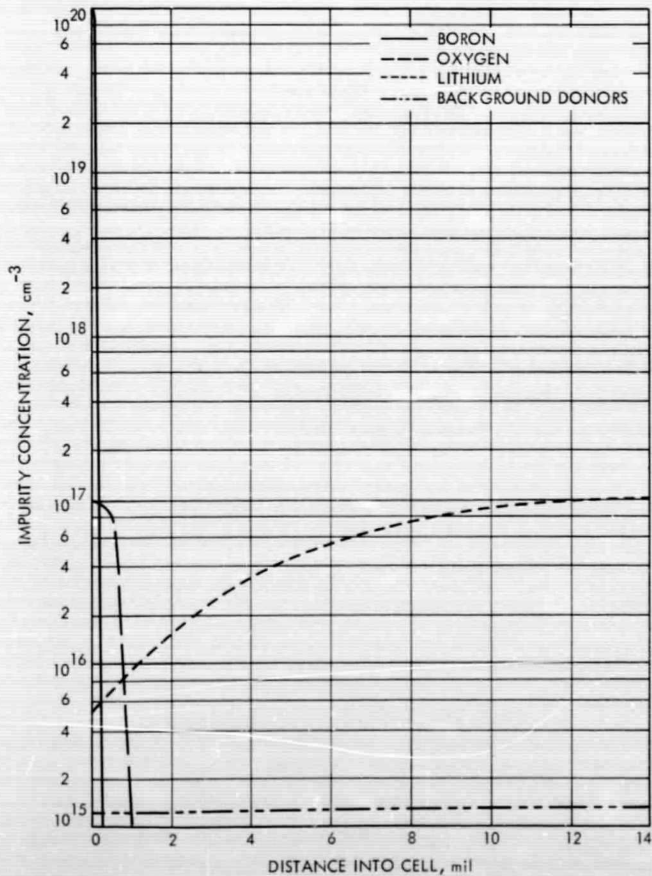

Fig. 12. Impurity distribution for oxygen-layer cells

Some cells with this structure have already been made and such cells will form half of the eighth shipment. The most encouraging result to date has been the surprisingly high quality of the bulk silicon after the severe oxygen diffusion schedule. Cells with outputs as high as 27mW have been obtained for Lopex and crucible-grown silicon, using moderate lithium doping.

A modification of this structure, close to that previously described for the $P^+/N^+/N$ structure, is also being investigated. The oxygen layer is formed and is then converted to a donor-rich layer by heat treatment at 450°C.

If successful, these oxygen layer structures should provide valuable information on the defect-lithium-oxygen interactions.

C. Front Surface Introduction of Lithium

The usual procedure, introducing lithium from the back surface of the cell, is convenient, but has some disadvantages. First, a fairly severe diffusion cycle is needed to build up sufficient concentration of lithium in the active part of the cell near the front surface. Attempts to increase the concentration in this region often leaves the rest of the body of the cell with excess lithium, or with severe concentration gradients. Second, the indiffusing lithium front has a gradient (often large) near the P/N junction, and this may lead to unstable cell behavior.

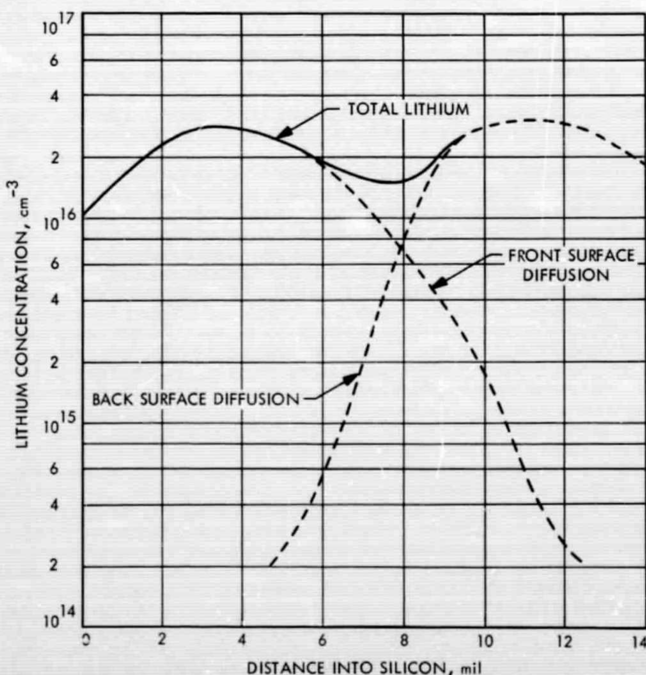

Fig. 13. Lithium distribution resulting from short tack-on cycles with lithium applied to both front and back surfaces

At present, no P+ formation methods have been found which can produce good lithium cells on silicon already diffused with lithium near the front surface.

Diffusion of lithium through an already formed P+ layer on the cell front can avoid some of the shortcomings of the usual method, but may, in turn, lead to other problems. These new problems are: (1) it has been proven difficult to diffuse lithium through the front surface with contacts and coating already formed; (2) if the contacts and coating are applied after lithium diffusion, the range of contact firing treatments is limited; and (3) if the lithium builds up concentration in small areas, it is possible to degrade the P/N junction seriously.

Despite the difficulties, some cells have been made by diffusing lithium through the front surface, and some cells of fair quality have resulted. Using a short cycle of 400°C for 10 min, more than 10^{16} lithium atoms per cm^3 can be provided throughout the cell, and the following I-V values were obtained: I_{sc} ~60 mA, V_{oc} ~590 mV, and I_{450} ~56 mA corresponding to $P_{450} = 25$ mW.

Measurements show that there is still a slump in the measured lithium in the first few mils of the cell (Fig. 13). However, the lithium distribution is sufficiently different to warrant some irradiation tests on cells of this structure.

If successful, this structure could be effective for high fluences. Half of the eighth shipment will include these front surface introduction cells.

Front surface introduction of lithium can be combined with the various boron diffusion methods or with the structures described.

D. Partial Compensation of P-Silicon

More attempts were made to controllably dope the low resistivity P-type silicon to around 10 Ω-m by lithium diffusion. Success depends on getting lower and controllable lithium concentration, with low gradient throughout the P-type silicon. Now, more control exists on lithium introduction methods; this structure is worth trying again.

IX. Conclusions

This year's work has seen consolidation and improvement of fabrication processes with more flexibility, allowing a wider range of structures to be tested. More understanding and control of the lithium distribution in cells has been achieved.

More emphasis was directed toward crucible-grown silicon, because previous work indicated that for real-time space conditions on many missions, the slower rate of recovery could be tolerated to gain the advantage of greater initial output and general stability. Closer examination of results on crucible-grown silicon ingots shows that there is still need for closer control of the properties of these ingots and, hopefully, the results presented at this conference will indicate the main variables needing attention. Crucible-grown silicon cells with lithium recover very well with only slightly accelerated annealing (80–100°C); thus, show good promise now for missions in which this forced annealing can be provided.

Oxygen-lean silicon still has advantages in fast recovery at room temperature, but seems to suffer from possible instability. However, more study is needed because understanding of the deficiencies in this material can be gained more quickly on the shortened time scale, and can complete the overall picture of lithium cells. Some of the more complex structures are of help in understanding, but the goal now is to try and develop the "conventional" lithium cell into a usable space component.

N70-12107

The Effect of Lithium Doping on Silicon Solar Cells

R. G. Downing
TRW Systems
Redondo Beach, California

I. Introduction

This paper covers the majority of the efforts expended at TRW Systems under JPL Contract 952251, concerning the effects of lithium in silicon solar cells. Since this program is not yet complete, the information presented herein will be concerned only with the highlights of information obtained to date. Complete coverage and more detailed information will be contained in the contract final report. Since the principal concern of this meeting is the overall status of the state-of-the-art of lithium-doped silicon solar cells, information obtained under other contractual support will be mentioned when this information pertains to the specific problems of concern here. Acknowledgement is therefore given to efforts conducted jointly with Heliotek under Air Force Contract F33615-68-C-1198.

There are two basic objectives in our program concerning the role of lithium in irradiated silicon and silicon solar cells. The first objective is the evaluation of lithium-doped silicon solar cells provided through JPL by Centralab, Heliotek, and Texas Instruments. This evaluation concerns the determination of the response characteristics of lithium-doped cells as a function of material type, diffusion schedule, and manufacturing techniques. The second objective of this program is the study of the basic kinetics of the interaction of lithium with radiation induced defects in order to better utilize the role of lithium in producing silicon solar cells with both desirable radiation damage annealing characteristics, competitive solar illumination efficiencies, and long-term stability.

II. Solar Cell Evaluation

In the three previous papers, the various manufacturers involved in the production of lithium-doped silicon solar cells have described in detail the characteristics of the various cells produced and the manufacturing techniques involved in their production. For this reason, the various cells evaluated will be referred to only by lot number with

 PRECEDING PAGE BLANK NOT FILMED.

the specific details available from the previous papers. The cell groups tested in this program consisted of C1, 2, 5, and 6; H1, 2, 4, 5, 6, and 7; and T2 through 8. To date, detailed time-dependent analysis is available only on groups C1 and 2, H1, 2, and 4, and T2 and 3. The remaining groups, though now under evaluation, are not complete for detailed analysis, but they will be mentioned when outstanding responses are clearly evident.

A. Crucible-Grown Cells

The first series of cells evaluated in this program consisted of crucible lithium-doped cell groups C1 and 2, H1 and 2, and T2. The test program for the crucible cells consisted of irradiation of 3×10^{15} e/cm^2, 1 MeV with subsequent storage at 60, 80, and 100°C. The fluence was chosen on the basis of the maximum that might be expected under severe orbital conditions wherein lithium exhaustion represents a potential problem, and for comparison with previous data. The storage temperatures were chosen to yield sufficient data in a reasonable period of time and to allow extrapolation to room temperature conditions.

The characteristics of this series of cells are shown in Table 1. The lithium concentrations range from 1 to 4×10^{14} Li/cm^3 with the exception of the C2 group in which lithium concentrations near the junction were undetectable.

The response of this series of cells is widely divergent as shown in Table 2. The C1 group exhibited high initial efficiencies and reasonably good recovery levels, but rather slow annealing times, while the C2 group exhibited no annealing, which is consistent with the observed absence of lithium near the junction. However, the diffusion schedule used for the C2 group should have produced an adequate lithium concentration, but it did not, implying that either the antimony doped initial material does not respond in a normal fashion to lithium diffusion, or some unidentified factor in the diffusion process produced this anamolous result. A later group of cells using antimony doped material is being prepared for further evaluation in this regard.

The H1 and H2 groups of cells responded in a normal fashion, exhibiting response characteristics very similar to those observed in previous experiments. It is emphasized that the recovery times at slightly elevated temperatures are the same as those observed for float-zone cells at room temperature.

The T2 group of cells were superior in that their initial characteristics were very good, their maximum recovered levels were the highest in this series, and their recovery times were faster than either of the C or H groups. The faster recovery times of the T2 group seem inconsistent with their relatively lower lithium concentrations.

Table 1. Crucible-grown lithium solar cell manufacturing parameters

Cell group	Base material		Dopant	Lithium introduction			
	Base growth	Resistivity, Ω-cm		Source	Diffusion, min/°C	Redistribution, min/°C	N_{Li}, cm^{-3}
C1	Crucible	25–35	Arsenic	Paint-on	5/150	40/450	2×10^{14}
C2	Crucible	5–10	Antimony	Paint-on	90/425	120/425	—
H1	Crucible	100–200	Arsenic	Paint-on	90/425	60/425	4×10^{14}
H2	Crucible	20	Phosphorus	Paint-on	90/425	60/425	4×10^{14}
T2	Crucible	>20	Phosphorus	Evaporated	90/400	120/400	1×10^{14}

Table 2. Crucible-grown lithium solar cell recovery characteristics

Cell group	N_{Li}, cm^{-3}	Electron fluence, e/cm^2, 1 MeV	Initial level I_{sc}, mA	Damaged level I_{sc}, mA	Recovered level I_{sc}, mA	Time to 1/2 recovery point at 100°C, h	Time to 1/2 recovery point at 25°C (extrapolated), days
C1	2×10^{14}	3×10^{15}	61–65	23–26	38–41	7.0	—
C2	—	3×10^{15}	52–60	18–24	none	—	—
H1	4×10^{14}	3×10^{15}	40–48	20–23	36–39	1.2	56
H2	4×10^{14}	3×10^{15}	50–55	20–22	35–37	0.6	61
T2	1×10^{14}	3×10^{15}	58–63	19–22	40–46	0.4	10

Figure 1 shows the typical short-circuit current versus time data for this series of cells. The particular group chosen is the T2 group due to its superior response. However, as is evident in Fig. 1a, degradation in short-circuit current, though less than 10%, has initiated. During this slight degradation, the open-circuit voltage is continuing to anneal and the shape of the I-V characteristic near the maximum power point is unaffected, as is the case for this whole series of cells.

Figure 2 illustrates the capacitance versus voltage characteristics for this series of cells. This relationship predicts

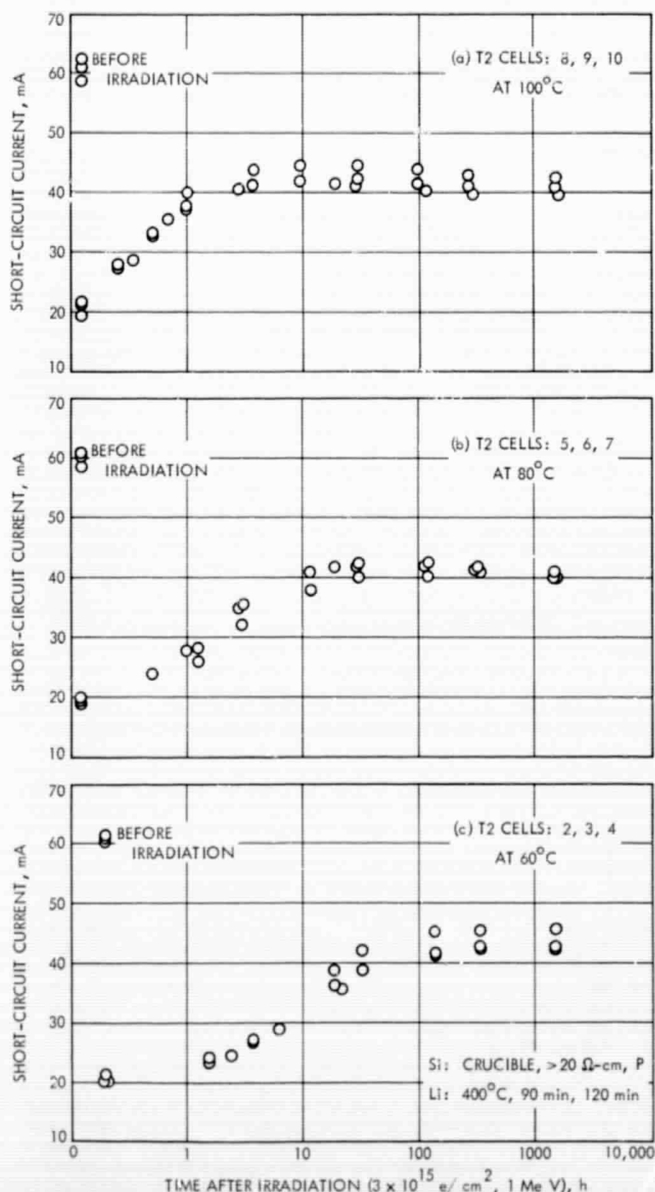

Fig. 1. Recovery of group T2 lithium solar cells

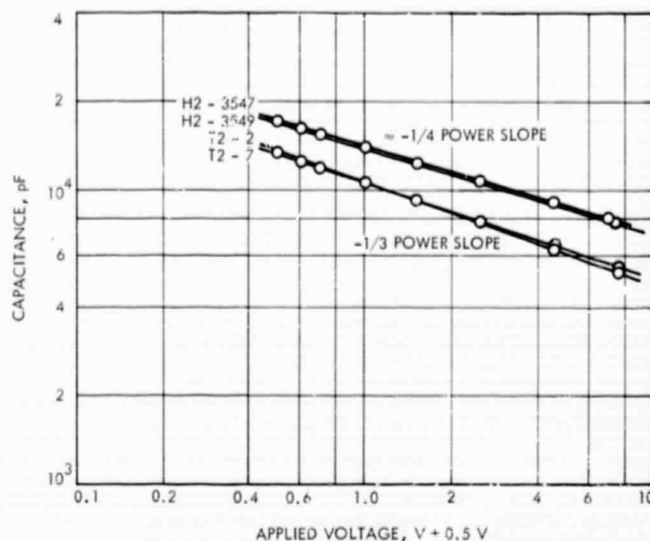

Fig. 2. Capacitance vs voltage for group H2 lithium solar cells

a $-1/2$ slope for a step junction, a $-1/3$ slope for a linear donor concentration gradient near the junction, and a $-1/4$ slope for a quadratic concentration gradient near the junction. Thus, one would expect, depending on the diffusion schedule, a capacitance versus voltage relationship of $-1/4$ (or possibly $-1/3$) if lithium has diffused to the junction region, and $-1/2$ if lithium is absent in the junction. Figure 2 illustrates the $-1/4$ and $-1/3$ relationship for the H2 and T2 groups, respectively; both groups exhibited favorable annealing characteristics. The C2 group of cells, which exhibited no annealing, had a $-1/2$ slope, verifying the absence of lithium as previously indicated.

B. Float-Zone Cells

A similar series of experiments have been continued on float-zone lithium-doped silicon solar cells. For these types of cells, fluences of 3×10^{14} and 3×10^{15} e/cm^2 were used followed by time-dependent measurements with storage at room temperature.

The first groups of cells tested were T3 and H4, which were fabricated as shown in Table 3. The response of these cells under irradiation is shown in Table 4. In general, the lithium concentrations near the junction are higher for float-zone silicon than normally found with crucible-grown silicon processed in a similar fashion.

It is of interest to note that the T3 cells exhibit a considerably higher initial output in spite of the indicated

Table 3. Lithium solar cell manufacturing parameters

Cell group	Base material		Dopant	Lithium introduction			
	Base growth	Resistivity, Ω-cm		Source	Diffusion, min/°C	Redistribution, min/°C	N_{Li}, cm^{-3}
T3	Lopex	>50	Phosphorus	Evaporated	90/400	None	4×10^{15}
H4	Float zone	80–120	Phosphorus	Paint-on	90/425	60/425	1×10^{15}

Table 4. Lithium solar cell recovery characteristics

Cell group[a]	N_{Li}, cm^{-3}	Electron fluence, e/cm^2, 1 MeV	Initial level, I_{sc}, mA	Damaged level, I_{sc}, mA	Recovered level, I_{sc}, mA	Time to 1/2 recovery point at 25°C, h
T3 (L)	4×10^{15}	3×10^{14}	51–54	24	44–46	0.5
H4 (FZ)	1×10^{15}	3×10^{14}	33–37	25–28	34–36	0.5
T3 (L)	4×10^{15}	3×10^{15}	49–53	15	32–34	2.0
H4 (FZ)	1×10^{15}	3×10^{15}	32–35	21	33	3.0

[a](L) = Lopez cell; (FZ) = float-zone cell.

higher lithium concentration. However, since the electrical response of the cells are a bulk phenomena whereas the measured lithium concentrations pertain only to the region near the junction, the different lithium concentration profiles in the bulk produced by the different diffusion schedules may account for this observation.

The annealing rates of the two groups of cells were approximately the same, and the maximum recovered levels for the 3×10^{15} e/cm^2 irradiation were approximately equal. For the 3×10^{14} e/cm^2 irradiation, the maximum recovered level for the T3 group is considerably higher than the H4 group; however, this higher level is considered to be due to the higher initial ouput rather than a lithium controlled annealing phenomena. In terms of response under irradiation, the two groups are considered relatively alike. Of primary importance here, however, is the fact that the T3 group possesses a higher initial output than the H4 group; this fact implies that either the different diffusion schedules used or the different manufacturing techniques used are a very important parameter in producing high initial efficiency lithium doped cells. It is stressed, however, that these measurements are acquired under tungsten illumination, which emphasizes differences due to bulk characteristics as opposed to solar illumination wherein the output is less affected by bulk properties, such is minority carrier diffusion length.

Figures 3 and 4 illustrate typical time-dependent recovery data for these two groups of cells. Once again, initiation of redegradation of short-circuit current is evident in the T3 group of cells. As in the previous case of the T2 group of cells, however, this degradation is evident only in the short-circuit current and, to date, is relatively small; i.e., of the order of 10% or less.

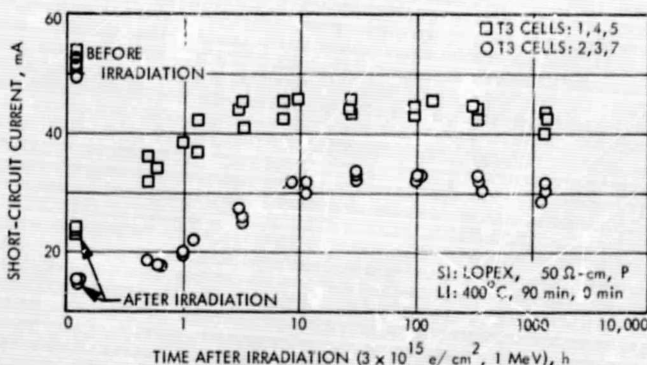

Fig. 3. Recovery of group T3 lithium solar cells

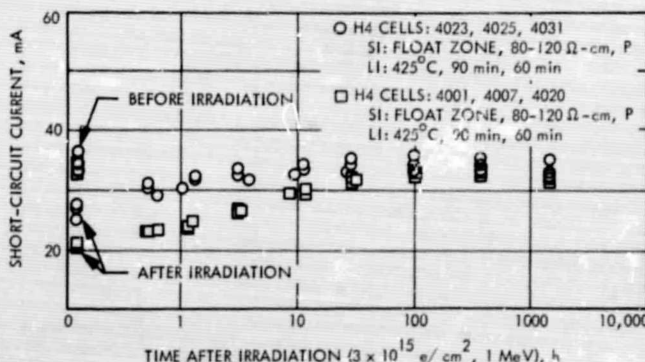

Fig. 4. Recovery of group H4 lithium solar cells

It is not understood at this time why the T3 group of cells exhibits the significantly higher initial output in the presence of the high lithium concentrations as indicated by capacitance voltage measurements. The existence of a high lithium concentration in the bulk material is further confirmed by the very high open-circuit voltage of approximately 590 mV and by the very low bulk resistivity as evidenced by the very high initial degradation to 15 mA after irradiation as opposed to approximately 20 mA for contemporary lithium-doped cells. Figure 5 shows the anticipated $-1/4$ capacitance versus voltage for the T3 cells; this result was also shown by the H4 group of cells.

C. Comparison of Data

The relationship between the short-circuit current and the lithium concentration for both the crucible and float-zone cells is shown in Fig. 6. Also shown in this figure are similar relationships obtained last year for a limited number of Heliotek and Centralab cells. As is evident in the figure, most of the cells exhibited a reproducible decrease in short-circuit current with increasing lithium concentration in the 10^{14} to 10^{15} Li/cm^3 range. The T3 group of cells, however, as previously indicated, do not follow this relationship in that their indicated short-circuit currents are considerably higher than would be anticipated. More recent groups of cells now in evaluation confirm this trend of higher outputs for the Texas Instruments groups of cells as a whole. The reason for these apparent higher outputs is not clear at this time, but may depend on some manufacturing parameter not associated with the lithium diffusion such as the different boron diffusion techniques utilized by Texas Instruments relative to those used by Centralab and Heliotek.

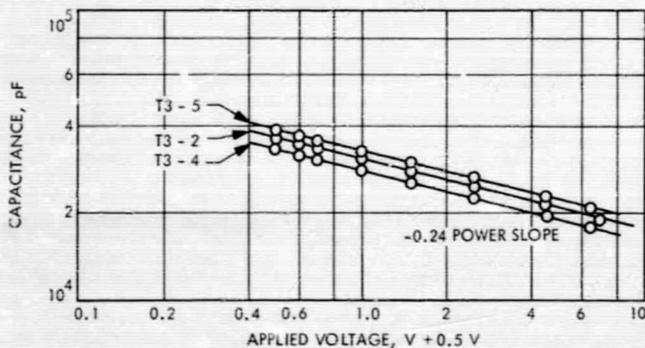

Fig. 5. Capacitance vs voltage for group T3 lithium solar cells

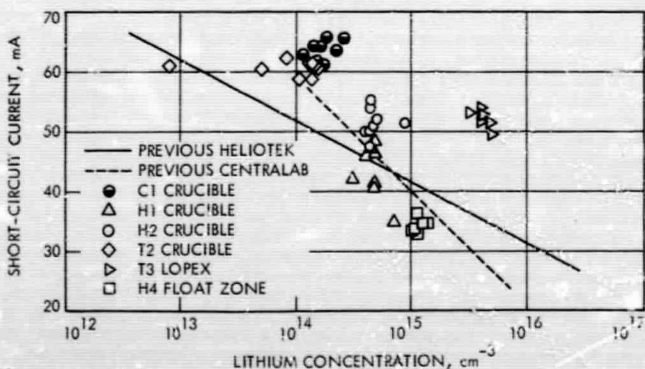

Fig. 6. Short-circuit current vs lithium concentration

The recovery characteristics for these initial groups of cells are listed in Tables 2 and 4. Of particular interest is the evidence that crucible cells exhibit annealing characteristics at slightly elevated temperatures, which are equivalent to those obtained with float-zone cells at room temperature. Other experiments concerned with the evaluation of lithium-doped cells under neutron irradiation indicate, in general, recovery characteristics very similar to those shown here for electron irradiation.

In comparing contemporary lithium-doped cells with contemporary 10-Ω-cm N/P silicon solar cells, it is generally observed that the better lithium-doped cells are only equal to or slightly better than contemporary N/P cells under electron irradiation, but they are superior by approximately an order of magnitude under neutron irradiation. Other workers have shown that the lithium-doped silicon solar cell is also far superior after annealing under proton irradiation.

The neutron experiments have also shown that, after 1-yr storage at room temperature, crucible lithium-doped cells have recovered to levels higher than initial outputs of float-zone lithium-doped cells, and further that redegradation of float-zone cells is observable whereas crucible lithium-doped cells have exhibited no redegradation. It has also been observed that unirradiated control cells fabricated for float-zone silicon evidence the same degree of degradation as the irradiated and recovered cells, strongly implying that the redegradation phenomenon is associated only with lithium diffusion in float-zone silicon after long storage periods, and that redegradation is essentially independent of irradiation history.

The more recent groups of cells now in evaluation are as yet insufficiently complete for the presentation of detailed data. Several interesting observations are evident, however, and they will be discussed very briefly here.

The T4 group of cells, which are identical to the T3 group except that they are constructed from float-zone material instead of Lopex material, exhibit very nearly the same response characteristics as the previously discussed T3 group, implying that there is not a strong dependence on the type of material in this case.

The T5 group of cells, which were not sliced until after all the diffusion processes had been completed to eliminate potential edge effects as previously discussed, are also now in evaluation. The data on the T5 group to date indicate that, at best, they are only as good as the T3 and T4 groups previously discussed. This comparison would imply that the nonuniform edge distribution obtained with normal diffusion techniques is not responsible for limiting the maximum recovered level of lithium-doped cells evaluated in this program.

Finally, the T6 group of cells, which were fabricated using a long diffusion time at lower temperature (i.e., 8 h at 325°C), exhibit very high initial characteristics and recover to the highest recovered level yet observed, i.e., 51–52 mA as opposed to the more normal maximum recovered level of 40–45 mA normally observed in the better lithium-doped cells after 3×10^{14} e/cm^2. Also the T7 group of cells utilizing the same diffusion schedule but are made from crucible rather than Lopex material also exhibit very good initial characteristics and maximum recovered outputs in the 43–44 mA range after 3×10^{15} e/cm^2, which is similar to the previously discussed T2 group.

It is not clear, at this time, whether the superior performance of the Texas Instruments cells, in general, in terms of both initial characteristics and maximum recovered outputs is due to the lithium-diffusion techniques or some other portion of the manufacturing process relative to the other manufacturers. Once again it is emphasized that the measurements presented here are obtained under tungsten illumination and that observed differences between various groups of cells would be less but still significant under solar illumination.

III. Kinetics of Lithium in Silicon

In this phase of the program, a variety of different techniques are being utilized to study the phenology of the interactions between lithium and radiation induced defects in silicon. Techniques included in this study are Hall effects, carrier removal rates, capacitance versus temperature, minority-carrier diffusion length versus temperature, X-ray topography, redistribution studies, other lithium sources, and other cell structures. Although only minority-carrier diffusion length versus temperature measurements will be discussed, complete detail and coverage of all our efforts in these various areas will be included in the final report. Choice of minority-carrier diffusion length measurements for presentation is predicated on understanding the nature of the recombination center and its subsequent removal, because this particular site is of principal importance in the degradation of silicon solar cells.

Data acquired several years ago on contemporary 1 Ω-cm P/N crucible silicon solar cells after irradiation with 1×10^{14} e/cm^2, 1 MeV electrons is given in Fig. 7. A fit of the data with the Hall–Shockely–Read single level statistics indicates a dominant recombination center at 0.17 eV below the edge of the conduction band. This particular energy level for minority-carrier recombination in electron irradiated N-type silicon has been reported by many other workers and is generally attributed to an oxygen-vacancy defect referred to as an A-center.

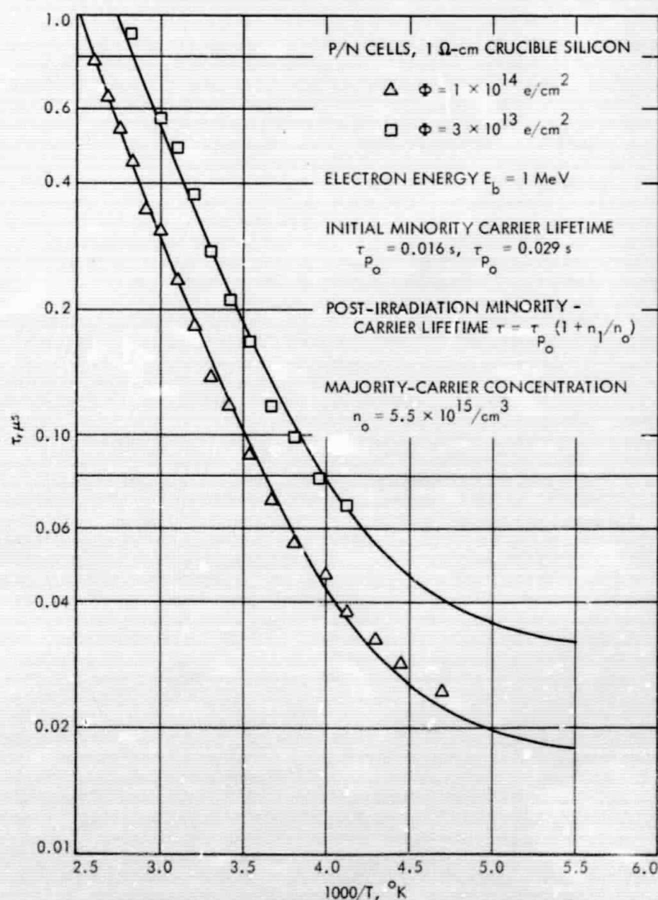

Fig. 7. Post irradiation minority carrier lifetime measurements

The measurements are performed by using a 1-MeV dc electron beam from the Van de Graaff to uniformly generate hole electron pairs in the bulk material. Collection of the current output from the cell can then be related to the minority-carrier diffusion length. Performing the experiment as a function of temperature and using published diffusion coefficient versus temperature relationships yields a steady-state minority-carrier lifetime, which is independent of trapping effects.

Prior to initiation of the present experiments, a 1 Ω-cm P/N cell was irradiated to 3×10^{13} e/cm^2 and the lifetime versus temperature characteristic, as shown in Fig. 7, was obtained. The reproducibility of the measurement is very good, indicating that the technique and associated instrumentation are adequate.

Figure 8 shows the minority-carrier lifetime versus temperature relationships for a lithium-doped crucible silicon solar cell before irradiation, immediately after irradiation, and after annealing. Using the same equations and assuming the same constants as in the previous case for the nonlithium-doped cell, an indicated activation energy of only 0.06 eV was obtained.

Figure 9 shows a similar set of data for a lithium-doped float-zone silicon solar cell before irradiation, immediately after irradiation, and after annealing. Using the same set of assumptions and constants, an activation energy of 0.06 eV is indicated after irradiation and an even shallower level is indicated prior to irradiation and after annealing.

It is not suggested that the recombination level is a 0.06-eV level, but rather that the dominant recombination center in lithium-doped N-type silicon is not the same level as that found in nonlithium doped N-type silicon. This would tend to imply that the initial defect site is not the A-center, but rather a more complex defect site involving lithium in its initial formation in both crucible-grown and float-zone material. Further, it appears from the data

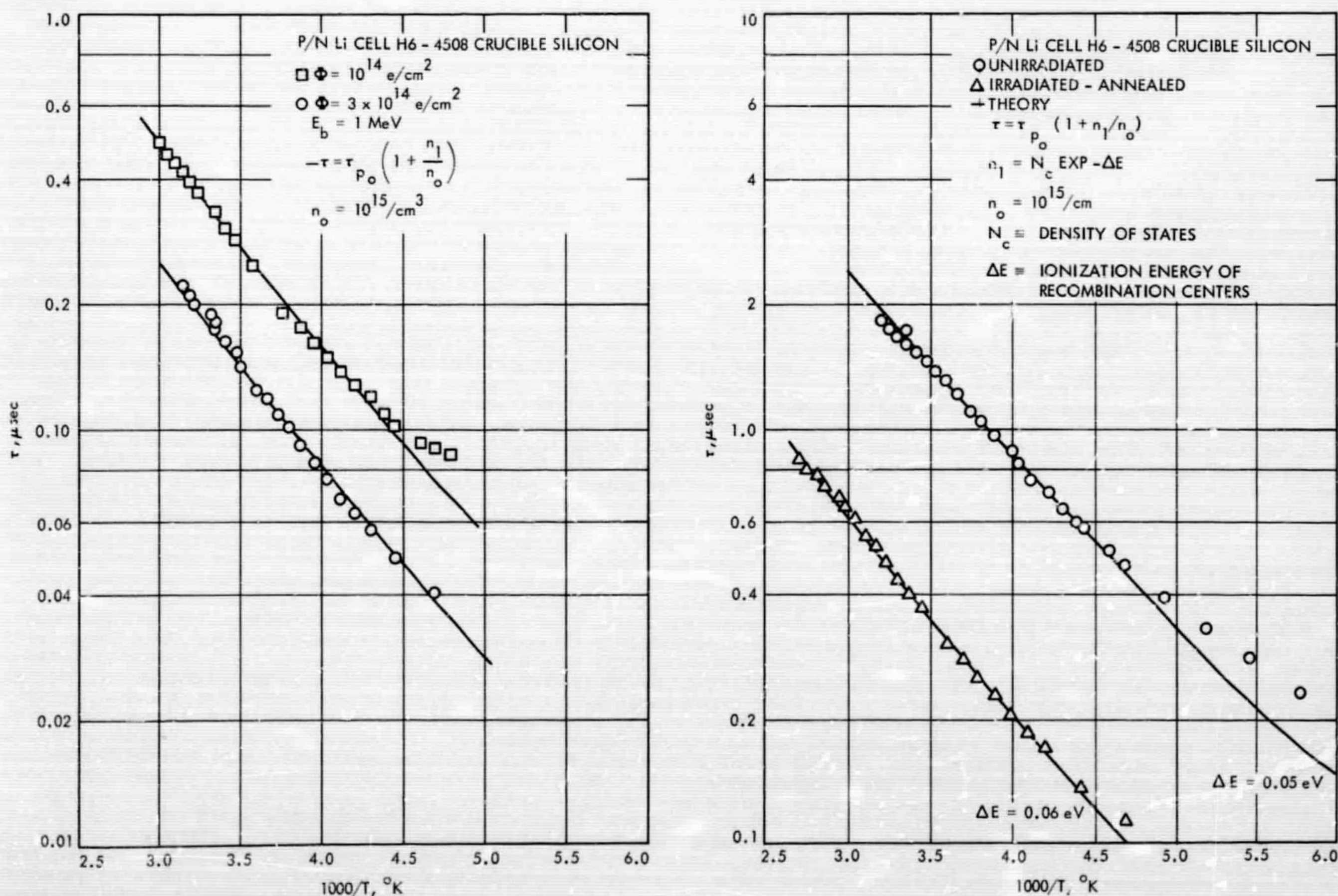

Fig. 8. Minority-carrier lifetime vs temperature relationships for lithium-doped crucible-silicon solar cell

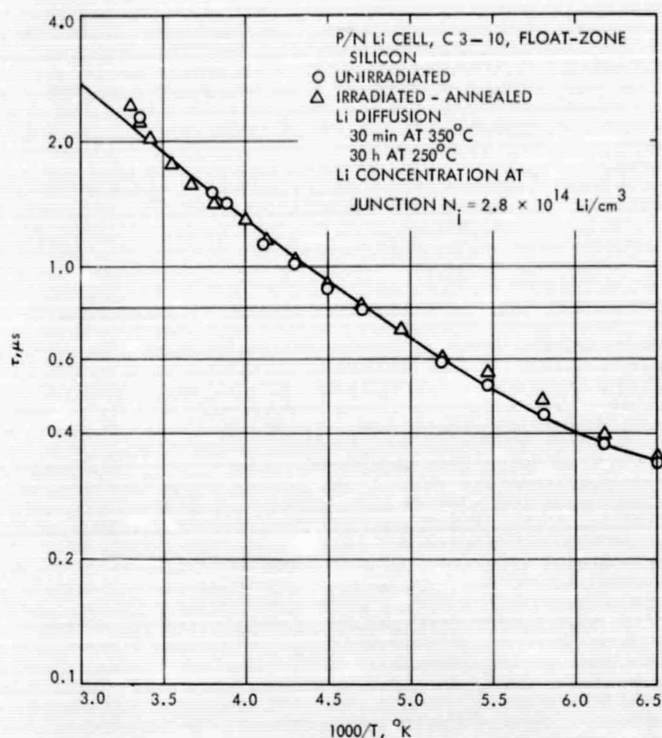

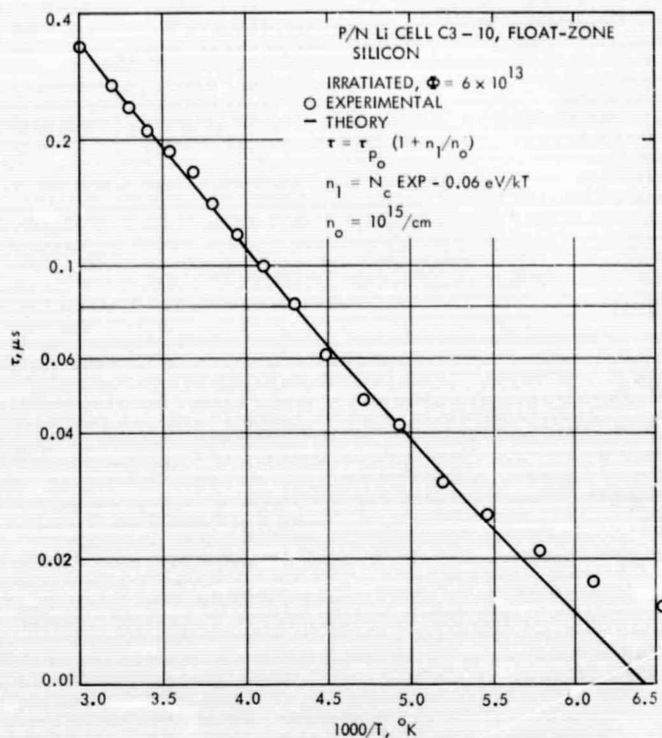

Fig. 9. Minority-carrier lifetime vs temperature relationships for lithium-doped float-zone solar cell

presented that the assumption of single-level recombination theory with the recombination site lying in the top half of the band is inadequate for the determination of the recombination center activation energy. Additional data from Hall mobility measurements also indicate that lithium is involved in the formation of majority carrier removal sites. Although the defect responsible for majority-carrier removal need not necessarily be the same defect site responsible for minority-carrier recombination, the fact that both sites appear to involve lithium in their initial formation is interesting.

IV. Conclusions

Although the program is not yet complete and a large amount of data remains to be analyzed, several tentative conclusions can be drawn at this time. It appears, in general, that crucible-grown lithium-doped cells have higher initial efficiencies, slower recovery times, and better long-term stability than float zone lithium doped cells at room temperature. It also appears that elevation of crucible-grown lithium-doped cells to temperatures in the 60–80°C range results in annealing times identical to those observed in float-zone lithium-doped cells at room temperature.

The limitation on maximum recovered level does not appear to depend on edge effects as shown by the almost identical responses of the T3 and T5 groups of cells. Cells fabricated by Texas Instruments generally tend to have initial outputs and maximum recovered levels that are equal to or better than cells fabricated by other manufacturers. It is not known, at this time, whether this relative superiority is due to the use of an evaporated lithium source, a different boron diffusion technique, or some other manufacturing process or starting material difference peculiar to Texas Instruments cells. The longer time lower temperature diffusions utilized in the more recent group of cells indicate a tendency toward higher recovered levels; however, this is only a tentative conclusion based on preliminary data and a statistically small group of cells.

Finally, it appears that the initial defects formed in lithium-doped silicon are complex and involve lithium atoms in their formation.

N70-12108

Electrical Studies of Electron-Irradiated Lithium-Containing Silicon and Silicon-Solar Cells

G. J. Brucker
Astro-Electronics Division
Radio Corporation of America
Hightstown, New Jersey

I. Introduction

The contract effort reported here represents an experimental investigation of the physical properties of lithium-containing silicon and P/N silicon solar cells, and of the processes that occur in these bulk samples and devices. The objectives are to identify the parameters affecting cell radiation recovery and long-term stability characteristics, and to generate information leading to the optimization of these parameters. The bulk silicon studies provide the basic information required to understand the physical interactions of lithium with radiation-induced defects. The eventual goal is to exploit this phenomenon of interaction for adaptation to the production of solar cells for the space environment. In this direction, it is anticipated that (1) realistic predictions of lithium cell performance can ultimately be developed, and (2) optimum designs of lithium cells for space use can then be specified.

The discussion will deal with the more important results obtained on solar cells, the results of the electrical studies on bulk silicon, and finally, the status of our research in lithium-containing silicon and its implication on solar cell development.

II. Solar Cells

The information on the characteristics of lithium-diffused P/N solar cells irradiated by electrons has been obtained from studies of cells furnished by JPL during the present contract and in the past by NASA. These studies have been concerned with the properties of the initial radiation damage and of the post-irradiation recovery. Both the short-term and long-term stability of the post-irradiated solar cell are important characteristics of the cells and considerable efforts have been concentrated on this subject.

One of our investigations of stability involves a large group of cells that were irradiated more than two years ago and since that time, their characteristics have been studied. Evidence of redegradation of short-circuit current and power loss due to increased series and shunt resistance were observed. The general conclusion of that study was that cells irradiated to a fluence of 10^{16} e/cm^2 did not redegrade after recovery unless the initial concentration of lithium near the junction (N_{Li}) was greater than 5×10^{15} cm^{-3}. It has become apparent that there exist several types of instability or redegradation. Evidence for

a mechanism of life-time or short-circuit current redegradation to occur will be presented in the discussion of results obtained on bulk silicon. In contrast to this type of instability, a serious loss of open-circuit voltage has been observed in cells following their recovery from irradiation.

Figure 1 illustrates this effect with the photovoltaic characteristics for cell TI-978 taken at three different times: before bombardment, at the time of maximum power after recovery, and as of the latest reading, 331 days after bombardment. The shape of the curve taken 331 days after bombardment indicates a severe redegradation due to a $\approx$15% drop in filling factor in addition to the redegradation caused by the $\approx$20% drop in open-circuit voltage. By comparison, the decrease in short-circuit current is only 6%; that is, within experimental uncertainty. Figure 1 clearly demonstrates that the stability of short-circuit current is not a sufficient criterion for lithium cell stability. A sufficient stability criterion is obtained only through examination of the entire photovoltaic response characteristic.

This same type of effect has also been observed in unirradiated cells, as shown in Fig. 2. Cell TI-979 showed significant degradation between 4 and 8 mo after the first measurement and as of the latest measurement was $\approx$35% below the initial value obtained in November 1967. This 35% is the same as the amount of redegradation suffered by a similar TI cell (978) shown in Fig. 1. In fact, as Fig. 2 shows, the changes in I-V characteristic in TI-979 are approximately the same as were the changes in I-V characteristic in TI-978 (Fig. 1). Figure 2 gives photovoltaic characteristics for TI-979 as of November 1967 and October 1968. A decrease in open-circuit voltage from 0.570 to 0.510 V has occurred in addition to a severe drop in filling factor, as seen from Fig. 2, $f = 0.64$ in November 1967 to $f = 0.48$ in October 1968. During the same time period, the short-circuit current has remained constant within experimental uncertainty.

The degradation in power of these two cells, and the stability (within experimental uncertainty) in the short-circuit current in the same cell, again points out the insufficiency of the latter as the stability criterion in lithium-doped cells.

Despite these results, many solar cells do not exhibit redegradation of any type for long periods of time, as shown in Fig. 3. This figure shows a typical set of photovoltaic characteristics for one of the cells, He-810, taken: before bombardment, 35 days after bombardment, and 206 days after bombardment. The characteristics of He-810 cell are representative of six of the seven cells of this group. No sensible redegradation was evident in these six cells.

The question also arises as to why the Heliotek cells, those irradiated to 10^{14} e/cm^2 and those left unirradiated, have not (in most cases) redegraded (or degraded). A

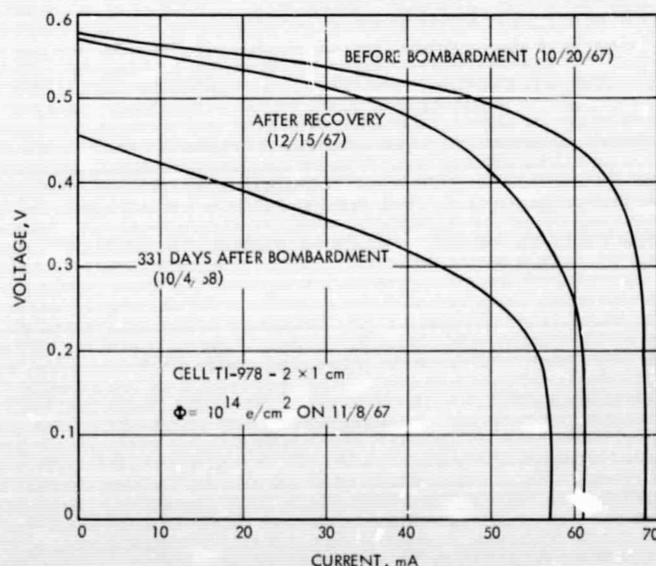

Fig. 1. Comparison of photovoltaic characteristics of Lopex cell TI-978

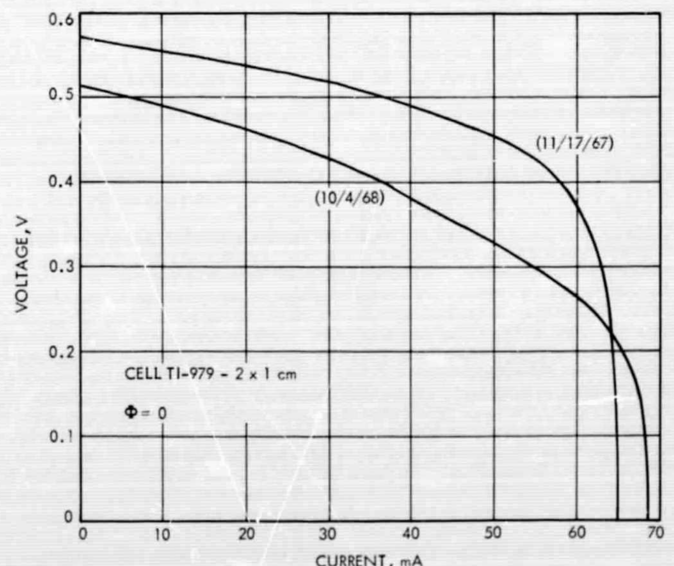

Fig. 2. Comparison of photovoltaic characteristics of unirradiated Lopex cell TI-979

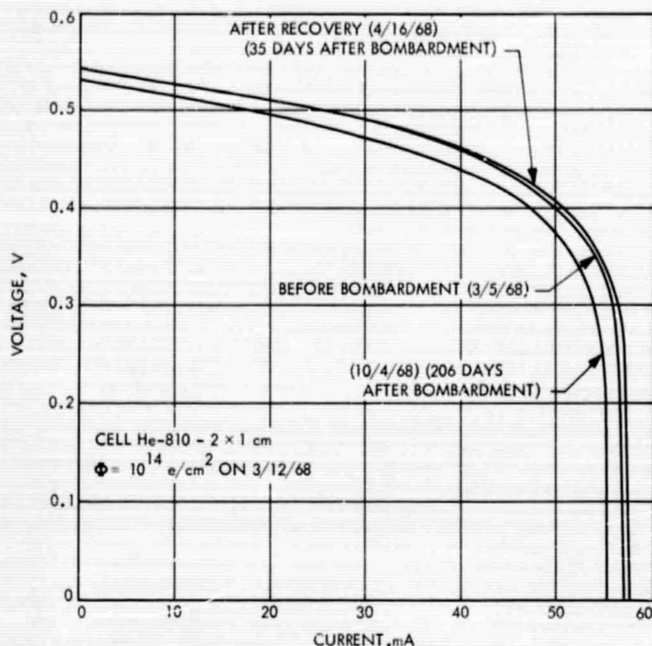

Fig. 3. Comparison of photovoltaic characteristics of float-zone cell He-810

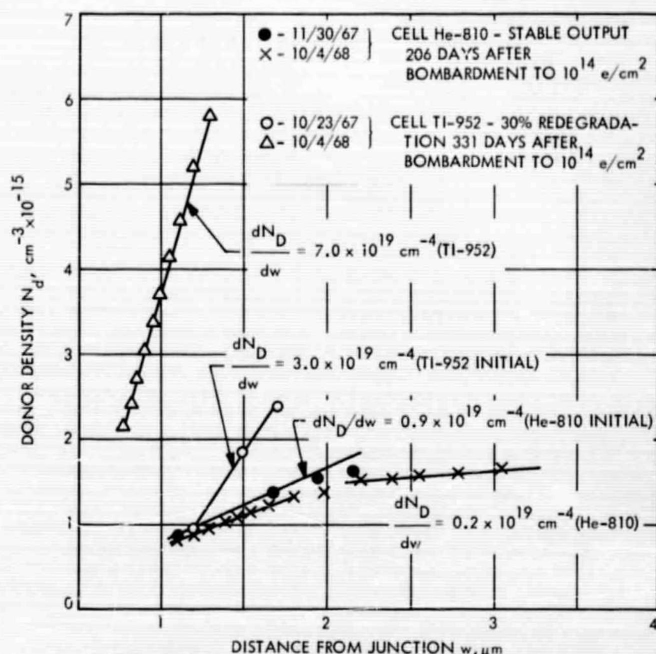

Fig. 4. Comparison of donor density profile histories of cells He-810 and TI-952

possible explanation for this is contained in Fig. 4, which gives density profiles for two cells on two dates approximately 11 mo apart. Both of the cells were fabricated from 20 Ω-cm float-zone silicon and both were irradiated to 10^{14} e/cm^2. One of the cells, TI-952, started to redegrade ~100 days after bombardment and had redegraded ≈30% in power 331 days after bombardment. The other, He-810, had shown no sensible redegradation 206 days after bombardment.

The initial densities of the two cells at zero bias (as measured on 10/23/67 and 11/30/67, respectively) were equal within the ≈±5% experimental uncertainty of the measurement; the initial density for TI-952 was 9.5×10^{14} cm^{-3} and that for He-810 was 9.0×10^{14} cm^{-3}. However, this is where the similarity ends. The slope dN_D/dw of the initial TI-952 profile was 3.0×10^{19} cm^{-4}, more than three times the 0.9×10^{19} cm^{-4} of He-810. The density profiles, taken approximately 11 mo later on October 11, 1968, showed an even more striking contrast. The TI-952 cell displayed a large increase in density near the junction as had the other TI cells. On the other hand, He-810 had a density profile similar to the initial profile. In addition, whereas the density gradient in TI-952 was 7.0×10^{19} cm^{-4} giving a density of 5.8×10^{15} cm^{-3} at a distance of 1.3 μm from the junction, the density gradient in He-890 decreased at ≈2 μm to 0.2×10^{19} cm^{-4}, a factor of 70 below that of TI-952.

Thus, although the initial densities of the two cells at the edge of the depletion region were approximately equal, their density profiles and the subsequent behavior of these density profiles were enormously different. The behavior of He-810 was typical of all the Heliotek cells. It is, therefore, inferred that the lithium motion in the junction region in the Heliotek cells is much less than that in the TI cells, and that this reduced motion is responsible for the better stability of the Heliotek cells.

The more recent batches of cells received from JPL demonstrate that high-performance cells can be made from quartz-crucible silicon. Figure 5 shows the normalized performance parameter and maximum power versus time after bombardment of six quartz-crucible cells irradiated to a fluence of 1×10^{14} e/cm^2. The initial and post-bombardment values of power for standard N/P cells of comparable power irradiated at the same time are shown in Fig. 5.

This group of cells recovered surprisingly rapidly—within ≈10 days as indicated by spot checks on individual cells (not indicated in Fig. 5). The recovery was particularly rapid considering the low lithium density in the T2 cells, and it is suspected that the oxygen density in these cells is considerably below that normally encountered in quartz-crucible cells. The cells have maintained substantially stable performance between the 45th

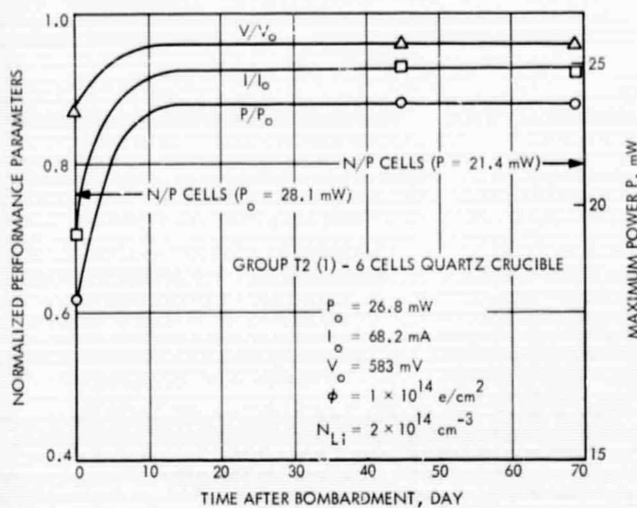

Fig. 5. Cell performance vs time after irradiation

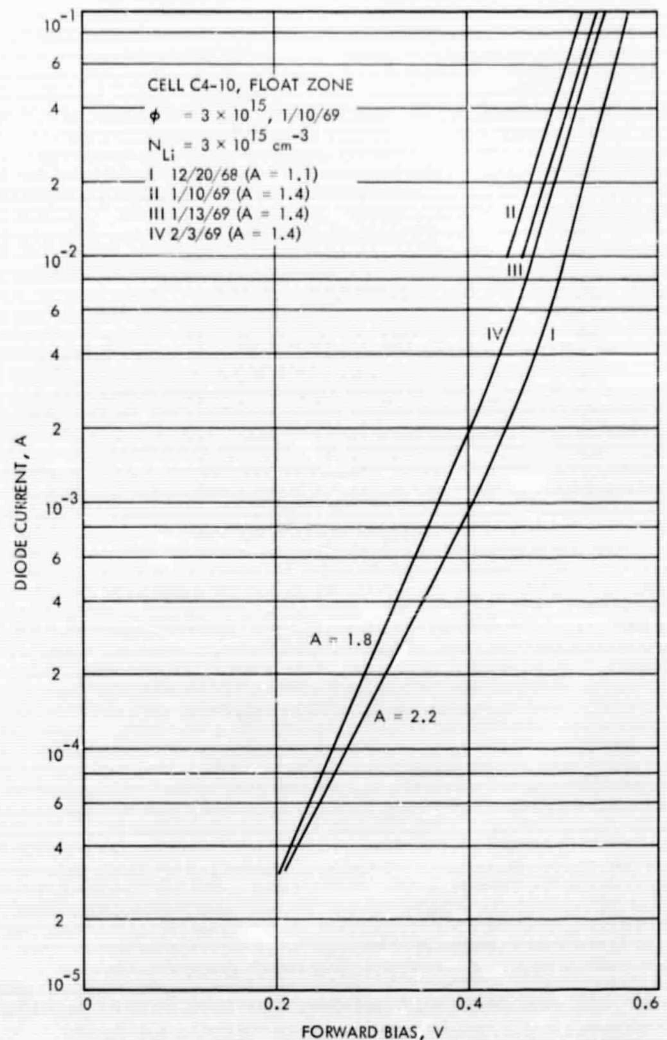

Fig. 6. Forward diode characteristic of cell C4-10, before bombardment and postrecovery

and 69th day after irradiation. The post-irradiation series resistance is $\approx 1\ \Omega$, the same as the pre-irradiation value. Thus, it appears that stable (at least within the period of these measurements) and high-efficiency cells can be fabricated from quartz-crucible silicon.

It was stated before that the higher density cells tended to be more unstable and redegraded by means of a decrease in short-circuit current. In contrast to this method of redegradation, other cells redegraded by a decrease in open-circuit voltage. A further illustration of a stable and unstable cell is shown in Figs. 6 and 7, in which the diode current characteristics versus forward bias voltage of cells C4-10 and C4-56 are shown.

Curve I of Fig. 6 is the pre-bombarded characteristic and curves II, III, and IV are the immediate post-bombardment and recovery characteristics. The A-factor increased after bombardment and remained constant during recovery. This recovery behavior is the normal one observed in a stable cell.

In contrast to this, Fig. 7 shows the V_{oc} instability that occurs during recovery in cell C4-56. Curve I is the pre-bombarded characteristic, curve II is the immediate post-bombarded characteristic, and curves III and IV are recovery characteristics. This cell exhibits redegradation of V_{oc} and, thus, characteristics in curves III and IV shifted to lower voltages during the post recovery period. However, the short-circuit current of this cell recovered to $\approx 90\%$ of its initial value during this same period of recovery. The lithium density of cell C4-56 is nearly an order of magnitude less than cell C4-10.

Thus, this instability is associated with low densities of lithium. The explanation appears to be the increase of resistivity ρ_n due to lithium losses that take place during recovery. Additional information concerning this effect was obtained in the measurements on bulk silicon and will be presented later in the discussion.

III. Bulk Silicon

Bombardment of silicon crystals by high-energy particles introduces intrinsic defects in the crystals. These defects consist of interstitial–vacancy pairs, which are mobile at temperatures as low as 4°K for the interstitial and 75°K for the vacancy. Electrical properties of electron-irradiated silicon at moderate electron energies ($E = 1$ to 2 MeV) are dominated by the secondary defects

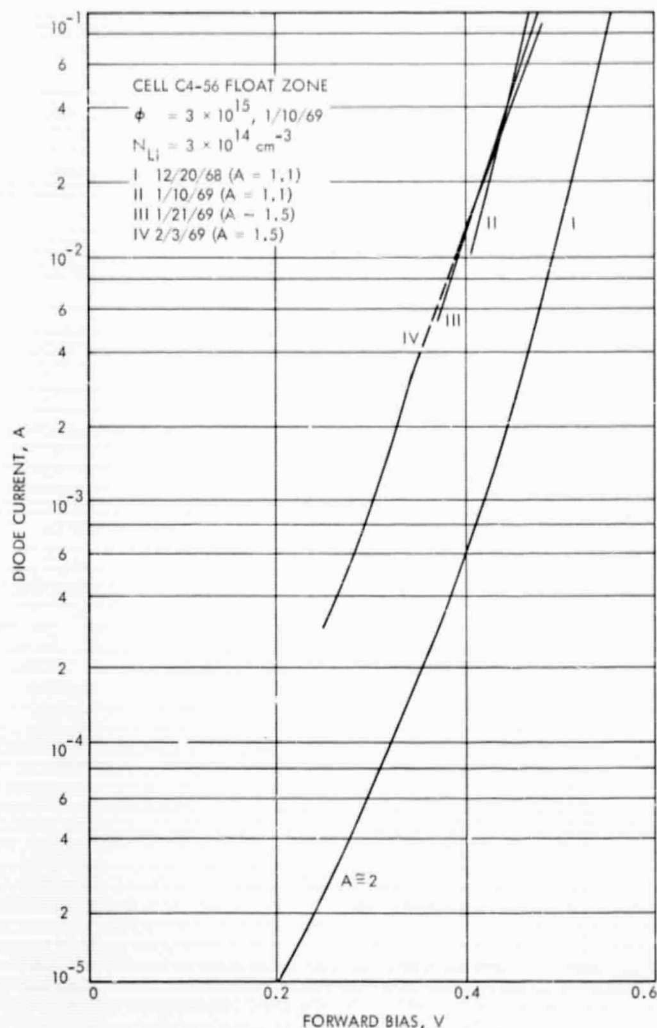

Fig. 7. Forward diode characteristic of cell C4-56, before bombardment and postrecovery

formed by the interaction of primary defects with impurities in the crystal.

In general, impurities are immobile at or below room temperature, but lithium is an impurity that is highly mobile at room temperature. This mobility makes it possible for lithium to diffuse to radiation-induced defect sites. However, at a temperature of about 250°K, lithium is virtually "frozen" in the silicon lattice, and the diffusion constant of lithium is reduced to about 1/50 the room temperature value. Thus, by irradiating samples at temperatures for which lithium is immobile and then raising the temperature, it is possible to investigate the processes by which lithium interacts with the primary and secondary defects, and to measure the introduction rates of carrier-removal defects without the interference of the mobile lithium ion.

The Hall-effect and resistivity measurements were obtained by direct current-voltage techniques on Hall bars of ≈0.3-Ω-cm lithium-doped N-type quartz-crucible grown and float-zone refined silicon. The resistivity of the starting material before diffusion with lithium was 30-Ω-cm phosphorus-doped quartz-crucible, and ≥1500-Ω-cm float-zone silicon. Samples were sequentially bombarded from the lowest to the highest bombardment temperature in any series of irradiations.

A. Carrier-Removal Rates

In these experiments, measurements of carrier losses as a function of electron fluence at any bombardment temperature are used to compute a carrier-removal rate $-\Delta n/\Delta\Phi$ in cm, and the results for both crucible-grown and float-zone silicon are shown in Fig. 8. These removal rates are those rates that remain after the irradiated samples were annealed to 200°K (measurements at 79° to 81°K). Therefore, these rates represent carrier-removal rates of defects that are independent of temperature and that have been called ITD defects in previous studies.

The additional defect, which only occurs in oxygen-containing silicon at a bombardment temperature of $T_B = 250$°K, produced a peak in the $-\Delta n/\Delta\Phi$ curve for crucible silicon. This defect has been attributed to an oxygen complex since it does not occur in oxygen-lean float-zone-refined silicon as indicated in Fig. 8. The curve of $-\Delta n/\Delta\Phi$ for zone silicon decreases with decreasing temperature at a faster rate than the curve for crucible silicon. The slopes of these carrier-removal curves were determined to be 0.09 eV and 0.055 eV for the zone and crucible-silicon curves, respectively. Apparently the defect-production mechanisms are different in these two types of silicon. Thus, this result suggests that different defects are produced in oxygen-containing silicon compared to oxygen-lean silicon.

Carrier-removal rates obtained on crucible and zone silicon doped with phosphorus to 5×10^{14} cm^{-3} are also shown in Fig. 8 for comparison. The temperature dependence of $\Delta n/\Delta\Phi$ shifted to higher temperatures relative to the results obtained on the phosphorus-doped samples of higher resistivity. This dependence on resistivity was predicted by the charge-state-dependent theory.

The higher damage rates of the phosphorus-doped samples for both types of silicon are due to the higher energy electrons ($E = 1.7$ MeV) used to obtain these data, and also to the higher phosphorus-doping density,

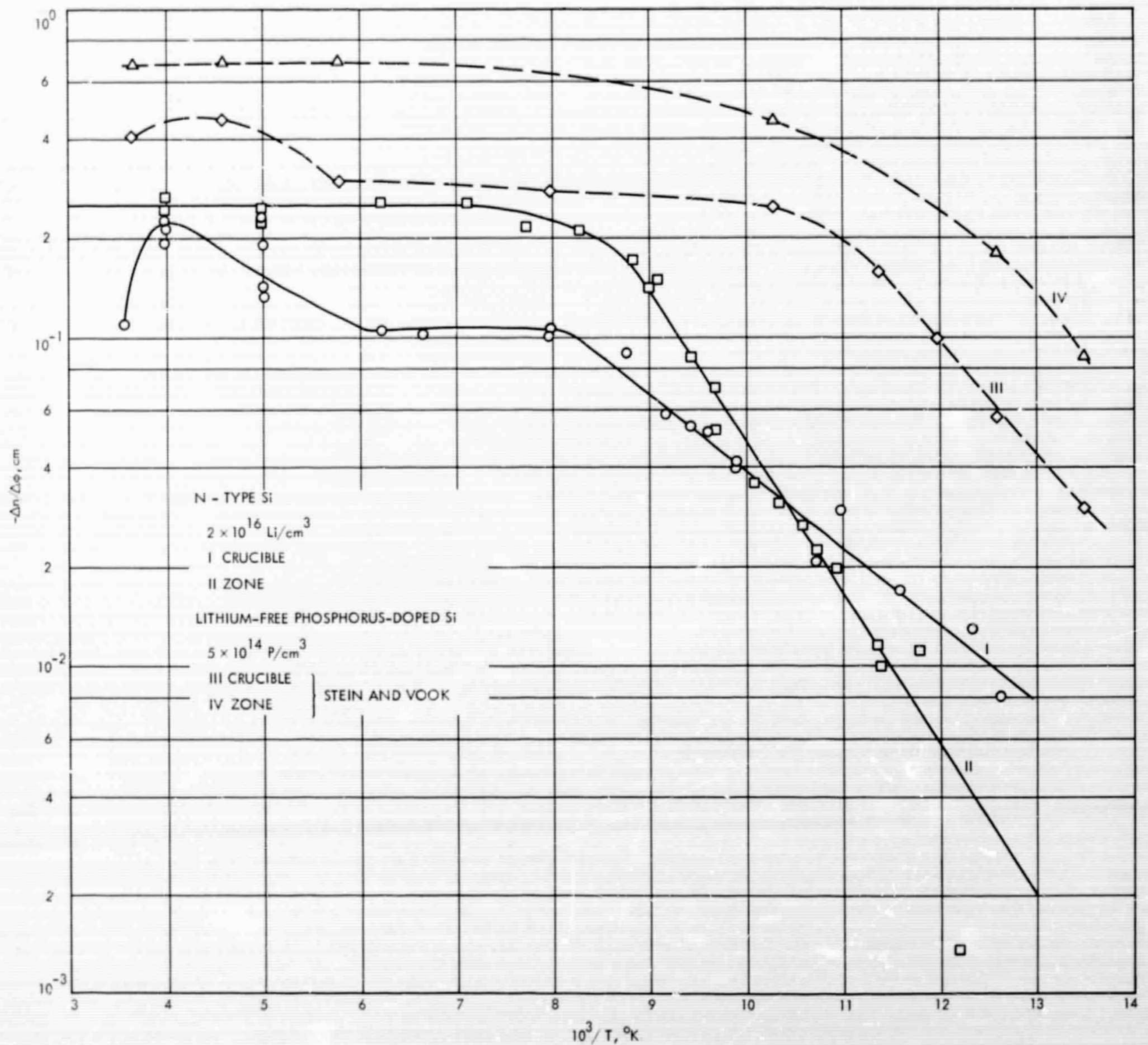

Fig. 8. Carrier-removal rates vs reciprocal bombardment temperature for float-zone and quartz-crucible silicon

which causes greater E-center production. It should be noted that the high temperature carrier-removal rate of zone silicon is greater than that of crucible silicon by a factor of ≈ 2.5.

A defect complex such as the LiO-V defect is an acceptor that removes two carriers from the conduction band. In a similar way, Li-V defect will remove two carriers in oxygen-lean silicon. In contrast to this effect, the A-center (OV) removes only a single carrier. Thus, either the production rate of Li-V defects is higher than the LiO-V defect or more A-centers than LiO-V defects are produced in crucible silicon under the conditions of this experiment.

Following the completion of irradiations at all bombardment temperatures, the sample temperature was allowed to increase to room temperature, and the interaction of lithium with radiation-induced defects was determined from measurements of the Hall-effect and resistivity on samples that had annealed at this temperature of 297°K.

B. Carrier Density Changes of Quartz-Crucible Lithium-Doped Silicon

Curves of carrier density n versus reciprocal temperature measured at different times before and after bombardment are shown in Fig. 9. (The carrier-removal rates that one would calculate from Fig. 9 will not correspond

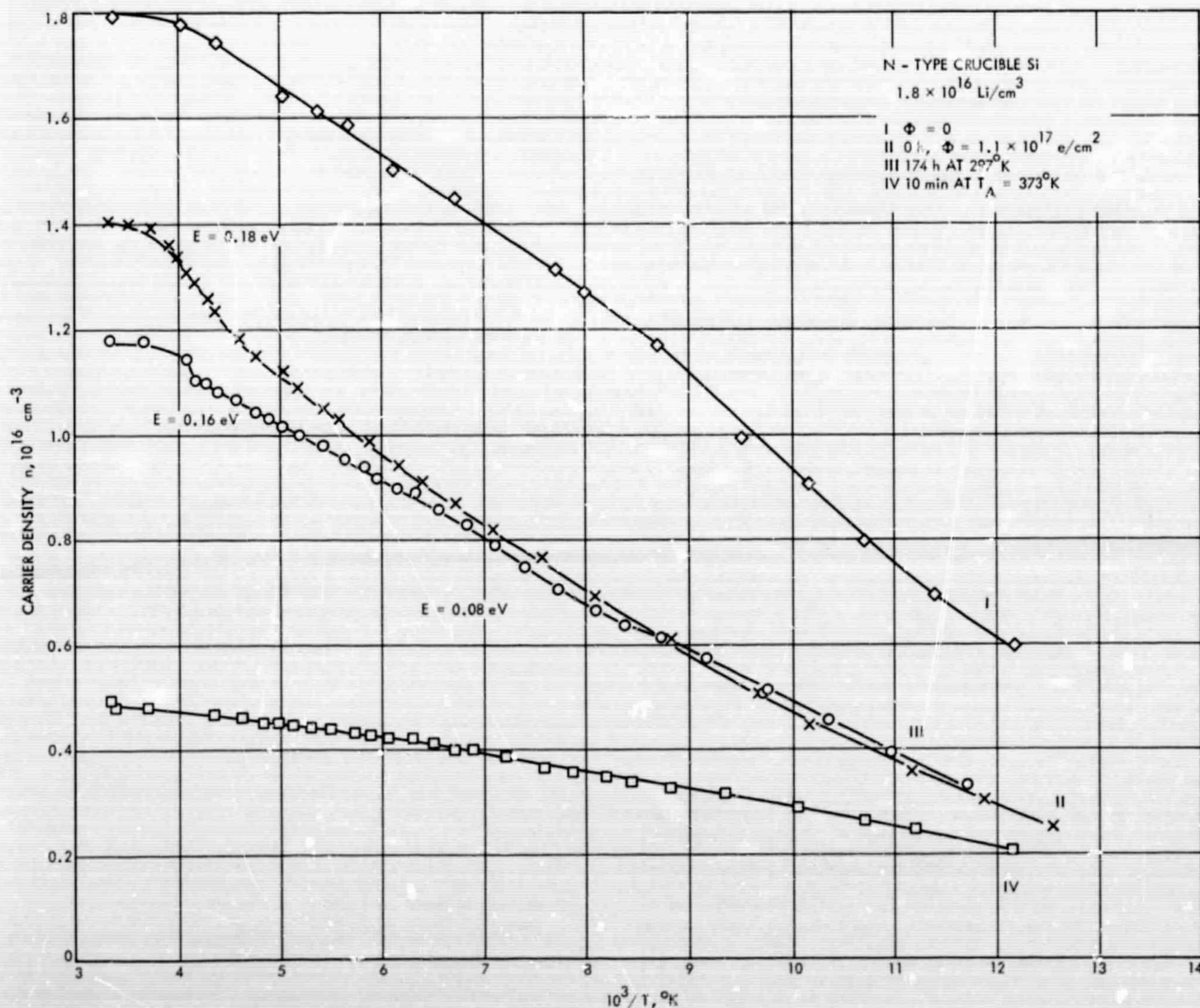

Fig. 9. Carrier density vs reciprocal temperature for crucible-grown silicon

to any unique data point in Fig. 8.) The pre-irradiation measurements of carrier densities versus temperature are shown in curve I of Fig. 9. A decrease in temperature shifted the Fermi-level towards the conduction band, and consequently the percentage of ionized donor levels decreased. Thus, the carrier density varied in accordance with the dependence of Fermi statistics on temperature.

Curve II of Fig. 9 is the temperature dependence of carrier density measured immediately after the completion of all bombardments. A defect-energy level located near 0.18 eV is identified as the A-center. The defect density is about 1×10^{15} cm^{-3} with a temperature $T = 220°K$ at half-filling of the defect level. This A-center concentration is about 1/3 of the total carrier-removal defects calculated from carrier-removal rates and fluences at each bombardment temperature. Since the A-center removes one electron and the LiO-V defect removes two electrons, A-center production appears to be about equal to the LiO-V defect production in the samples of this experiment.

Curve III of Fig. 9 is the temperature dependence of carrier density obtained on the sample after it annealed for 174 h at 297°K following the completion of bombardment. Both a decrease of carrier density at high temperature and a slight increase of carrier density at low temperature occurred during this annealing period. The decrease of carrier density at room temperature can be attributed either to the formation of additional deep-lying acceptor levels, and/or to a loss of lithium due to the complexing of lithium with A-centers or LiO-V centers. This latter possibility of a lithium loss to explain the decrease of carrier density at high temperature is strongly supported by the increase of the Hall mobility at low temperature.

In addition to these changes in carrier density, the defect center previously located near 0.18 eV shifted to 0.16 eV below the conduction band. The formation of a new level located near $E_c - 0.08\,\text{eV}$ is indicated by curve III.

Curve IV of Fig. 9 was obtained after annealing for 10 min at a temperature of 373°K. The purpose of this technique was to speed up the interaction of lithium with radiation-induced defects. This final curve showed that all defect levels have disappeared, and the carrier density had decreased extensively at all temperatures. Thus, the interaction time of lithium with defects was accelerated considerably by the high-temperature annealing. All defects appeared to be neutralized at an annealing temperature and for a duration that is insufficient to anneal normal defect centers (e.g., A, E, C, etc.).

C. Mobility Changes of Quartz-Crucible Lithium-Doped Silicon

The Hall-mobility data gives strong support to the suggested annealing mechanism of lithium complexing with defects and neutralizing their electrical effects. Figure 10 shows the Hall-mobility versus reciprocal temperature measured on the same sample and under the same conditions as in Fig. 9.

Curve II of Fig. 10 is the mobility measured immediately after bombardment. Curves III and IV show that the mobility is progressively recovering from the state of damage after 34 and 174 h at 297°K following bombardment. Clearly, charged-scattering centers are being neutralized, since the mobility varies inversely with the number of charged centers. Curve V is the mobility measured on the sample after it was annealed for 10 min at a temperature of 373°K.

These measurements showed that the mobility recovered to approximately the pre-irradiation values. Therefore, the scattering conditions in the sample, after this annealing process, were equivalent to the initial conditions before bombardment.

D. Carrier Density Changes of Float-Zone Lithium-Doped Silicon

In order to study the effect of oxygen on the results, samples fabricated from float-zone refined silicon were irradiated and measured. The low oxygen content ($\leqq 10^{14}$ cm^{-3}) and high resistivity ($\geqq 1500$ Ω-cm) of the starting silicon prevented a significant number of impurity-defect complexes from forming, except for lithium-defect complexes.

Initially, the float-zone samples were bombarded at several temperatures to determine the carrier-removal rates as a function of temperature. Immediately after completion of these bombardments, carrier densities were measured as a function of temperature, and then the samples were allowed to anneal at room temperature. Figure 11 shows the carrier density versus reciprocal temperature measured before bombardment, immediately following bombardment, and after 17 h at room temperature following bombardment. Irradiated float-zone silicon exhibited an increase of carrier density at all temperatures upon annealing, instead of a spontaneous de-

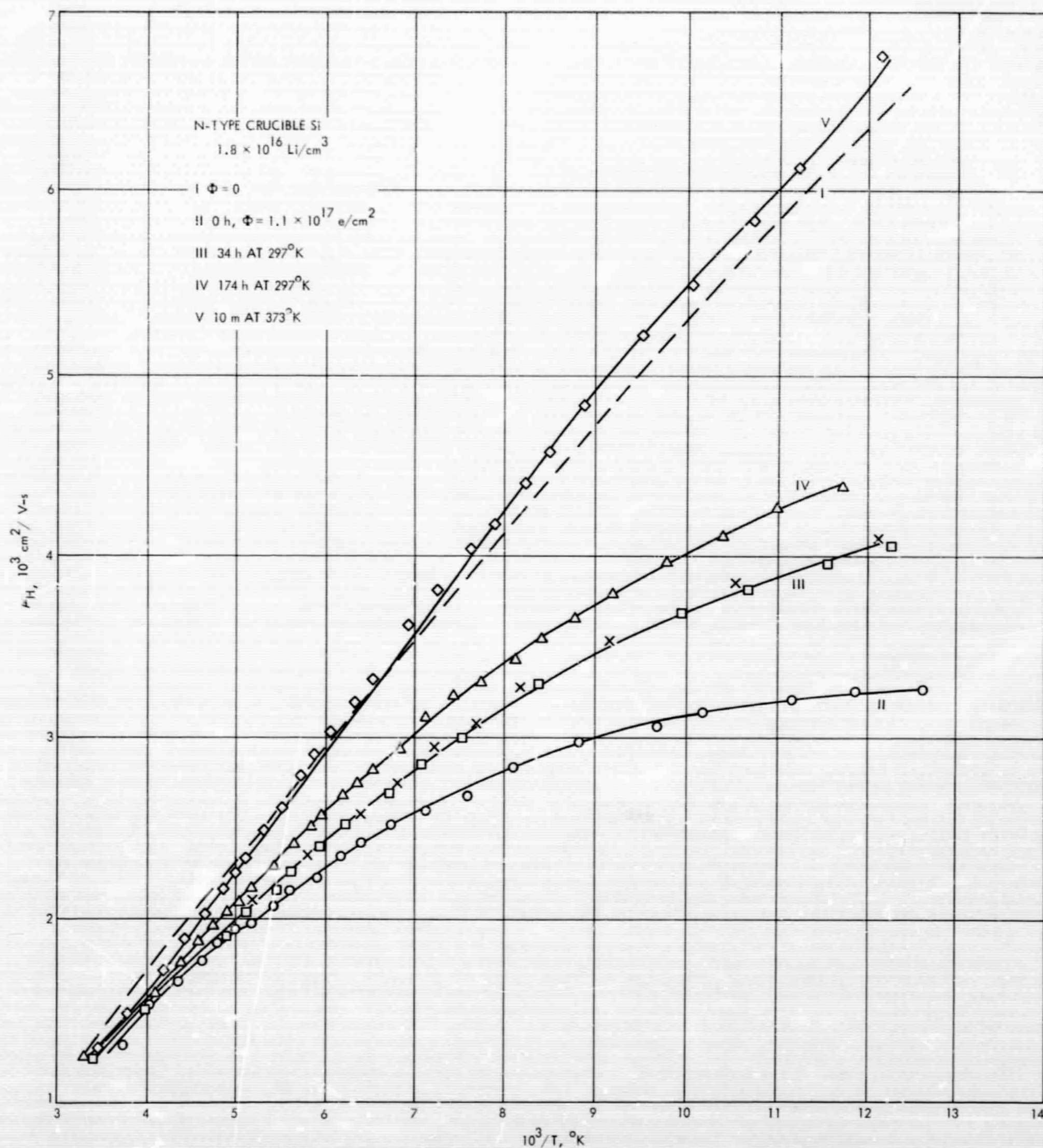

Fig. 10. Hall mobility vs reciprocal temperature for crucible-grown silicon

crease of carrier density, occurring in crucible silicon after annealing at room temperature.

Both mechanisms of dissociation of carrier-removal defects, and neutralization of these defects by lithium takes place in irradiated float-zone silicon soon after bombardment. The fast reaction at room temperature observed in these samples of float-zone silicon is due to the lack of oxygen, which combines with lithium and decreases the free-lithium diffusion constant in crucible silicon.

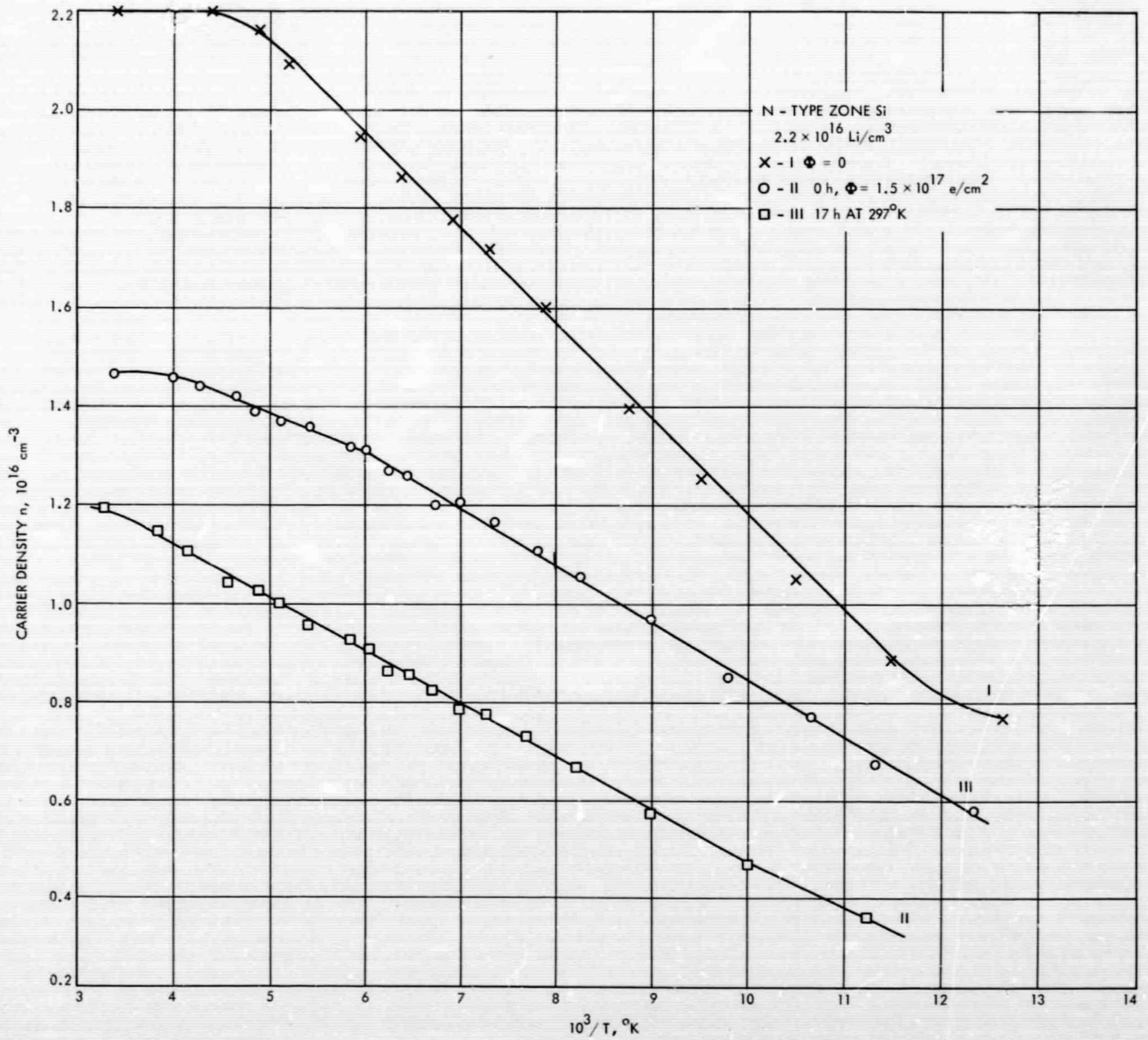

Fig. 11. Carrier density vs reciprocal temperature for float-zone silicon

E. Mobility Changes of Float-Zone Lithium-Doped Silicon

The decrease of the mobility is consistent with the introduction of charged-scattering defects in samples bombarded by electrons. Figure 12 shows the mobility dependence on temperature for the same sample and conditions described in Fig. 11. After the 17-h annealing period, the mobility recovered to slightly better than the initial values. This speed of recovery is to be contrasted with the speed of mobility-recovery in crucible silicon, as shown in Fig. 10. Measurements on a crucible-silicon sample, annealed at 297°K for 40 days after bombardment, showed that the mobility had not fully recovered. Thus, without the necessity of annealing to a temperature of 100°C, irradiated-zone silicon exhibits neutralization and dissociation of all charged scattering centers in ≤17 h at room temperature after completion of bombardment.

Recovery of mobility is dominated by the complexing mechanism of annealing if the assumption is made that only one lithium donor is required to neutralize a lithium-defect complex. Thus, there is no effective change in carrier density, but there is a decrease in the number of

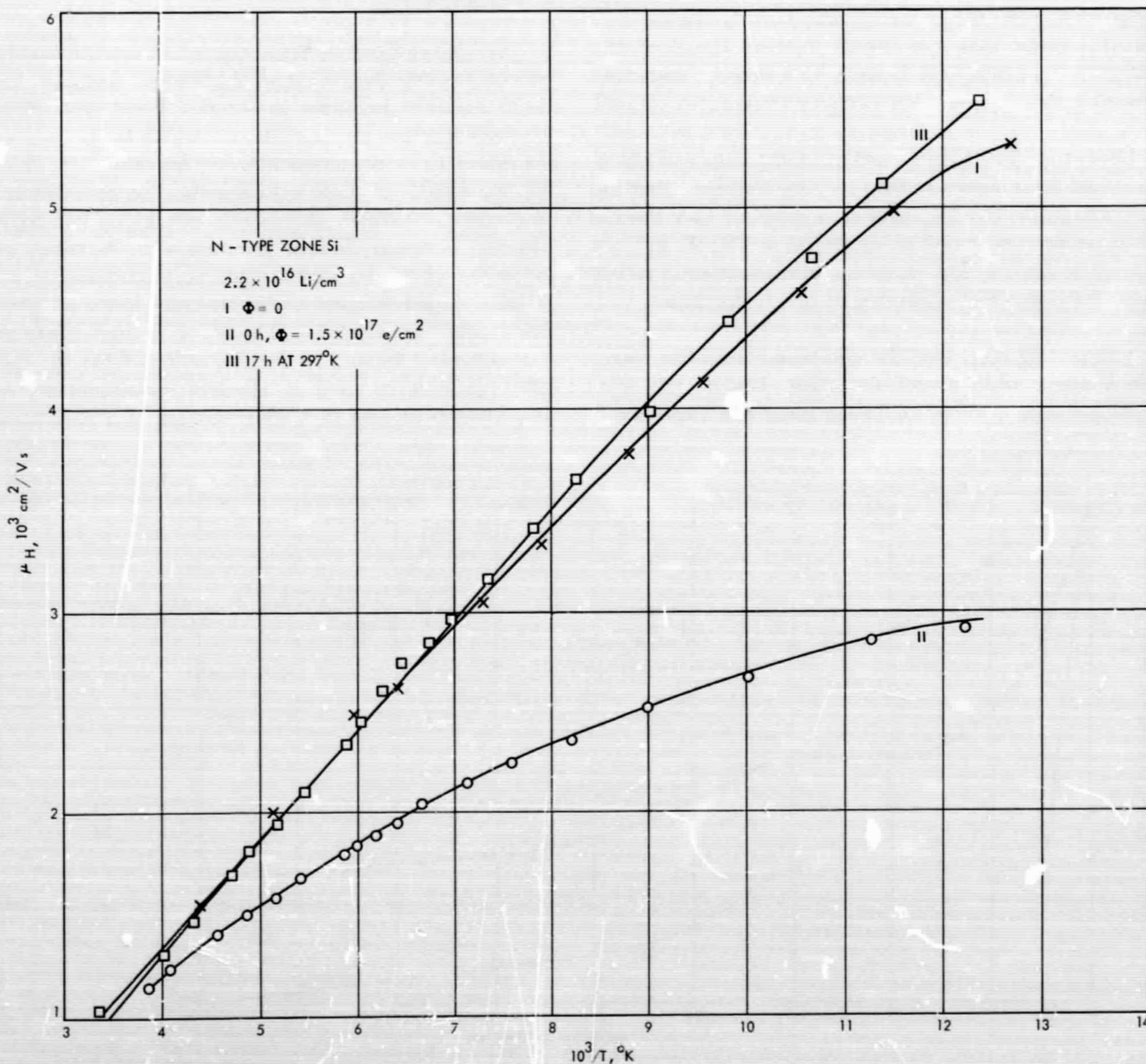

Fig. 12. Hall mobility vs reciprocal temperature for float-zone silicon

charge-scattering centers. In contrast to this effect, the increase of carrier density is dominated by the mechanism of dissociation. Therefore, a detailed measurement of recovery kinetics would indicate the existence of the two processes.

Accordingly, a sample of zone silicon was irradiated to a fluence of 2×10^{15} e/cm^2 at a bombardment temperature of 250°K, and then isothermally annealed at a temperature of 297°K. Measurements of mobility and carrier density were made at temperatures of 83 and 297°K. The results are shown in Fig. 13 in which the unannealed fraction of reciprocal mobility f_μ and of carrier density f_n are plotted versus the annealing time. Clearly, the mobility recovers faster than the carrier density. However, the recovery from radiation damage by a defect-complexing process and by a defect-dissociation process act in parallel.

The carrier density measured at a temperature of 297°K increased, as is shown in Fig. 13. This indicated that the free-lithium density increased as a result of Li-V defects dissociating. The mobility measured at 297°K did not change, since it is dominated by lattice scattering rather than charged-defect scattering at this temperature.

A surprising result was the additional annealing stage, which commenced at an annealing time of 120 min. Measurements made at annealing times of 63 and 255 h indicated that this second annealing stage was unstable, since the mobility and carrier density returned to the recovery levels achieved after the first stage of recovery.

The float-zone silicon samples used in obtaining carrier-removal rates were remeasured 79 days after bombardment to check the long-term stability of the annealed samples. They did not show any significant change from the recovered-carrier density and values of mobility indicated in Figs. 11 and 12.

F. Carrier Density Changes of High-Resistivity Crucible Silicon

The high concentration of oxygen (10^{18} cm^{-3}) in crucible silicon prevents the formation of lithium-defect complexes in measurable quantities in samples doped with lithium to concentrations of $\approx 2 \times 10^{15}$ cm^{-3}. This has been shown in recent EPR measurements, and has also been shown by the results of these experiments. The production of A-centers dominates in crucible silicon of low-doping density. However, lithium interacts with A-centers and other defect centers that are normally produced in non-lithium doped samples of quartz-crucible-grown silicon bombarded by electrons. Therefore, to investigate this interaction, a sample of crucible silicon from the same 30-Ω-cm material used in all these measurements was doped with lithium to a concentration of 2×10^{15} cm^{-3},

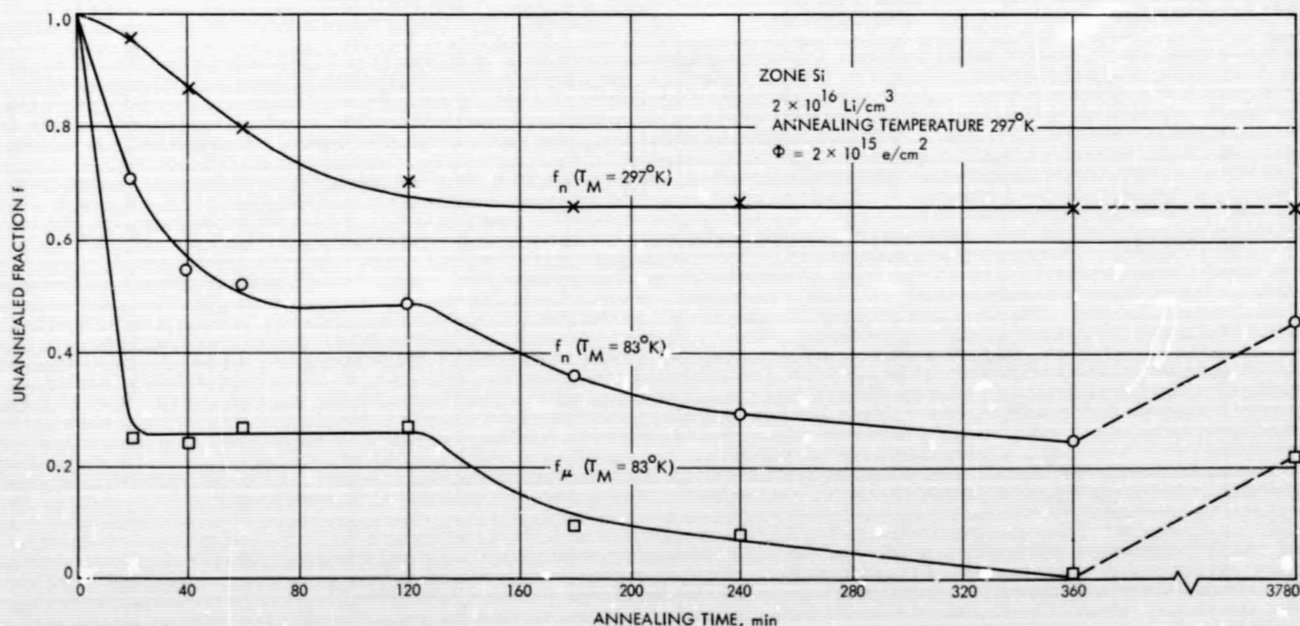

Fig. 13. Unannealed fraction of carrier density f_n and unannealed fraction of reciprocal mobility f_μ versus annealing time

and irradiated with electrons at bombardment temperatures of 79 and 250°K.

Carrier density measured immediately after each irradiation and then measured as a function of time after the last irradiation with the sample annealing at room temperature is shown in Fig. 14. The two most interesting results in the data of Fig. 14 are the interaction of lithium with the radiation-induced defects as demonstrated by the temporal behavior of n during the annealing process at room temperature, and the location of defect-energy levels in the carrier density versus temperature curves. The temperature at which the half-filling of the defect level occurs is indicated in Fig. 14.

It can be seen that two energy levels are indicated in Fig. 14 by curve II, which is the data taken after completion of the annealing cycle (from bombardment temperature of 79 to 250°K) following the irradiation at a temperature of $T_B = 79°K$. These levels were determined to be 0.18 and 0.13 eV below the conduction band.

The data of curve III for $T_B = 250°K$ in Fig. 14 indicates an energy level extending over a broad temperature range with an approximate temperature $T_{1/2} = 208°K$ for the half-filling of the level. This locates the level at an energy of 0.16 eV below the conduction band. The determination of the half-filling point is not accurate, since the energy of this defect level appears perturbed or smeared out over a broad energy range. Merging of the levels at 0.18 and 0.13 eV would produce a broad energy level, such as this one.

Examination of curve IV of Fig. 14 measured after 63 h at room temperature following bombardment, shows that the level at 0.17 eV (A-center) is still present, and the

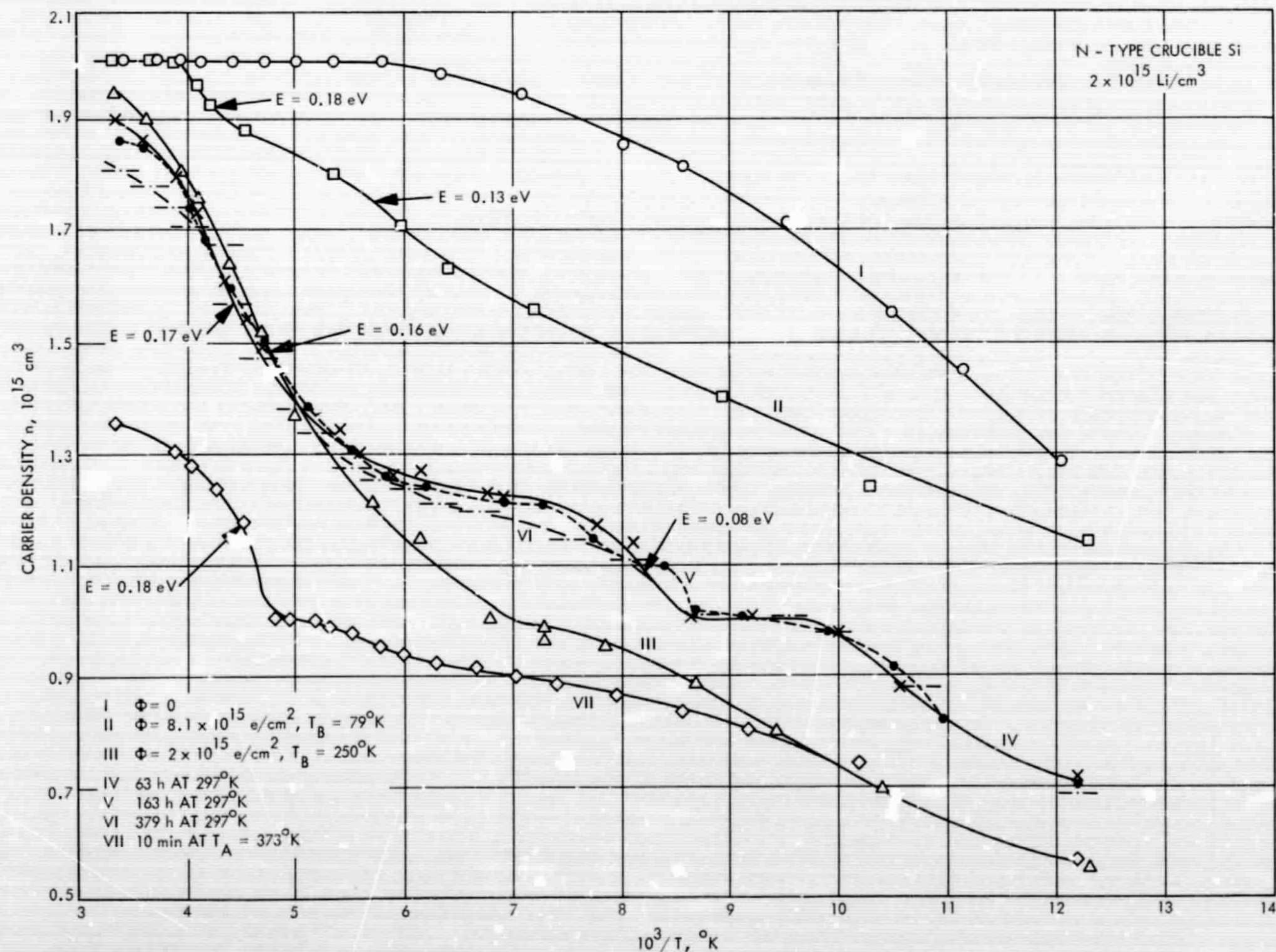

Fig. 14. Carrier-density vs reciprocal temperature for high resistivity (2.5 Ω-cm) crucible-grown silicon

Table 1. Status of research on lithium in silicon

Research area	Material type	Process	Remarks
Damage centers from reaction of Li^+ and LiO^+ with V	Float zone	$Li^+ + V^- + e \rightarrow [Li\text{-}V]^-$	Carrier-removal center
	Quartz crucible	$[LiO]^+ + V^- + e \rightarrow [LiO\text{-}V]^-$	Carrier-removal center
Room-temperature recovery is complexing of Li with damage centers	Float zone	$[Li\text{-}V]^- + Li^+ \rightarrow Li\text{-}V\text{-}Li$	Annealed center
	Quartz crucible	$[LiO\text{-}V]^- + Li^+ \rightarrow LiO\text{-}V\text{-}Li$	Annealed center
If oxygen is not involved in the initial damage center, the center is unstable and dissociates		$[Li\text{-}V]^- \rightarrow Li^+ + V^- + e$	

0.13-eV level has disappeared; however, a new level at 0.085 eV has formed. Curves V and VI are measurements taken at $t = 163$ and 379 h after completion of the irradiation. The 0.085-eV level is still present, but the carrier density progressively decreased at high temperature.

Loss of carrier density at high temperature as a function of annealing time at room temperature is similar to the behavior observed in the measurements on crucible silicon of low resistivity. The explanation is the same as the one suggested before, namely lithium complexes with defects to neutralize their electrical effect on carrier density. However, now it is predominantly the A-center that has been affected. The number of LiO-V centers is small and unimportant.

Table 2. Impact on solar cell design

Findings	Possible uses
Confirms O yields stable recovery state	Optimize O
Li can be recovered from defect complexes	Optimize
Temperature dependence	Use of Li in low-temperature orbits
New recovery centers	Research may extend Li efficiency

Curve VII of Fig. 14 is the result of annealing the sample to 373°K for 10 min, thereby accelerating the interaction of lithium with defect complexes. A defect level approximately located at 0.18 eV (A-center) and distributed over a wide energy range still remains. The behavior of the mobility substantiated this fact, since it did not recover to its initial value as did the mobility in the low-resistivity sample. Some residual damage remained even after the high-temperature annealing process.

IV. Summary

The status of our research on lithium in silicon is summarized in Table 1 and the impact of this research on solar cell development is given in Table 2.

N70-12109

Annealing of Electron Damage in Lithium-Doped Silicon at 300°K

J. E. Stannard
U. S. Naval Research Laboratory
Washington, D. C.

I. Introduction

The Hall effect has been used extensively to measure impurity and damage center concentrations in semiconductors. In fact, it is still the most sensitive tool available for such determinations. The measurement, when performed as a function of temperature between 4 and 300°K on a semiconductor containing one type of acceptor and one type of donor, allows a separate determination of these two concentrations. In addition, the location of one of the levels in the forbidden gap may be determined.

The Hall-effect studies of radiation damage in lithium-doped silicon have been limited until now to temperatures above 77°K. Such a measurement allows a quantity equal to the donor concentration minus the acceptor concentration to be determined. This means the creation of an acceptor affects the measured quantity in the same way as the loss of a donor. Both of these processes are presumed to occur for radiation damage in Si (Li) and cannot be separated in a measurement restricted to high temperatures.

The experiment to be described here was designed to separate these effects by making Hall effect measurements over the full range from 4 to 300°K.

Preliminary work had indicated that the 1-MeV electron irradiation of float-zone silicon containing 10^{16} lithium cm^{-3} and performed at 300°K, did not cause the increase in acceptor concentration expected from present models of radiation damage. A similar experiment but with the irradiation performed at 80°K did show an increase in acceptor concentration. These results indicated that to separate the effects of damage from those of annealing, irradiation must be performed at low temperature.

In this experiment, the sensitivity of the Hall effect was exploited by using a sample that contained less than 10^{14} lithium/cm^3. This provided two major advantages. First, the anomalous dependence of the Hall constant on temperature characteristic of heavily irradiated material was avoided. Secondly, it was arranged so that, at

some point in the experiment, the free lithium would be depleted. This last point proved to be vital to the success of this experiment.

II. Hall Effect

Before discussing experimental results, some comments on the Hall effect at low temperatures and, in particular, the application of this tool to damaged material is in order. The Hall effect allows the carrier concentration to be measured to within a proportionality factor, known as the Hall factor. This factor is a function of temperature and magnetic field varying between 0.9 and 2 in magnitude.

Under the conditions of this experiment, the Hall effect may be assumed to give the carrier concentration directly for temperatures below 100°K. Above 100°K, corrections were necessary. The statistics relating carrier concentration to defects present in the solid require two adjustable parameters, concentration and ionization energy, for each type of defect. In the case of material damaged by radiation, a wide variety of defects are present, causing an exact theory to involve large numbers of adjustable parameters.

In this experiment, a simple four-parameter model presuming only one type of acceptor and one type of donor was used to fit the data. The applicability of this model can best be seen intuitively by considering the situation that exists at absolute zero. This condition of minimum energy, shown in Fig. 1, is reasonably accurate to 40°K in Si (Li). Several types of donors and acceptors are shown in the forbidden gap of silicon. An electron added to this system would fill the lowest lying unfilled state. The choice of which level will be partially occupied is determined entirely by the balance between the number of acceptors of lower energy and donors of higher energy. If acceptor states deep in the gap are added in sufficient quantity, the partially filled defect may become entirely depopulated, causing a deeper lying level to become partially filled. However, the addition of a donor deep in the gap affects nothing and is not detectable.

The Fermi level is that position in the gap where the probability for a level to be filled is 1/2. In general, this position is fixed very near the level that is partially occupied. Therefore, a measurement of the depth of the Fermi level below the bottom of the conduction band can give the ionization energy of the partially filled level. As temperature is increased from 0°K, the population of only those levels within KT (Boltzmann constant and temperature) of the Fermi energy change.

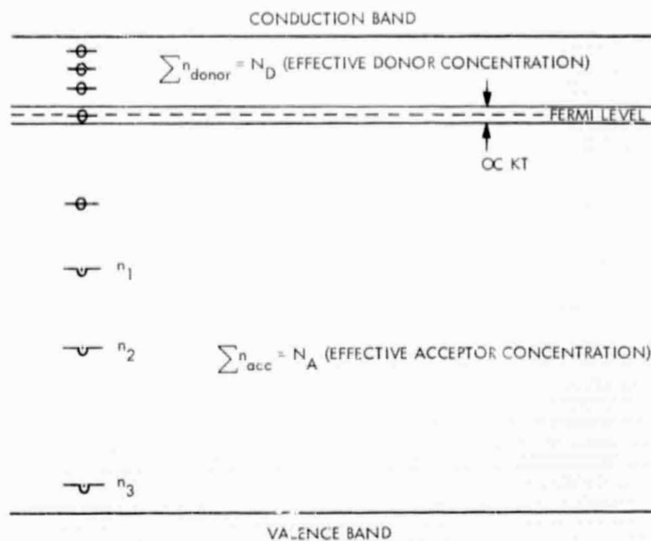

Fig. 1. Two-impurity model

The use of a two-impurity model with four parameters (number of acceptors N_A, number of donors N_D, ionization energy, and degeneracy factor) is rationalized as follows. The acceptors in the lower half of the gap are always filled so that their presence can be approximated by a single acceptor level of concentration N_A. The donors near the conduction band are assumed to be one type of donor lying at the energy of the partially filled donor and with a concentration equal to the sum of the separate densities. The fact that there are really not N_D donors at this energy but a smaller number, causes a physically unrealistic value of the degeneracy factor to be obtained when the two-impurity model is fit to the data. Degeneracy factors of as low as 1/60 were obtained where 1/2 is expected theoretically.

The validity of this model was verified by fitting it to false data calculated, assuming three impurities. The results indicated concentrations were accurate to within 20 to 30%. However, this model is less accurate when the Fermi level is part way between two levels of similar ionization energy, both of which are partly occupied.

III. Experiment

The plan of this experiment is as follows. A sample of 100 Ω-cm float-zone silicon was doped with lithium by diffusion to a total donor concentration of 10^{14} cm^{-3}. The ratio of the concentration of lithium to that of phosphorus was about 3 to 1.

After the Hall measurements were made, it was irradiated at 77°K with 4×10^{14} 1 MeV e/cm^2 and remeasured.

Subsequently, it was remeasured after annealing at 200°K to remove intrinsic defects and after five periods of increasing duration at 300°K.

The resultant data were fit to a two-impurity model with four adjustable parameters, using the method of least squares. (Credit for the fitting program is given to W. Daniels of the University of Maryland.) It was not possible to include a control sample of Si(P) to guard against anomalous annealing not due to lithium. The effects of this on the conclusion will be noted as they arise.

IV. Measurements Below 100°K

The results obtained from measurements made below 100°K are discussed first. The experimentally determined electron concentration as a function of inverse temperature is shown in Fig. 2. Electron concentration changed over eight orders of magnitude as the temperature changed from 100 to 14°K. The low-temperature limit was set by the inability of the apparatus to measure potentials from a source whose impedance was greater than 10^{10} Ω. The slope of the curves in the linear portion represents the Fermi level at low temperature. Comparison of these curves shows that the Fermi energy moved deeper into the gap as the experiment proceeded. The value of the electron concentration at high temperature equals $(N_D - N_A)$ and decreased on annealing at 300°K. The form of this decrease was in agreement with the carrier-removal studies by Carter.[a]

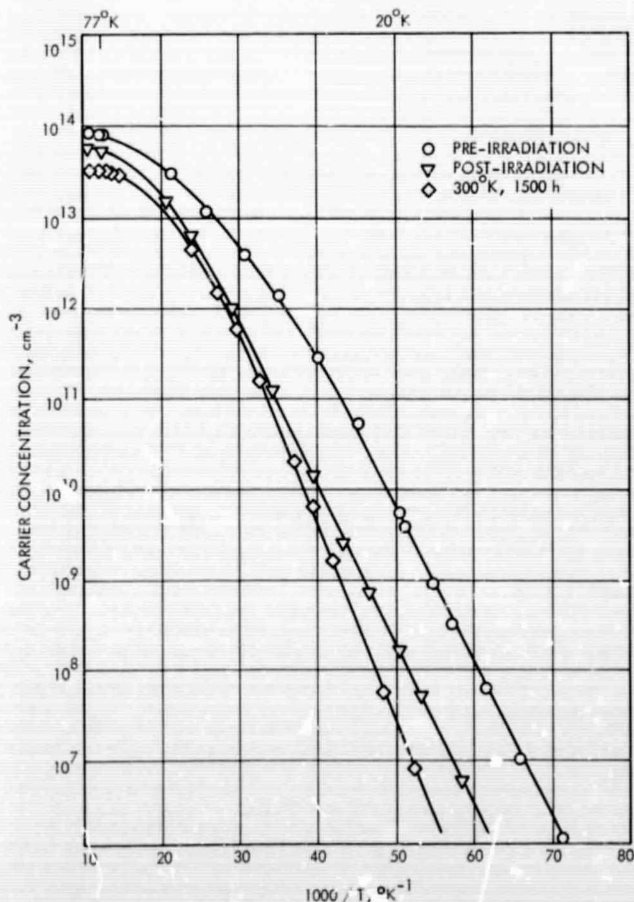

Fig. 2. Effect of electron irradiation and annealing on carrier concentration

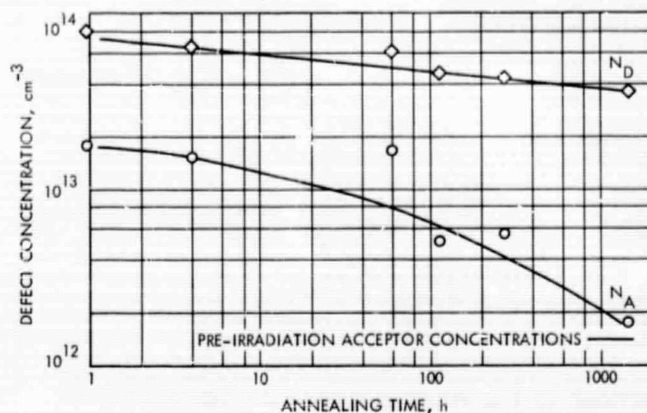

Fig. 3. Effect of annealing at 300°K on defect concentration

The explicit dependence of the donor and acceptor concentrations on time of annealing at 300°K is shown in Fig. 3. Donor and acceptor concentrations are represented by the upper and lower traces, respectively. Both show a decrease with annealing time. The acceptor concentration decreases a full order of magnitude; after 1500 h, it is near the acceptor concentration measured before irradiation. The majority of the acceptor concentration indicated here is due to the irradiation, and it does anneal at room temperature. Two points shown off scale to the left represent the values measured after annealing at 200°K. The large error in the point corresponding to 61 h is attributed to the fact the Fermi level at low temperature was located midway between the energy levels of the free [Li] donor and the [LiO] pair donor.

The decrease in acceptor concentration shown in Fig. 3 is vital to the argument presented with Fig. 4. During the course of the experiment, the Fermi energy at low temperature moved deeper into the gap. At the same time, the donor concentration decreased. The points shown in

[a] Carter, J. D., Jr., and Downing, R. G., Semiannual Progress Report on Contract NAS 5-10322, Aug. 28, 1966.

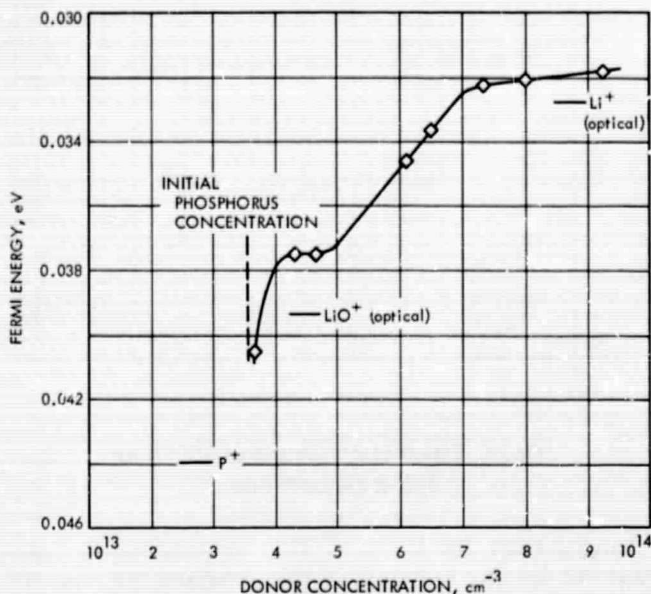

Fig. 4. Effect of annealing on Fermi energy

Fig. 4 were obtained in sequence moving from right to left. As annealing proceeded, the Fermi level moved from the vicinity of the lithium donor level to that of the lithium-oxygen donor. Then as the donor concentration approached the initial phosphorus concentration, the Fermi energy began to move toward the phosphorus donor level.

This movement of the low-temperature Fermi energy through a donor level can be brought about either by a large decrease in the concentration of that donor or by an increase in acceptor concentration; thereby, depopulating that donor completely. Figure 3 shows that the acceptor concentration was in fact decreasing not increasing; thereby, ruling out the second alternative. In addition, the decrease in donor concentration presumed by the first alternative was observed. This data establishes that the free lithium concentration is depleted and, subsequent to this, the LiO concentration is similarly depleted. It would seem that free lithium is removed by some process and this removal drives the lithium-oxygen pairing reaction to completion in the direction of decreasing lithium-oxygen pair concentration.

Several more interesting points can be made here. First, if it is assumed that the data shown here indicates the thermal ionization energies of the Li and LiO donors, the differences between the thermal and optical values are found to be about 1 MeV for Li and 2 MeV for LiO as compared to the known difference of 6 MeV for phosphorus. These differences seem quite reasonable within the framework of the Franck Condon principle, which is used to explain the differences between thermal and optical values.

Second, the times required for the depletion of the LiO donor are an order of magnitude greater than that required to deplete the free Li. Free Li is depleted in 100 h or less, while LiO donors are almost gone by 1500 h.

Third, when the Fermi level is near the LiO donor, it can be stated that the free Li concentration must be less than the measured acceptor concentration. Using Pell's disassociation constant, an estimate is obtained that the oxygen concentration must be greater than about 2×10^{15} cm^{-3}. Infrared absorption measurements were performed and showed no 9-μm absorption other than that attributable to the lattice. This result is the same as would be expected for float-zone material.

Finally, while this is float-zone material, the behavior of the lithium in oxygen content is somewhat characteristic of quartz-crucible type. That is, the free lithium content is at least partly determined by the disassociation of lithium-oxygen pairs.

However, it must not be presumed that the lithium is lost due to precipitation, which was the case in Pell's work with unirradiated quartz-crucible material. In Pell's work, the lithium concentration was orders of magnitude greater than the solid solubility for free Li and the donor concentrations remained always above this solid solubility.

The data in Fig. 3 is shown again in Fig. 5 in order to demonstrate that something quite different is occuring in this sample. Since the total donor concentration is less than four times the solid solubility of Li at 300°K, precipitation can be neglected. In addition, the donor concentration falls below the solid solubility for lithium. Clearly, some extremely active center is removing free lithium.

One further point can be made concerning the sinks to which the lithium is being removed. What is the relationship between the lithium loss and acceptor loss? The answer is that, in both the slow and the fast parts of the annealing process, approximately two donors were lost for each acceptor neutralized. If the change in acceptor concentration between time zero and time T is added to the donor concentration at time T, the lower curve of Fig. 6 is obtained. If twice the integrated acceptor change is added to the donor concentration, the upper, nearly flat curve is obtained.

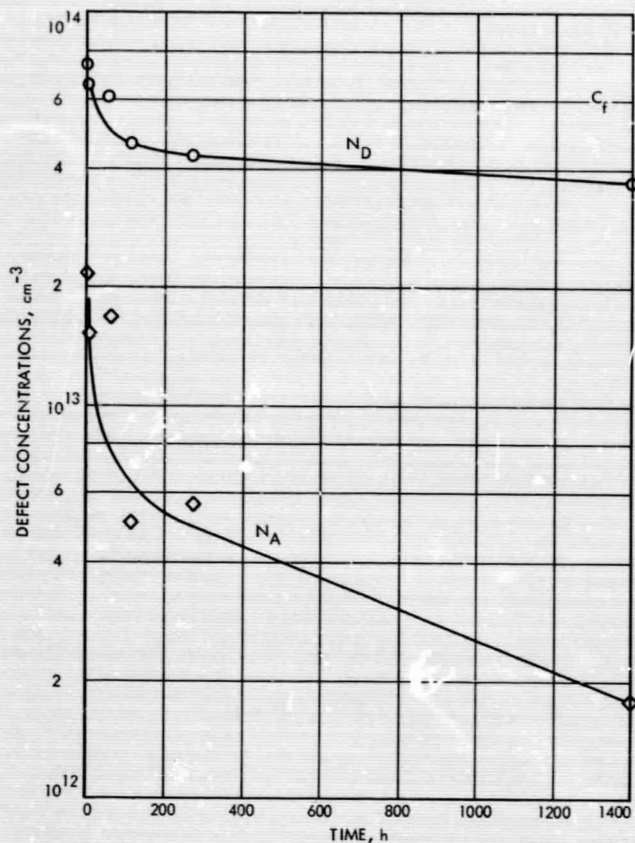

Fig. 5. Effect of annealing on defect concentrations

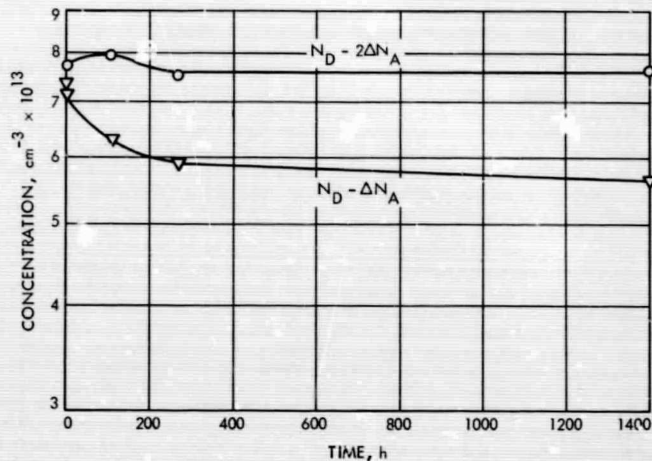

Fig. 6. Relative changes in acceptor and donor concentration

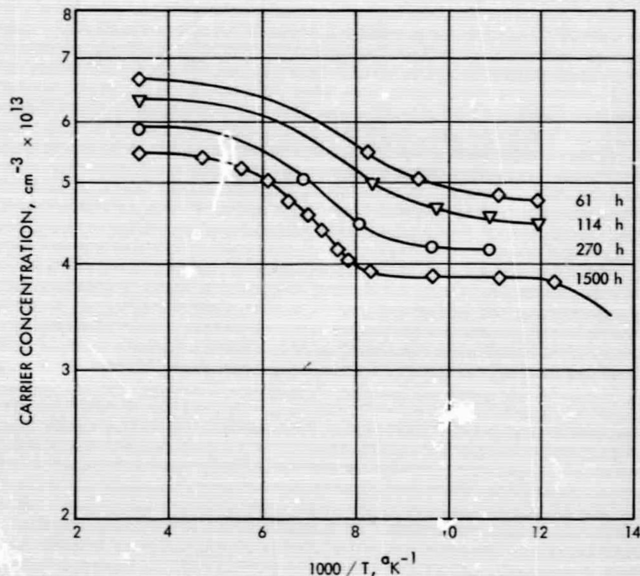

Fig. 7. Effect of deep donor energy on Hall data

V. Measurements Above 100°K

As the temperature is increased above 40°K, the Fermi energy tends to move downward toward the center of the gap. At 300°K, it can be as low as 0.3 eV below the bottom of the conduction band. At such high temperatures, the concept of filled versus unfilled loses meaning. If the Fermi level passes through a level as it moves downward, the population of that level will change and will thus produce a structure in the Hall data. Corrections for the Hall factor were necessary and were made using the Hall factor determined from the data taken before irradiation.

Structure due to A-centers at 0.185 eV below the conduction band was not observed in the measurements made after 61 h at 300°K. Structure due to a deep level was observed, however, and its effect on the Hall data is shown in Fig. 7. The various curves were taken at the indicated annealing times.

Analysis indicates a concentration of about 1.5×10^{13} cm^{-1} and is apparently independent of annealing time. This level may well have been present immediately after irradiation. Also, since its concentration far exceeds the acceptor concentration measured from the low temperature data, it must be concluded that this center is a donor. As such, it was neutral and undetected for all the measurements made below 100°K.

The depth of this level can be seen in Fig. 8. The dotted lines are carrier concentrations calculated for several values of deep-donor ionization energy. Apparently the shape of the data agrees well with theory, and the level is near 0.15 eV below the conduction band. Structure due to the A-center would be near the 0.19 eV curve and is clearly not observed. Since there was no control

sample, the importance of Li to this donor is an open question.

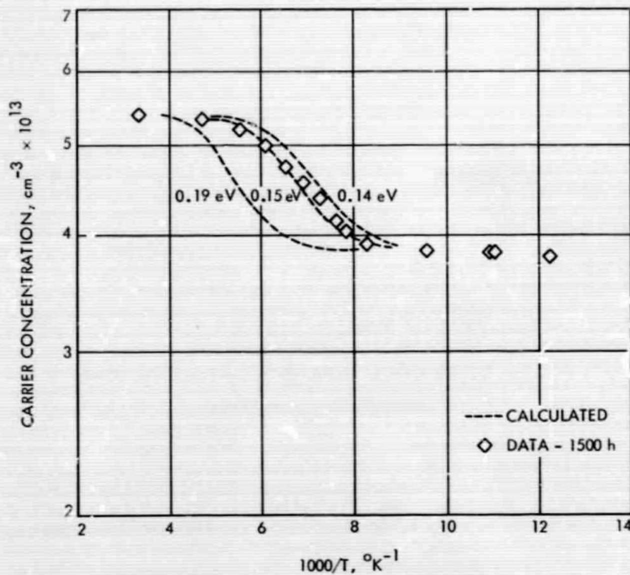

Fig. 8. Effect of deep donor energy on carrier concentration

VI. Summary

The results of this experiment utilizing the Hall effect can be summarized as follows:

(1) Acceptor defects introduced in silicon containing lithium and phosphorus become electrically neutral on annealing at 300°K.

(2) A decrease in concentration of both free lithium and lithium-oxygen pairs occurred concurrently with the decrease in acceptor concentration.

(3) Lithium was removed much more strongly than would be expected from a mechanism such as precipitation.

(4) In all phases of the annealing process, the loss in donor concentration was approximately twice the loss in acceptor concentration.

(5) A deep donor level 0.15 eV below the conduction band was observed; its concentration was independent of annealing at 300°K.

(6) No A-centers were detected after 61 h at 300°K.

N70-12110

Production and Annealing of Defects in Li-Diffused Silicon After 30-MeV Electron Irradiation at 300°K

J. A. Naber, H. Horiye, and R. A. Berger
Gulf General Atomic Incorporated
San Diego, California

I. Introduction

The effects of impurities on the production and annealing of radiation-induced defects in silicon has been studied extensively. It is known that impurities do play a significant role in the production and annealing of defects in silicon irradiated with 30-MeV electrons. Lithium as an impurity has been of particular interest because of its ability to diffuse through silicon at room temperature (Ref. 1).

The present work, supported by NASA Contract No. NAS 7-289, was undertaken to investigate the effects of lithium on the production and annealing of defects after 30-MeV electron irradiation in which some clustered damage is expected. Most of the radiation damage work on lithium-diffused silicon reported to the present time has been with 1-MeV electrons (Refs. 2–4). Bulk silicon was used during the present work making it possible to determine bulk damage effects. Lithium effects on the degradation and annealing of the minority-carrier lifetime, electrical conductivity, and Hall coefficient were studied. Comparisons with the results of silicon device studies (Refs. 4 and 5) were made because these parameters are important in the operation of silicon devices.

The effect of lithium on the production and annealing of known radiation-produced defects was also investigated using electron spin resonance. Emphasis was placed on a study of the silicon B-1 center (vacancy-oxygen complex) as presented in Refs. 6 and 7.

II. Experiment

Measurements of minority-carrier lifetime and electrical-conductivity were performed by standard methods. The electrical-conductivity measurements were performed by the four-probe method. Photoconductivity decay, obtained with the four-probe method, was used for the determination of the minority-carrier lifetime. The minority-carrier-lifetime measurements were taken at low injection levels ($<1\%$).

The electron-spin-resonance measurements were performed by the use of a superheterodyne spectrometer at 9.2 GHz with the magnetic field modulation at 100 Hz. These measurements were made at 20°K. Annealing of these samples was performed in an oil bath.

The samples were vacuum float-zone and quartz-crucible grown phosphorus-doped silicon with initial resistivities of 0.4 to 10^4 Ω-cm. The samples were lithium-diffused by painting the sample with a lithium-oil suspension and then diffusing for 1 to 2 h at 400 to 500°C.

Measurements of the minority-carrier lifetime were made immediately after 30-MeV electron irradiations at room temperature. The samples used in the electron-spin-resonance experiments were stored at liquid-nitrogen temperature from immediately after irradiation until they were measured. Storage at this temperature prevented annealing in the irradiated samples. In all experiments, the elapsed time during irradiation at room temperature was very small compared to the annealing time at room temperature.

A. Results and Analysis of Minority-Carrier-Lifetime Measurements

1. Float-zone silicon. The minority-carrier-lifetime measurements were performed on the lithium-diffused float-zone N-type samples with donor concentrations of 3×10^{16} cm^{-3} and with initial room-temperature minority-carrier lifetimes of 2 μs.

The samples were irradiated at room temperature with 30-MeV electrons. The degradation of the lifetime with electron fluence is plotted in Fig. 1. The data is plotted in accordance with

$$\frac{1}{\tau} = \frac{1}{\tau_0} + K\Phi \qquad (1)$$

where τ is the measured lifetime after an electron fluence Φ, τ_0 is the initial lifetime, and K is the degradation constant.

The inverse lifetime is linear with fluence, and the degradation constant is $1.1 (\pm 0.2) \times 10^{-7}$ cm^2/s-electrons. This value of the degradation constant is twice as large as the degradation constant for nonlithium-diffused float-zone silicon of the same resistivity (Ref. 8).

The isochronal annealing experiments of the minority-carrier lifetime consisted of 5-min anneals at the annealing temperature with the measurements made at 300°K.

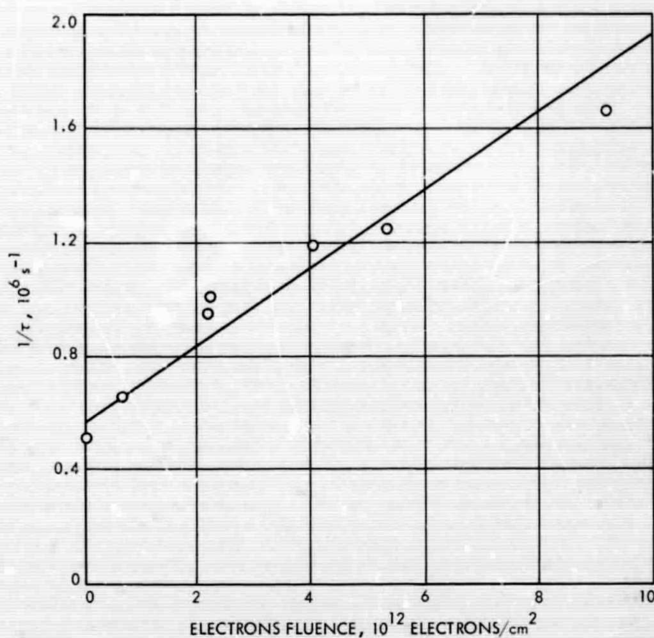

Fig. 1. Inverse minority-carrier lifetime as a function of 30-MeV electron fluence at 300°K for lithium-diffused float-zone N-type silicon

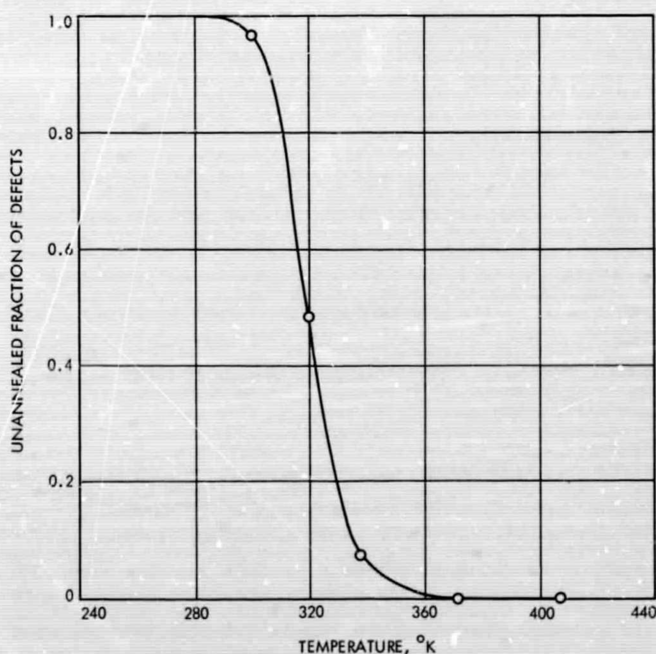

Fig. 2. Five-minute isochronal annealing of lithium-diffused float-zone N-type silicon after 30-MeV electron irradiation

This isochronal annealing is shown in Fig. 2. The data is plotted as an unannealed fraction of annealable damage as a function of the annealing temperature and is related to the lifetime by

$$\text{Unannealed fraction of annealable damage} = \frac{\dfrac{1}{\tau_t} - \dfrac{1}{\tau_f}}{\dfrac{1}{\tau_0} - \dfrac{1}{\tau_f}} \qquad (2)$$

where τ_f is lifetime after complete annealing, τ_0 is initial lifetime before annealing, and τ_t is lifetime at any time t.

The isochronal annealing was centered at 320°K, and all the recombination centers introduced by the irradiation were annealed. Isothermal annealing measurements were also performed; analysis of the isothermal annealing data at 300°K indicated that this annealing was first order.

Analysis of the isochronal data, assuming first-order kinetics, yields an activation energy of 0.85 ±0.10 eV with a frequency factor of 10^{11}/s for the annealing of the lithium-diffused float-zone N-type silicon.

2. *Quartz-crucible silicon.* The experiments on the Czochralski-grown N-type silicon were performed on samples with carrier concentration of 3×10^{16} cm^{-3}.

The lifetime degradation as a function of electron fluence is shown in Fig. 3, the associated degradation constant being 1.1 (±0.2) × 10^{-7} cm^2/s-electrons. This value is twice as large as for nonlithium-diffused silicon (Ref. 8); however, it is about the same as for float-zone lithium-diffused silicon.

Isochronal annealing experiments of the degraded lifetime were performed using 5-min anneals at elevated temperatures, and the measurements were made at 300°K. The data is plotted in Fig. 4 in accordance with Eq. (2). This annealing was centered at 360°K, and the annealing was complete; i.e., all the recombination centers introduced by the irradiation were annealed. Isothermal annealing experiments of the damage were also performed. Analysis of the isothermal annealing data showed that annealing was first order at 360°K.

The analysis of the isochronal annealing, assuming first-order kinetics, yields an activation energy of 0.75 ±0.1 eV and a frequency factor of 10^8/s.

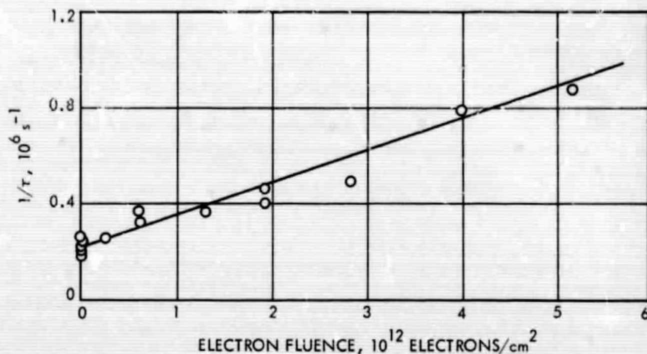

Fig. 3. Inverse minority-carrier lifetime as a function of 30-MeV electron fluence at 300°K for lithium-diffused quartz-crucible N-type silicon

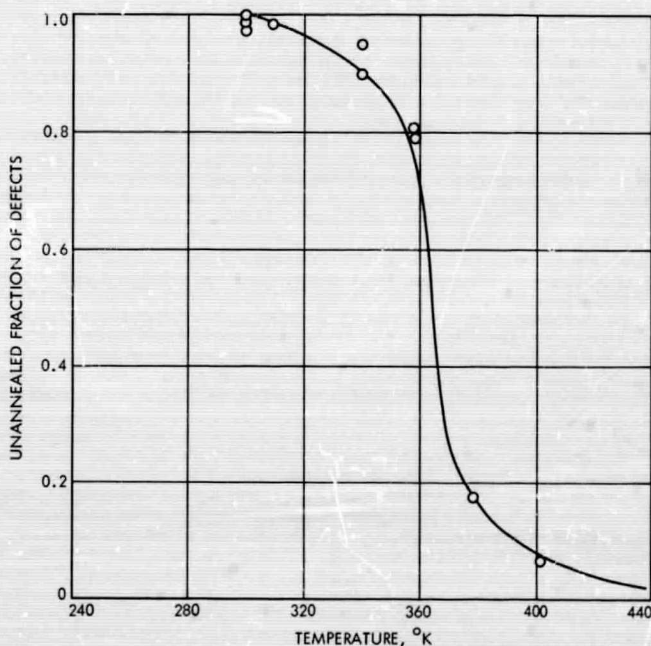

Fig. 4. Five-minute isochronal annealing of lithium-diffused quartz-crucible N-type silicon after 30-MeV electron irradiation

B. Results of Electron-Spin-Resonance Measurements

Quartz-crucible silicon samples (10^{16} P atoms/cm^3 before lithium diffusion) were diffused to a donor concentration of approximately 5×10^{17}/cm^3, as determined by electrical-conductivity measurements. A large-resonance signal, assumed to be due to the LiO donor (Refs. 9 and 10), was seen in this material. The concentration of these centers was estimated to be about 0.7×10^{18} to 1×10^{18} centers/cm^3.

Since the absolute number of centers derived from electron-spin-resonance measurements is not easily obtained, this concentration should be normalized to that obtained by the conductivity measurements. This procedure assumes that this resonance center is equal to the total donor concentration.

The samples were irradiated with 30-MeV electrons at 300°K to fluences between 1×10^{17} to 2×10^{17} electrons/cm^2. The average introduction rate observed for the B-1 center was 0.025 (±0.01)/cm. The carrier removal rate, as determined by electrical conductivity, was 1.7 (±0.2)/cm, whereas a value of 1.5 (±0.5)/cm was obtained from the decrease in the LiO resonance.

The sample was annealed in steps. The B-1 center annealing is shown in Fig. 5, along with the change in electrical conductivity and LiO resonance. It should be noted that simultaneous with the B-1 center anneal at about 325°K, there was a decrease in the electrical conductivity. Above 373°K, the concentration of B-1 centers remained undetectable, whereas the electrical conductivity increased.

C. Analysis of Electron-Spin-Resonance Measurements

The LiO resonance decreased with irradiation. The loss in resonance could be due to the depopulation of the donor levels by deeper radiation-induced acceptors, or to a conversion of some of these donor levels into acceptors.

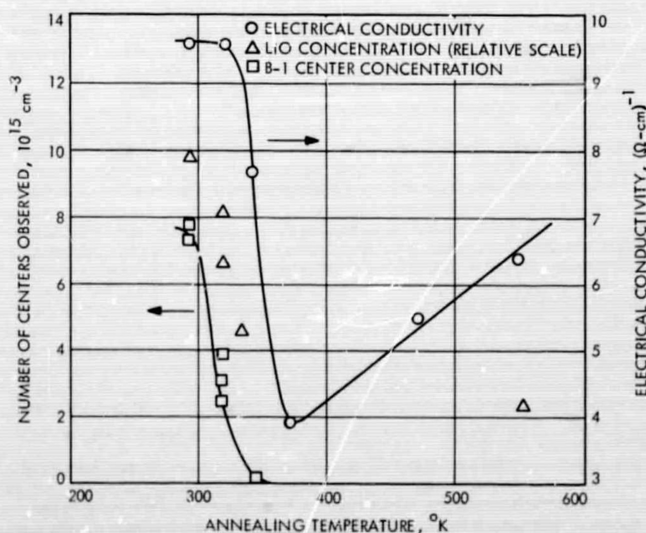

Fig. 5. Isochronal annealing of electrical conductivity, LiO concentration, and B-I center concentration after 30-MeV electron irradiation at 300°K

This loss in resonance intensity is accompanied by a decrease in electrical conductivity. In lithium-diffused quartz-crucible silicon with a carrier concentration of approximately 4×10^{17} carriers/cm^3 (assumed to be due to the LiO donor), the B-1 introduction rate is about 0.02/cm. The dependence of the B-1 introduction rate on the carrier concentration in lithium-diffused silicon is similar to that observed by Watkins (Ref. 11) in phosphorous-doped silicon, and indicates a competition for the irradiation-induced vacancy by the oxygen and the donor.

The annealing of the sample with the high lithium concentration (Fig. 5) is centered near 320°K. The decrease in B-1 resonance is not due to a depopulation of its electrical level, since the value of the conductivity and the fact that the LiO donor signal was seen throughout the temperature range indicate that the B-1 center, if present, is in the right charge state to be seen by the electron-spin-resonance measurement. Since the B-1 center anneals in silicon without lithium near 600°K (Ref. 7), the disappearance of the B-1 center must be due to the presence of lithium.

Figure 5 indicates that, since the change in conductivity is too great, the center causing the drop in conductivity is not the B-1 center only.

The electrical conductivity in the quartz-crucible silicon decreases during irradiation. This decrease is consistent with the formation of acceptors in N-type silicon. Upon annealing, the electrical conductivity decreases in the same temperature region that the B-1 center disappears, and the LiO resonance decreases. This decrease in conductivity upon annealing is interesting since it is seen that the minority-carrier lifetime increases in this temperature range.

III. Discussion of Results

The experimental results presented in the previous sections have shown some specific properties of the defects introduced in lithium-diffused N-type silicon by 30-MeV electron irradiations at room temperature.

A. Irradiation

The lifetime degradation constants due to irradiations with 30-MeV electrons at 300°K for both the lithium-diffused float-zone and quartz-crucible N-type silicon

were higher than that for similar nonlithium-diffused silicon (Ref. 8). These K values were larger by at least a factor of two. In a like manner, the carrier-removal rate in the lithium-diffused quartz-crucible N-type silicon was larger than the carrier removal rate for similar nonlithium-diffused N-type silicon (Ref. 8). In quartz-crucible silicon, the removal rate of the donor resonance (LiO) was about the same as the carrier-removal rate. The B-1 center production in the quartz-crucible material with a large LiO^+ concentration was 0.02/cm, which is about ten times smaller than in nonlithium-diffused quartz-crucible material (Ref. 12).

The increases in the degradation constant and carrier-removal rates for the lithium-diffused N-type silicon imply that the production of the defect that is formed is dependent on the presence of lithium. This defect may either contain or not contain lithium; in either case, however, its production is somehow affected by the lithium present.

The cause of the low introduction rate of B-1 centers is not clear. The reason for the low introduction rate in the sample with the high concentration of lithium could be that, in this sample where the donor concentration is comparable to the oxygen concentration, most of the oxygen is in the form of the LiO donors and, therefore, is not free to form B-1 centers. The other possibility is that the negative vacancies produced are attracted to the positively charged donors. The higher concentration of the donors makes the probability of the vacancies combining with free oxygen smaller.

B. Annealing

The most interesting property of irradiated lithium-diffused silicon is its ability to anneal at lower temperatures than irradiated nonlithium-diffused silicon. Nonlithium-diffused silicon irradiated at room temperature does not show large amounts of minority-carrier-lifetime annealing at temperatures below 375°K (Ref. 13), whereas lithium-diffused-silicon annealing is centered as low as 320°K. This lowering of the annealing temperature is attributed to the presence of lithium, as is evident in a comparison of the lifetime annealing of lithium-diffused and nonlithium-diffused silicon. The kinetics for annealing of carrier lifetime of both the float-zone and quartz-crucible material indicate that it is a first-order process with activation energies of 0.85 ±0.1 eV for float-zone silicon and 0.75 ±0.1 eV for quartz-crucible silicon, and the effective frequency factors of 10^{11}/s for float-zone silicon and 10^{8}/s for quartz-crucible silicon.

The annealing temperature of the B-1 center is also decreased by the presence of lithium in the silicon lattice. The B-1 center usually anneals near 600°K in nonlithium-diffused silicon. However, when lithium is present in the lattice, this annealing takes place at a much lower temperature (about 320°K). The annealing kinetics of the B-1 center in lithium-diffused silicon seem comparable to the annealing times of the minority-carrier lifetime, although the data on B-1 annealing is not precise enough to determine the annealing kinetics for the B-1 center. This annealing is accompanied by a decrease in carrier concentration. This decrease implies that the center produced when annealing takes place is an acceptor, thereby removing another carrier from the conduction band.

The activation energy for annealing of recombination centers in both float-zone and quartz-crucible material is close to the activation energy of 0.66 eV, as determined by Pell (Ref. 1) for diffusion of interstitial lithium in the silicon lattice. This result suggests that the annealing mechanism is the Li^+ diffusing to the damage center and thereby annealing it. The ratio of the frequency factors for the float-zone and quartz-crucible Li-diffused silicon are consistent with the "effective diffusion" rate of lithium in both silicons as determined by Pell.

The above annealing experiments indicate that the Li^+ is responsible for the annealing of defects. The diffusion of Li^+ to the recombination center or electron-spin-resonance centers (B-1 centers) changes the electrical nature of the defects.

IV. Summary

The dominant defects introduced in lithium-diffused silicon by 30-MeV electrons contain lithium, or are affected in their production by lithium. The lifetime degradation constant and carrier-removal rates are larger in lithium-diffused silicon than in equivalent nonlithium-diffused silicon. The introduction rate of B-1 centers is a strong function of the lithium concentration. Defects (recombination centers and B-1 centers) are annealed at lower temperatures in lithium-diffused silicon than in nonlithium-diffused silicon by the diffusion of free lithium to the defect. The electrical conductivity undergoes a reverse anneal during the above annealing.

References

1. Pell, E.M., "Diffusion Rate of Li in Si at Low Temperatures," *Phys. Rev.*, Vol. 119, p. 1222, 1960.
2. Smirnova, L. V., Chapnin, V. A., and Vavilov, V. S., "Radiation Defects in Lithium-Doped Silicon," *Sov. Phys.–Solid State*, Vol. 4, p. 2426, 1963.
3. Carter, J. R., Jr., "Radiation Damage in Lithium-Doped Silicon," *IEEE Trans. Nucl. Sci.*, Vol. NS-14, p. 110, 1967.
4. Wysocki, J. J., "Role of Lithium in Damage and Recovery of Irradiated Silicon Solar Cells," *IEEE Trans. Nucl. Sci.*, Vol. NS-14, p. 103, 1967.
5. Fang, P. H., *Present Status of Lithium-Diffused Silicon Solar Cells*, Report X-713-67-136. NASA/Goddard Space Flight Center, Greenbelt, Md., March 1967.
6. Watkins, G. D., and Corbett, J. W., "Defects in Irradiated Silicon," *Phys. Rev.*, Vol. 121, p. 1001, 1961.
7. Corbett, J. W., et al., "Defects in Irradiated Silicon," *Phys. Rev.*, Vol. 121, p. 1015, 1961.
8. Flanagan, T. M., et al., *Transient Radiation Effects*, Report GA-8338. Gulf General Atomic, Dec. 1967 (AD-838-975).
9. Feher, G., "Electron-Spin-Resonance Experiments on Donors in Silicon," *Phys. Rev.*, Vol. 114, p. 1219, 1959.
10. Honig, A., and Kip, A. F., "Electron-Spin-Resonance of an Impurity Level in Silicon," *Phys. Rev.*, Vol. 95, p. 1686, 1954.
11. Watkins, G. D., Corbett, J. W., and Walker, R. M., "Spin Resonance in Electron-Irradiated Silicon," *J. Appl. Phys.*, Vol. 30, p. 1198, 1959.
12. Naber, J. A., Horiye, H., and van Lint, V. A. J., *Radiation Effects on Silicon*, Report GA-8668. Gulf General Atomic, Aug. 20, 1968.
13. Wilsey, N. D., Statler, R. L., and Faraday, B. J., "Defect Clusters in Electron-Irradiated Silicon," *IEEE Trans. Nucl. Sci.*, Vol. NS-15, p. 55, 1968.

N70-12111

Study of Dopants for Radiation-Resistant Silicon

O. L. Curtis, Jr. and R. F. Bass
Northrop Corporate Laboratories
Hawthorne, California

I. Introduction

In silicon, the participation of impurities in the formation of radiation-induced defect complexes and subsequent thermal annealing is well established. One aspect of this fact, of special interest to those attending this conference, is the remarkable effects that small amounts of lithium have on the stability of radiation-induced defects. However, along with decreased sensitivity to radiation, there appear to be instabilities in device performance when Li is present. It is natural to ask whether there might not be other impurities that are more useful from a practical standpoint than Li.

In the work we describe here, we have considered various impurities and have evaluated the effects of these impurities upon lifetime degradation and the stability of defects introduced by radiation. As a means of comparison and to provide additional information on the bulk properties of Li-associated defects, we are also studying bulk material into which Li has been diffused. Earlier studies (Ref. 1) showed that, in certain cases, complete lifetime recovery in electron-irradiated Si can be obtained by moderate anneals (~250°C). We are studying the dose dependence of this annealing, and also the dependence upon previous radiation and annealing history to see if a practical annealing schedule for solar cells might be developed.

II. Experimental Study

Several impurities have been selected for initial consideration. One of these is aluminum, a semi-conventional P-type dopant. Observations on neutron-irradiated Si indicate that Al-doped material is more radiation resistant than material doped with more conventional impurities, boron and gallium (Ref. 2). The data from these observations is shown in Fig. 1 in which the sensitivity to radiation is indicated by a damage constant K. The value of K represents the neutron fluence required to reduce the lifetime τ of an initially perfect sample ($\tau = \infty$) to 1 μs. The history of these samples may be important in their behavior.

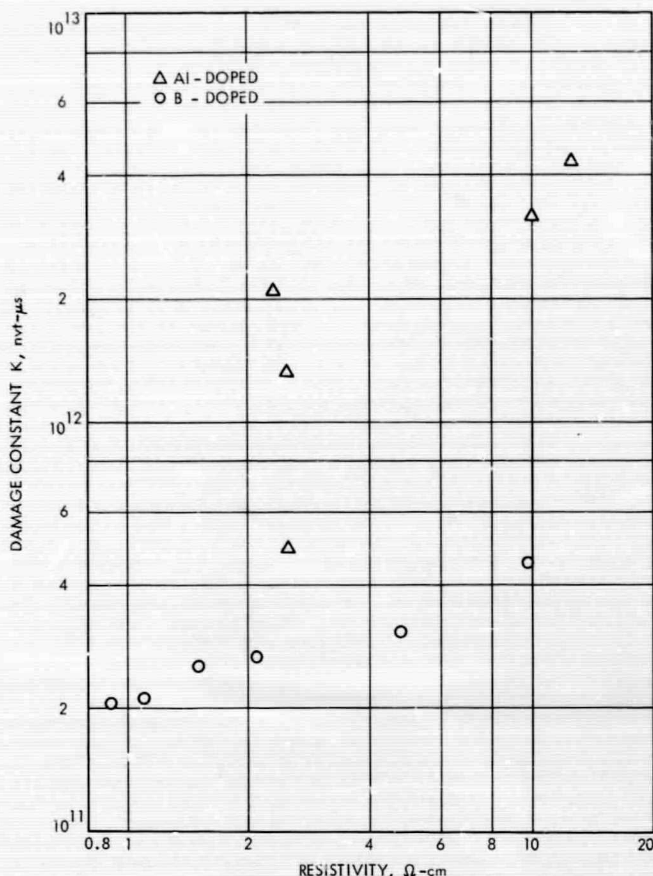

Fig. 1. Lifetime damage constant in Al-doped and B-doped silicon

Because of their low initial lifetime, the samples were annealed before irradiation at temperatures ~400°C. This improved the lifetimes, sometimes markedly, but it also increased the resistivity, evidently by redistributing some of the Al atoms.

The impurity that is perhaps best known for its influence on radiation-induced defects is oxygen. Gamma-irradiated Si exhibits a much smaller sensitivity to radiation when it contains appreciable amounts of oxygen (Ref. 3). This difference is also observed for N-type material, but to a lesser degree, following irradiation by 10-MeV electrons (Refs. 1 and 4). The variation in oxygen in these and many subsequent studies has been that which naturally occurs when different growth techniques are employed. Thus, it seems logical to attempt additional reduction in radiation sensitivity by purposely doping with higher concentrations of oxygen.

Another impurity with some appealing possibilities is beryllium. Diffusion and distribution coefficient data on Be is quite limited, but Trumbore (Ref. 5) discusses correlations between distribution coefficients and tetrahedral radii for elements in various columns of the periodic table. The tetrahedral radius of Be is 1.06 Å (Ref. 6), and the distribution coefficient is estimated to lie between 10^{-4} and 10^{-3}. The diffusion characteristics of Be are unknown, but it appears unlikely to diffuse easily because the solid solubility is low at temperatures much below the Si melting point.

A possible limitation is the deep levels that might be associated with Be and would act as recombination centers. In this regard, it is natural to make comparisons with magnesium and zinc, both of which show deep levels (Refs. 7–9). However, the levels might be expected to be shallower for Be.

Maximum solid solubility can be estimated (Ref. 10) from the distribution coefficient. It should be practical to introduce $\sim 10^{17}$ Be atoms/cm^3 by adding to the melt.

Other impurities that appear interesting are the halides; namely, fluorine, chlorine, and bromine. Again on the basis of discussions of Trumbore (Ref. 5), it appears that introduction would be feasible either by diffusion or by introduction into the melt. Recombination behavior is unknown.

Because of similarities to Li, sodium is another possible doping agent of interest. There is considerable controversy over the diffusion of Na in Si (Refs. 11–13). It appears that it would be best to introduce Na in the melt, rather than attempting to diffuse it because it would be very difficult to avoid Li contamination in the latter case.

III. Results

Table 1 lists special materials that have been investigated with the manufacturer, growth method, resistivity, and pre-irradiation lifetime of each. Four ingots of Al-doped material were obtained, all with usable characteristics. Suitable B-doped and P-doped material with excess oxygen were obtained from two sources. The two Be-doped ingots had lower resistivities than planned (in each material we aimed for resistivity values between 5 and 10 Ω-cm), but of greater consequence was the fact that the carrier lifetimes in both crystals were too low to be measured. Presumably, deep levels are introduced into Si by Be, resulting in a short lifetime for this material. It appears then, that Be is not a satisfactory dopant. The only Cl-doped material obtained had tn extremely high

Table 1. Special materials investigated

Dopant	Manufacturer	Growth method	Resistivity, Ω-cm	Lifetime, μs
Al	General Electric	Float zone (argon)	6	433–480
	General Electric	Float zone (argon)	10	150–470
	Texas Instruments	Czochralski	5	4.5–5.8
	Texas Instruments	Lopex	6	123–165
O(B)	General Electric	Czochralski	6	39.0–43.3
	Semi-Elements	Czochralski	7	13.0–24.5
Be	General Electric	Float zone (argon)	3	≤0.5
	Semi-Elements	Czochralski	0.9	≤0.2
Cl	Semi-Elements	Czochralski	$\sim 10^4$	—
Li	Northrop Corp. Laboratories	Diffused in Lopex (P)	1.0–2.5	107–130
Na	Semi-Elements	Czochralski	30	43.3–84.0
O(P)	General Electric	Czochralski	6	251–310
	Semi-Elements	Czochralski	4	18.0–24.5

resistivity. Perhaps this material has amphoteric characteristics, resulting in a highly compensated crystal. The Na-doped crystal obtained had a higher resistivity than desired, but was useful for experimentation.

Because of its availability and the fact that the energy distribution is reasonably similar to that occurring in space, a field-emission electron-beam machine (Febetron) was used as a radiation source to evaluate these materials. However, the photoconductivity decays of electron-irradiated samples were observed to be very nonexponential after irradiation. This behavior was initially attributed to nonuniform damage in the samples, but was later found to be partly due to trapping states introduced near the surface.

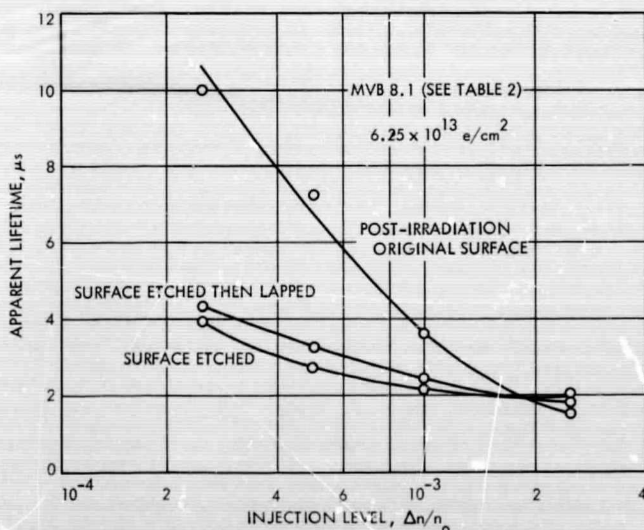

Fig. 2. Effect of surface condition on apparent lifetime of electron-irradiated silicon

Figure 2 indicates the sensitivity of the measured lifetime to surface condition, particularly at low injection levels. This behavior was surprising because the samples had lapped surfaces, which should provide a condition of maximum disorder and essentially infinite surface recombination velocity. However, when the surface was etched and subsequently lapped to approximately its initial condition, a large change in behavior was observed. (The difference in the bottom two curves is not believed to be significant.) Because of this instability and the difficulty in obtaining exponential decays and well-defined lifetimes, the decision was made to discontinue use of the Febetron.

Data was obtained, however, on N-type and P-type material with excess oxygen, and on Al-doped material. The data indicated that material doped with Al was less sensitive to radiation, and the General Electric material was found to be about twice as radiation resistant as normal B-doped material. However, the Lopex material grown by Texas Instruments did not indicate any improvement over normal material.

Studies are currently being performed using a Co^{60} source for radiation, and surface stability problems have been eliminated. Preliminary results are shown in Table 2. The damage constant used here is that gamma fluence required to reduce the lifetime of an infinite lifetime sample to 1 μs, so that, the higher the damage constant, the more radiation-resistant the material. The apparent radiation resistance of the Al-doped material is absent, which is quite surprising since gamma-irradiated material normally is much more sensitive to impurity effects than electron- and neutron-irradiated material. The anomalous relationship is under investigation. Some possibilities are discussed in the conclusion. However, as we will show later, at higher temperatures the Al-doped material again displays a lower sensitivity. As with the electron source, no particular advantage of high oxygen concentrations is apparent. The Na-doped material was P-type, and indicated no benefits of Na doping at room temperature.

Lithium-doped samples were prepared by diffusing Li from two sides into a slab of material ~7 mm thick. A small sample was cut from the center of this material so that its ends were the surfaces of the slab. The resistivity of the sample was probed following various treatments. The results, shown in Fig. 3, indicate that reasonably

Table 2. Lifetime-damage constant for Co^{60} γ-irradiated silicon[a]

Sample[b]	Co^{60} γ dose, γ cm^{-2} $\times 10^{16}$	Damage constant, γ cm^{-2} μs $\times 10^{16}$
GFAl 6	1.228	11.5
TCAl 5	1.228	10.1
TLAl 6	1.965	9.9
GFAl 10	1.965	38.2
GCBO 6	1.228	9.5
SCBO 7	1.965	36.2
DVB 2	1.228	29.8
DVB 10	1.965	44.7
MVB 8	1.965	41.0
DCB 2	1.228	26.2
SCNa 32	1.228	30.3
SCNa 32	1.965	37.7
GCPO 6	1.228	3.5
SCPO 4	1.965	2.2
KCP 6	1.965	4.4
DVP 8	1.228	0.3

[a]Values shown are average values for two or more identical samples.

[b]The sample designation indicates the crystal manufacturer (first letter), growth technique (second letter), dopant impurity (third and on letters) and nominal resistivity (numbers, in Ω-cm) at room temperature. Manufacturer D is Dow Corning, G is General Electric, K is Knapic, M is Merck, S is Semi-Elements, and T is Texas Instruments. Growth techniques C, F, L, and V represent the Czochralski (pulled), float-zone (argon atmosphere), Lopex, and float-zone (vacuum) methods, respectively.

uniform samples, approximately 3 mm thick, can be obtained.

The lifetime recovery reported (Ref. 4) at relatively low temperatures in electron-irradiated Si appears very promising as a means of providing annealing cycles for Si solar cells. However, the conflict of this data with those obtained by others (Refs. 14 and 15) suggests a possible dependence of this annealing stage on total damage.

Figure 4 presents data for five initially identical samples that were irradiated to various levels. As the dose is increased, the annealing stage moves to a higher temperature. This behavior suggests that a series of anneals after slight damage could be more successful than anneals after greater damage has occurred.

Figure 5 illustrates the annealing behavior at the higher temperatures of the same five samples after a subsequent irradiation in which all received the same dose. Those samples receiving the highest initial dose required a

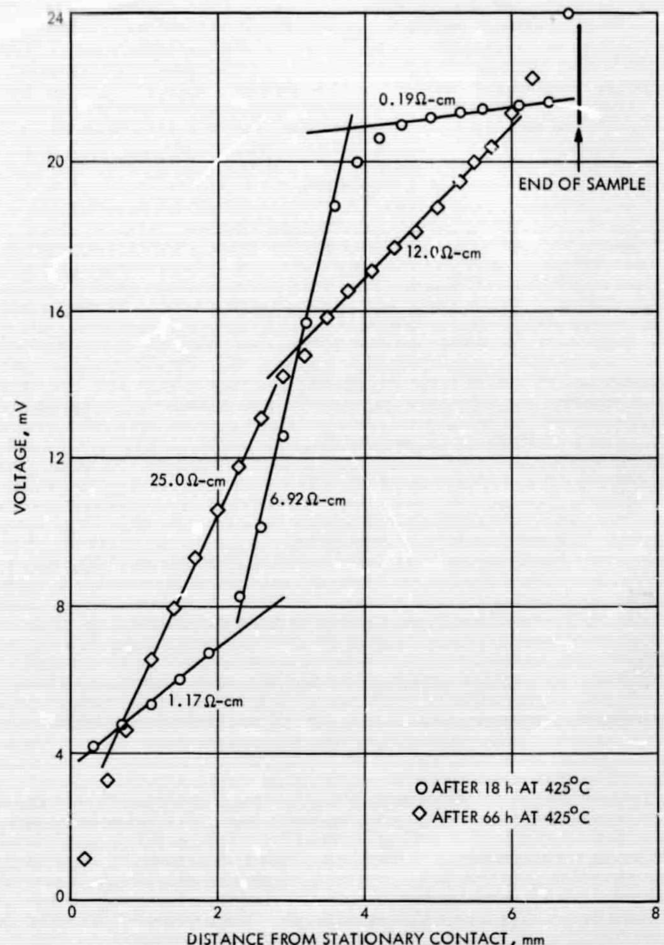

Fig. 3. Effect of heat treatments on distribution of lithium in silicon

higher temperature for subsequent anneal, even though the initial lifetime damage was completely removed from all samples after the first irradiation. Evidently, some low-density defect sinks exist in these materials. If they can be identified, it might be possible to introduce them in larger concentrations to provide annealing of more severe damage.

The annealing behavior of N-type material is similar for various oxygen concentrations. However, the large recovery stage is completely absent in vacuum-float-zone P-type material. Instead, significant reverse annealing occurs so that there is more damage, in terms of lifetime changes present, after 200–300°C anneals. This is true for all float-zone B-doped samples investigated. However, as shown in Fig. 6, Al-doped material grown by the float-zone or Lopex methods, either of which should have a relatively low oxygen concentration (GFAl 10 had

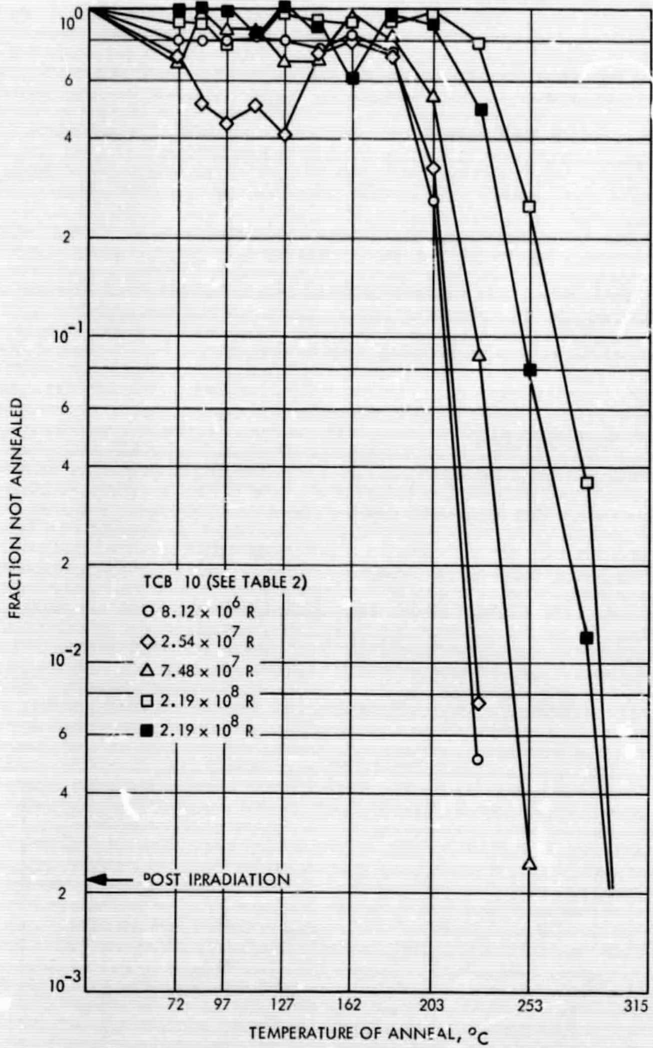

Fig. 4. Dependence of dose on lifetime recovery in Co^{60} gamma-irradiated silicon

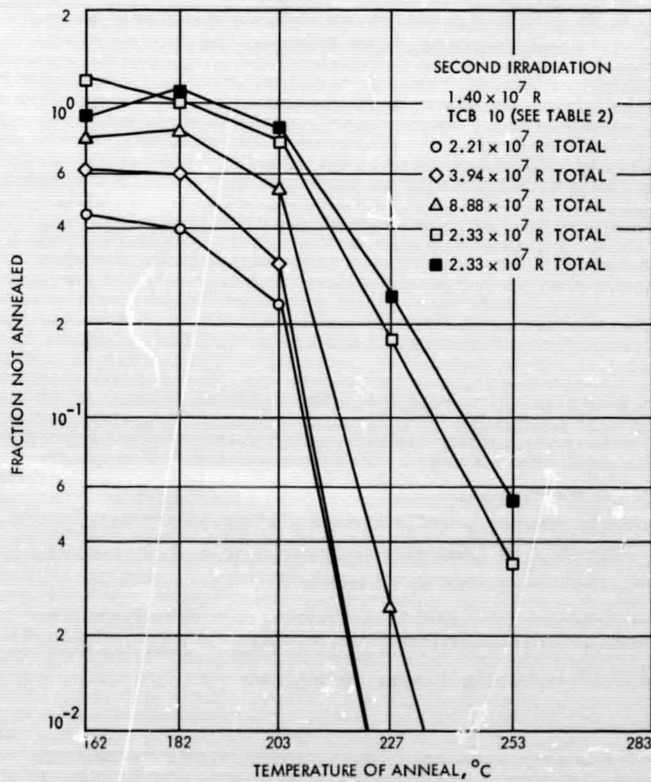

Fig. 5. Effect of total dose on lifetime recovery in silicon irradiated with Co^{60} gamma-rays in two different irradiations

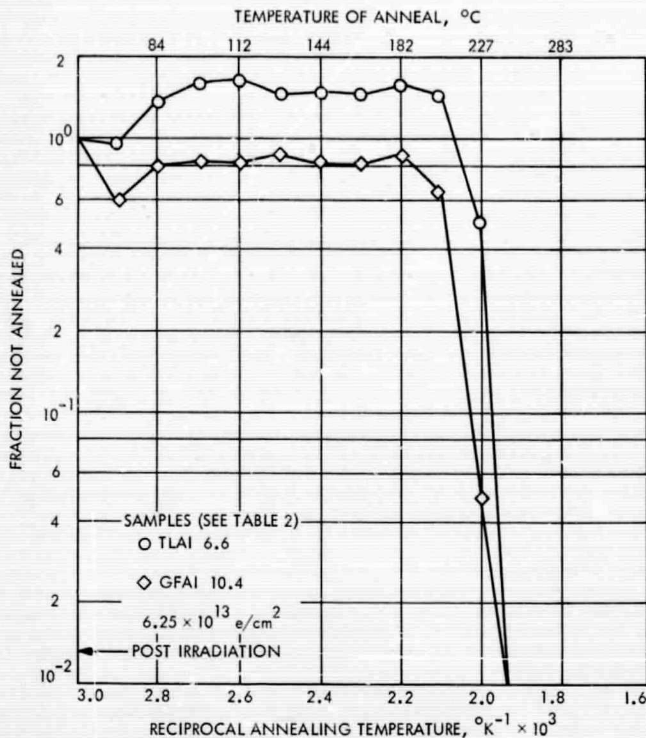

Fig. 6. Isochronal annealing of lifetime damage in electron-irradiated Al-doped silicon

an oxygen content $\lesssim 10^{16}$ cm^{-3}), shows the normal complete annealing at $\sim 250°C$. (This data is for electron-irradiated samples, but comparable results have been obtained from γ-irradiated samples.) It is not yet clear whether this difference is due to the presence of the aluminum or to other differences that may exist in the manufacturing process.

Figures 7 and 8 compare the annealing behavior of material containing high oxygen concentration ($\sim 10^{18}$ cm^{-3}) and that of similarly doped materials containing more normal oxygen concentrations ($\sim 10^{17}$ cm^{-3}). Surprisingly, the large amount of oxygen appears to suppress the annealing process in N-type material, and the annealing stage appears to lie between that for vacuum-float-zone (low oxygen) and Czochralski (medium oxygen) in its effect on P-type silicon. Again, similar data has been obtained following gamma irradiation.

As has been indicated, Na-doped material showed no improvement in terms of radiation resistance. In fact, if one considers the resistivity of the material (which should yield higher lifetimes), its showing was quite poor. It is to be anticipated, however, that Na would be more stable than Li, thus the interactions that take place at room temperature in Li-doped Si might not occur until higher temperatures in Na-doped material. Isochronal anneals have been performed on this material and the damage remained relatively stable up to $\sim 250°C$. Thus, the tentative conclusion is that the addition of Na did not improve the radiation tolerance of the material. However, since the resistivity of the material was higher than expected and no measurements of Na concentrations were performed, the Na concentrations may have been much lower than intended ($\sim 2 \times 10^{15}$ cm^{-3}).

IV. Conclusions

Silicon was doped with various impurities in an attempt to make the minority-carrier lifetime less sensitive to degradation by radiation. The impurities added were aluminum, excess oxygen, beryllium, chlorine, and sodium. The results indicated that both Be and Cl had adverse effects on the electrical properties of the material and are, thus, unsuitable for use. Since only one source of Cl-doped material was used, the conclusion should be

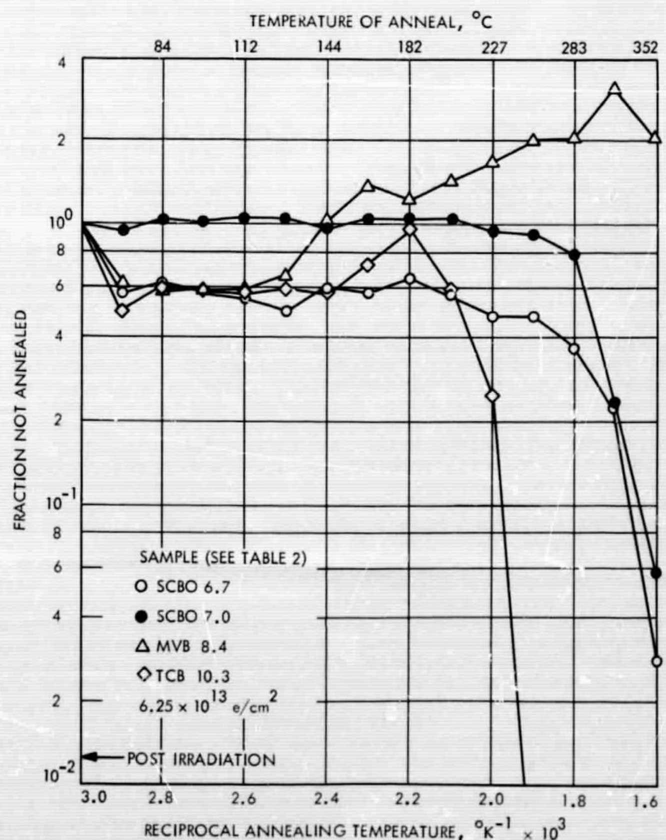

Fig. 7. Influence of oxygen on lifetime recovery in electron-irradiated B-doped silicon

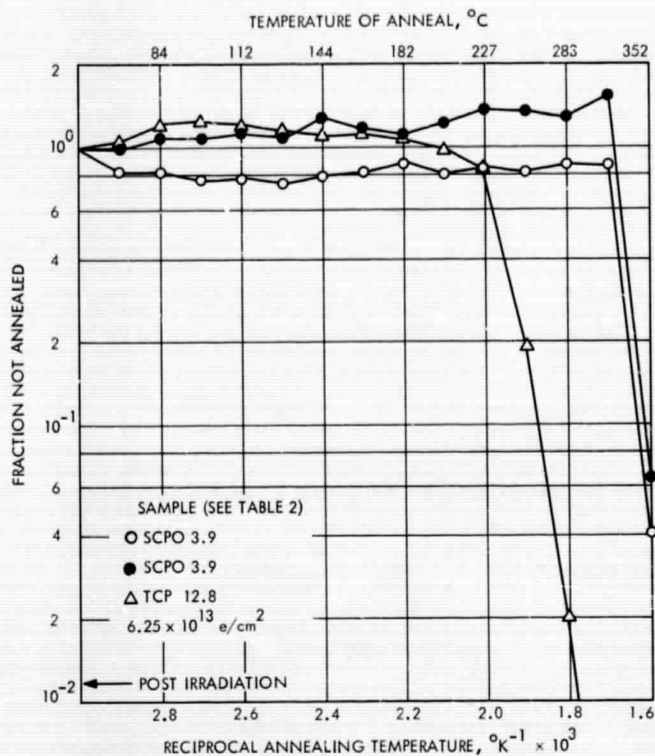

Fig. 8. Influence of oxygen on lifetime recovery in electron-irradiated P-doped silicon

considered tentative in this case. Excess oxygen did not appear to improve the radiation tolerance of either N- or P-type material. Materials containing excess oxygen, in fact, seemed somewhat less tolerant than normal Czochralski-grown material. However, it is possible that this material would exhibit greater merit at larger amounts of total damage. Na-doped material showed no improvement in radiation tolerance. However, only one ingot, with probably a fairly low concentration of Na, was investigated.

The greater promise appears to lie with material that has been doped with aluminum. Even here the sensitivity to electron irradiation is larger than had been anticipated on the basis of neutron irradiation results. Although the relatively high radiation resistance exhibited by Al-doped samples under neutron exposure may have been due to the pre-irradiation heat treatments given these samples, the greater impurity effect apparent in neutron-irradiated samples may be associated with the large fields surrounding disordered regions. It is possible that neutron damage consists of the disordered region itself, containing a high concentration of vacancies, surrounded by a cloud of aluminum interstitials displaced by the shock propagating from the disordered region. The charge state of the interstitial Al might cause it to be moved into the disordered region by the surrounding field. Such a model is, of course, highly tenuous and further consideration needs to be given to this subject. If such a conclusion is valid, Al may not be helpful when simple defects occur. Its effectiveness may be increased, however, through annealing or by increasing the apparent Al concentration through compensation. Such possibilities deserve further consideration.

It has been established that the total amount of damage is very important in determining the annealing behavior of electron- and gamma-induced defects. Furthermore, even when the induced damage has apparently been completely annealed, subsequent damage and anneal is affected by its earlier history. An understanding of this process should be important in ascertaining the feasibility of any scheme to increase the life of solar cells by thermal cycling.

References

1. Curtis, O. L., Jr., Bass, R. F., and Germano, C. A., *The Properties of Defects Introduced in Silicon by 10-MeV Electron Irradiation*, AFCRL-68-0368. Northrop Corp., Hawthorne, Calif., June 1968.

2. Curtis, O. L., Jr., Bass, R. F., and Germano, C. A., *Radiation Effects in Silicon and Germanium*, HDL-235-3. Northrop Corp., Hawthorne, Calif., 1967.

3. Inuishi, Y., and Matsuura, K., "Radiation Damage and Annealing of Carrier Lifetime in Silicon," *Phys. Soc. Japan*, Vol. 18, p. 240, 1963.

References (contd)

4. Bass, R. F., and Curtis, O. L., Jr., "Annealing of 10-MeV Electron Damage in Silicon," *IEEE Trans. Nucl. Sci.*, Vol. NS-15, p. 47, 1968.

5. Trumbore, F. A., "Solid Solubilities of Impurity Elements in Germanium and Silicon," *Bell Sys. Tech. J.*, Vol. 39, p. 205, 1960.

6. Pauling, L., *The Nature of the Chemical Bond*, Chapter 2. Cornell Univ. Press, Ithaca, N.Y., 1960.

7. Franks, R. K., and Robertson, J. B., "Magnesium as a Donor Impurity in Silicon," *Solid State Comm.*, Vol. 5, No. 6, p. 479, June 1967.

8. Carlson, R. O., "Double-Acceptor Behavior of Zinc in Silicon," *Phys. Rev.*, Vol. 108, p. 1390, 1957.

9. Kornilov, B. V., "Absorption in Silicon Doped with Si," *Sov. Phys. Solid State*, Vol. 5, p. 2420, 1964.

10. Schibli, E., and Milnes, A. G., "Deep Impurities in Silicon," *Matl. Sci. and Eng.*, Vol. 2, p. 173, 1967.

11. McCaldin, J. O., and Widmer, A. E. "Alkali Ion Doping of Silicon," *Proc. IEEE*, Vol. 52, p. 301, 1964.

12. McCaldin, J. O., Little, M. J., and Widmer, A. E., "The Solubility of Sodium in Silicon," *J. Phy. Chem. Solids*, Vol. 26, p. 1119, 1965.

13. Svob, L., "Solubility and Diffusion Coefficient of Sodium and Potassium in Silicon," *Solid State Electron.*, Vol. 10, p. 991, 1967.

14. Fang, P. H., and Liu, Y. M., "Temperature Dependence of Radiation Damage in Silicon," *Phys. Lett.*, Vol. 20, p. 344, 1966.

15. Tauke, R. V., and Faraday, B. J., "Annealing Study in Electron-Irradiated N-type Silicon," *J. Appl. Phys.*, Vol. 37, p. 5009, 1966.